Developmental programming of adipose tissue by maternal obesity

Dissertation zur
Erlangung des Doktorgrades (Dr. rer. nat.)
der Mathematisch-Naturwissenschaftlichen Fakultät
der Rheinischen Friedrich-Wilhelms-Universität Bonn

vorgelegt von
Manjusha Biswas
aus
Jalpaiguri, Indien

Bonn 2023

Angefertigt mit Genehmigung der Mathematisch-Naturwissenschaftlichen Fakultät
der Rheinischen Friedrich-Wilhelms-Universität Bonn

1. Gutachterin: Prof. Dr. Elvira Mass
2. Gutachter: Prof. Dr. Med. Alexander Pfeifer

Tag der Promotion: 16.01.2024
Erscheinungsjahr: 2024

Dedication

To my girls, Kalyani & Niharika ……..

Acknowledgements

It is said in the ancient scripts of Vedas that success cannot be achieved by a person alone, but only with guidance from the Guru (teacher). One can thus achieve impossible with the blessings from the Guru! I would like to thank all my gurus (teachers) who came in all forms in my life last few years to make my research possible with their guidance, contribution, motivation , support and knowledge transfer.

Undoubtedly my immense thanks goes to Prof. Dr. Elvira Mass for giving me opportunity to work in her lab and her support and guidance throughout my doctoral studies. I am grateful for her supervision and handholding from bedside to bench. I would like to thank Prof Dr. Alexander Pfeifer for his comments, questions and guidance through colloquiums, retreats and supervisors' meetings. His critical comments about the project and actionable suggestions are the cornerstone of refining my project towards success. I would specially want to thank Dr. Elisabeth Mies- Klomfass for her help starting even before I set foot to Bonn till end of the project in many different dimensions. Along with Prof Mass, I would also like to thank my dissertation committee members: Prof. Dr. Alexander Pfeifer, Prof. Dr. Christa Müller, and Prof. Dr. Maximilian Weigend, for evaluating my dissertation. Besides, I would like to thank DFG (Deutsche Forschungsgemeinschaft) for the research funding.

Furthermore, I would like to thank my colleagues Nora Balzar & Amir Hussain Kayvanju for their insight, with whom I made my initial experiments in the institute. I would add Conny and Carolin in my 'thank you' list for teaching me how to work with mice. I could not thank enough my lab mate Seyhmus Bayar for his constant support who made my life easier during the studies and also has become one of my best friends.

I would like to thank Sandra Ferring-Schmitt, Vanessa Barabasch, Dr Hannes Beckert and Dr Gabor Horvath from Uniklinilkumbonn's core facility for their support throughout my project. I would also like to thank my collaborators Dr Andreas Buness, Dr Farhad Shakeri (Insitute of Genomics, Statistics & Bioinformatics), Dr Jelena Zurkovic (AG Thiele), Dr David Bejarano (AG Schlitzer), Dr Jan Hansen, Dr Nora Matchat (AG Wachten). I would like to thank University of Bonn's Family office , Graduate center and International office to make my journey possible with my 2 years old.

I am thankful to Dr. Pradip Majumder for his advice and suggestions along the way. I would like to thank Prof Dr. AK Pal and Prof Dr. Pranita Medhi for their support in spite of their extremely busy schedule.

On a personal note, I would like to thank my mom Dr. Kalyani Biswas and my daughter Niharika for their constant sacrifice and encouragement, they helped me to go through the most difficult times. They are my rocks!

Last but most importantly, I express my gratitude to my patients battling with cancer in the farthest corners of India, whose courage has inspired me to go beyond my comfort zone, and try to understand the reason behind disease development. With minimal resources and even less money, they fought their best, which compelled me to pursue my journey in science to be able to bring a little more ray of hope & sunshine to the bedside….

Dated the 30th May, 2023
Bonn, Deutschland

Table of contents

Summary

Tissue resident macrophages are an integral part of the innate immune system, but their biology is not well understood in the context of metabolic diseases. Distinctive resident macrophage populations are identified in different organs in mice and in humans using fate mapping studies. They develop from the yolk sac and self-maintain themselves lifelong in specific tissular niche. Adipose tissue is the largest endocrine organ of the body which also takes part in energy balance and metabolic homeostasis. Adipose tissue macrophages have recently gained attention for being majority of immune cell type in steady state and metabolic imbalance and many studies are emerging to understand their mechanistic role in disease development. Adipose tissue resident macrophages are the guardian of immune metabolic gateway. However the full spectrum of adipocyte and adipose resident macrophage interaction is still a matter of current research. Moreover, on the verge of obesity pandemic , it is important to look beyond and try to understand the mechanism of transmission of metabolic disease to the next generation. Maternal obesity plays an important role on offspring's metabolic life , but the role of adipose tissue macrophages in this regard is an uncharted territory.

In this dissertation, it is shown using mouse models that maternal obesity leads to reprogramming of adipose tissue by adipose tissue macrophages in the offspring. The reprogrammed adipose tissue microenvironment showed adipocyte hypertrophy and increased crown like structure formation in maternal obese pups as delineated by histopathology. Moreover the gonadal adipose tissue was marked by infiltration of ontogenically diverse macrophage subsets as shown by high dimensional flow cytometry data. These macrophages were primed by specific immune-metabolic signaling aberration like HIF-1α and MYD88, Moreover, these maternal obese pups also showed delayed sensitivity to insulin in insulin tolerance tests and aberrant lipid subclasses in lipidomic profile. These adverse effects was observed to be rescued using myeloid lineage specific knock-out mice. It confirmed the role of adipose tissue macrophages in the pathogenesis of maternal obesity induced reprogramming of offspring adipose tissue.

All in all, the findings of this dissertation supports the hypothesis that maternal obesity is responsible for transmission of adverse metabolic signature to the offspring's adipose tissue and provide evidences that ontogenically heterogenous macrophages are responsible for such metabolic aberration.

1.Introduction

1.1. Macrophages

1.1.1. General concept

Macrophages were first described in the 19th century by Ilya Metchnikoff who received his Nobel Prize in Medicine for the work in 'Phagocytosis' in 1908[1], however, macrophages are considered to be evolved more than 500 million years ago[2]. In PubMed search, the first peer-reviewed reference on macrophage dates back to 1914, but it talks little about the cell itself. It is around 1925, macrophage as a cell started getting attention in several papers. In the next few decades,macrophage's function is considered primarily to be in infection control as a phagocytic cell. Its role was thought to be limited to eating and scavenging 'foreign' material. Almroth Wright brought to the table the importance of 'microphage' (as they were initially called), and opsonization, and George Bernard Shaw made it popular in his play, The Doctor's Dilemma[3]. In the first half of the 20th century, these cells were regarded as reticuloendothelial system(RES), later to be replaced by the name 'mononuclear phagocyte system'(MPS), and we already see the nomenclature is changing to address the possibility of different phenotypic signatures within these distinctive group of cells. 1970 was marked by the discovery of dendritic cells (DCs) by Steinman and Cohn which represents a further differentiated stage of cells from the same lineage[4]. Next big thing would be the Fc-receptor mediated phagocytosis by macrophage as a zipper-type mechanism[5]. However, in spite of these above game-changing discoveries, the beginning of modern macrophage biology as a discipline can easily be marked by the use of antigenic markers such as F4/80 in mice and CD68 in man which made identification of diverse phenotypes possible in different organs[6,7]. Later discoveries on the receptor families like TLR or NOD-like receptors pave the way for understanding systems biology better.

In adult mammals, macrophages are present in almost all tissues and show significant anatomical and functional diversity[8]. The functional ability of such a diversity makes macrophage a major player in different clinical fields like immunology, oncology, microbiology, virology, regenerative medicine and so on. The implication is deep, as understanding the minute difference within the lineage subpopulations would be key to many future therapeutic discoveries. With this understanding, there has been a passionate research in the last 2 decades to find the heterogeneity of this special cell. This led to the deeper dive into the developmental origin of macrophage -monocyte lineage.

1.1.2. Macrophage Ontogeny

Several studies started to talk about the macrophage ontogeny in the early 2000s. Three of them can be regarded as most impactful. Gordon & Taylor talked about monocyte heterogeneity in humans and corresponding identifying markers in mice[9]. While they correctly pointed out the heterogeneous nature of monocytes, they described them as the origin of tissue-resident macrophage and dendritic cells. However, they did admit the nature of the renewal capacity in the tissue macrophages is poorly understood[9]. On the other hand, Geissmann et al reviewed the importance of exploring developmental lineages because the origin and differentiation cues for many tissue macrophages, monocytes, and dendritic cell subsets in mice, and the corresponding cell populations in humans are areas of active interest[10]. In vitro lineage studies in microglia, the special macrophage in the brain showed it originates from primitive myeloid progenitors that arise before embryonic day 8, which clearly indicated the developmental origin of different macrophage populations beyond monocytic origin[11]. The importance of exploring effects of cytokines or microbial products or transcriptomic profiles is also discussed in different papers which possibly influenced macrophage development. However, it has been clearly mentioned that the activation status of many mature macrophage populations remained to be elucidated in special tissues or diseases like adipose tissue, atherosclerotic plaque, or cancer tissue[4]. Two problems remained. First, the idea of a common precursor for DC and macrophages clouded the understanding of ontogeny. Secondly, whether and how different macrophage populations played role, specifically in different tissues were not defined. The newly developed clonal culture assay was able to ascertain an absence of a common macrophage-DC-restricted precursor (MDP) leading to both macrophages and, resident conventional DCs and plasmacytoid DCs[12]. The use of conditional CX3CR1 promoter-driven Cre-recombinase expression to fate-map the MPS ultimately proved the existence and self-maintaining capacity of tissue-resident macrophage populations[13]. Our understanding becomes much clearer with description of fetal hematopoietic waves in multiple locations of the body: the first wave may give rise to microglia, independent of any further wave and the second wave leads to erythroid-myeloid precursors (EMPs) in yolk sac(YS), differentiating into pMac[14]. These can circulate and give rise to tissue-resident macrophages directly or via EMP-derived monocytes which generate long-lived tissue macrophages. The third wave of hematopoiesis gives rise to the hematopoietic stem cell derived monocytes which can be recruited in the tissues as macrophages[14]. However, the exact role of these macrophage subpopulations in context of different pathophysiology or specialized tissue microenvironments remains to be elucidated.

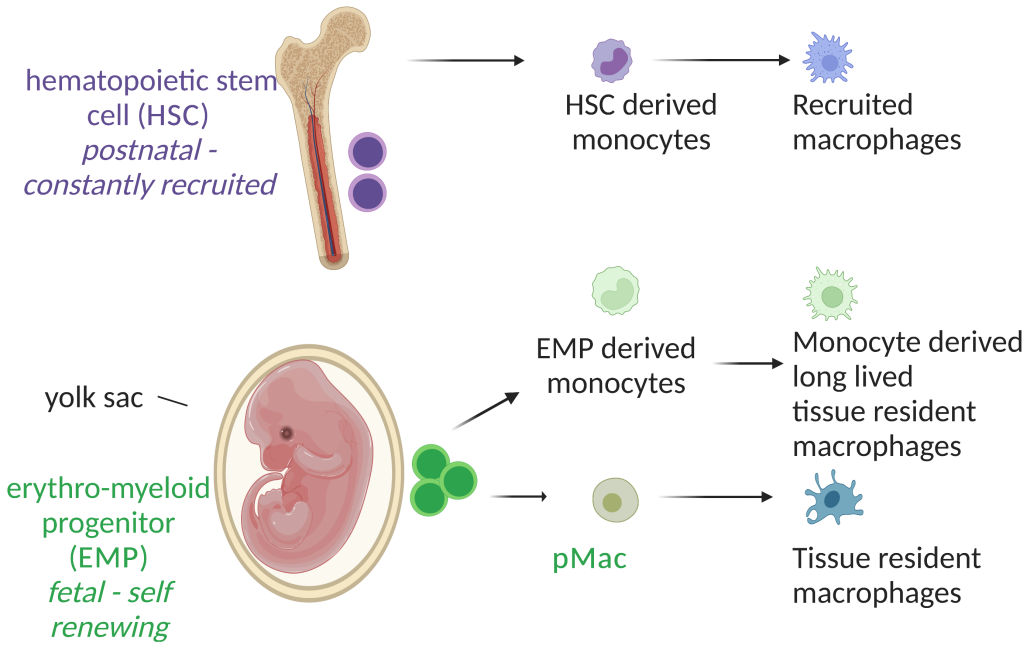

Figure 1: Model of mouse macrophage development & heterogeneity

1.1.3. Anatomical niche of macrophage

The idea of macrophage morphological niche is relatively new. Macrophages are not only functionally diverse but they also tend to show affinity for arranging themselves in close proximity to some tissue components such as nerves or blood vessels. In the context of sub-tissular microenvironment, they can also interact with fibroblast or stromal cells to promote fibrosis as seen in neoplasia. The significance of the macrophage niche is not well defined in different tissues. For alveolar macrophages, replenishing their niche depends on their self-renewal capacity and response to the local microenvironment[15]. Subsequently, scientists started asking questions about the deeper implications of the niches' subpopulations for example, if they are at different stages of maturation rather than a new population, what is their role in homeostasis and disease, and if they are also present in other tissues etc[16].

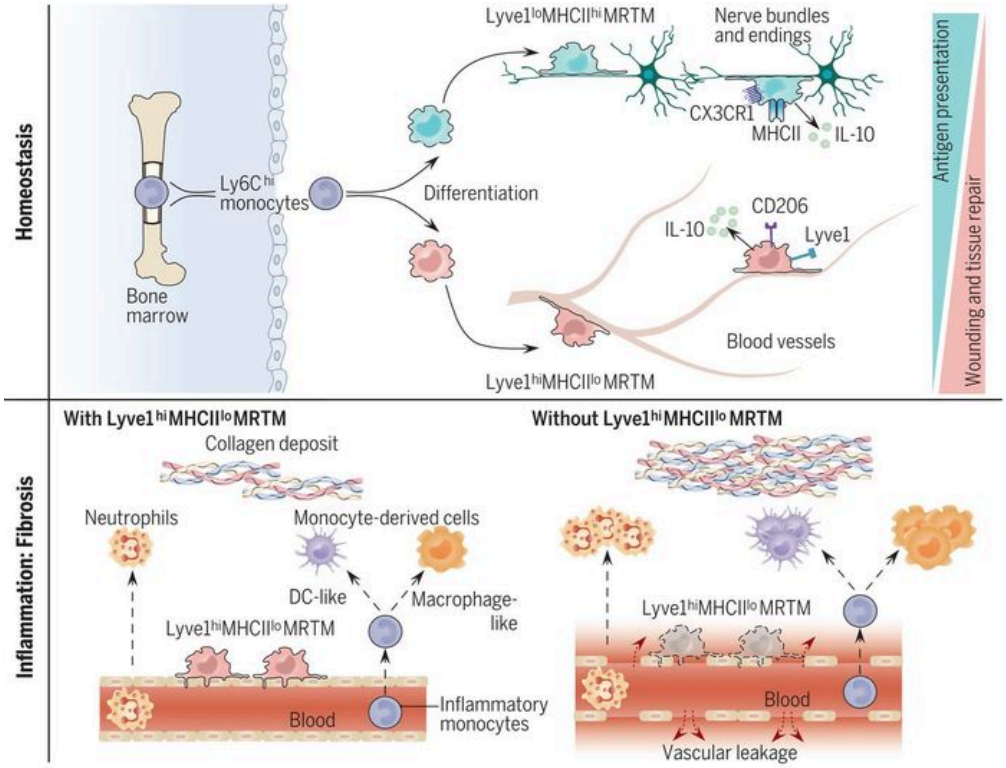

Figure 2. Anatomical niche of resident macrophages (Chakarov et al, 2019)

Chakarov et al showed using complementary fate-mapping models that 2 separate monocyte-derived resident macrophage lineages exist in multiple tissues like lung, heart, dermis, and in fat which preferentially reside in different sub tissular niches such as either close to nerve bundles and fibers (Lyve1^{lo} MHCII^{hi}) or towards blood vessels (Lyve1^{hi} MHCII^{lo})[16]. However, understanding the presence or role of similar niche in adipose tissue is still an area of active research.

1.2. Adipose tissue (AT)

Adipose tissue (AT) gained more clinical importance in recent years than the past, because of the onset of worldwide pandemic of obesity & obesity-related diseases. After all, obesity can be a major etiological contributor for life-crippling chronic diseases like Diabetes Mellitus, cardiovascular accidents and cancer. Adipose tissue is composed of many different cell types such as adipocytes, endothelial cells, immune cells, stromal cells, mesenchymal stem cells etc[17]. Normally, adipocytes are about 30-40% of the cells present in AT[18]. There are three different adipocytes described in mammals: white, brown, and beige adipocyte /brite.

These adipocytes have different morphological characteristics and diverse effects on lipid metabolism[19]. According to the dominant sorts of adipocytes, there are two types of AT: brown and white. The distribution of adipose tissue in humans and in mice is shown in figure 3.

(a) (b)

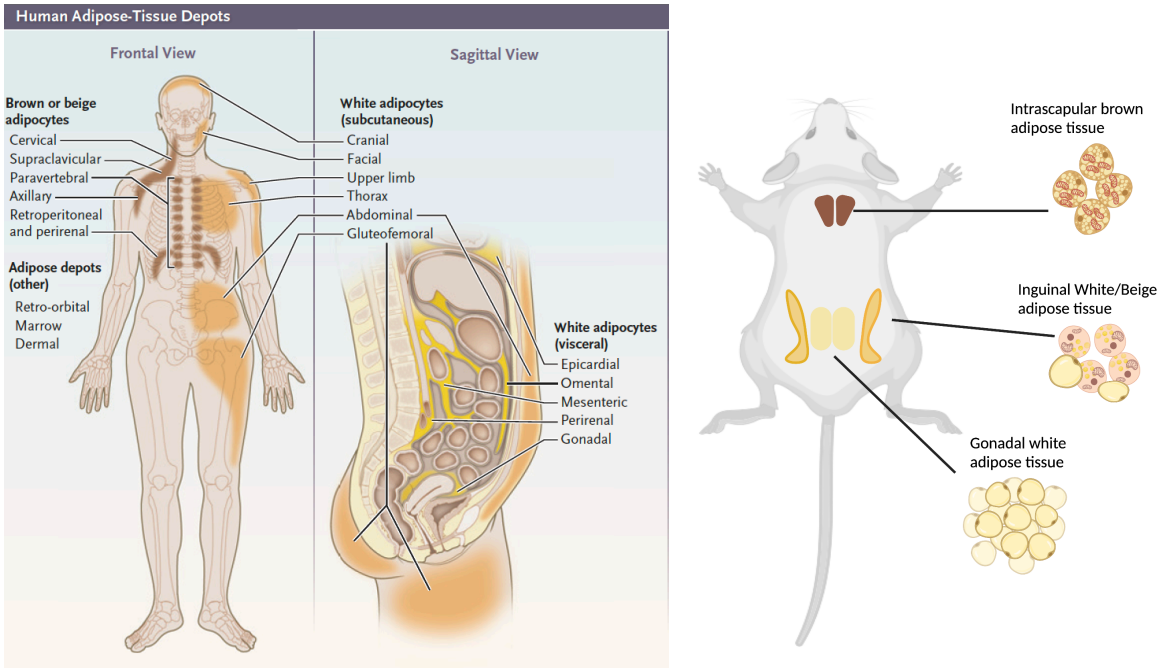

Fig3: Localization of adipose tissue in Human (a) (Aaron M Cypess, 2022) and in mice (simplified)(b)

The stromal vascular fraction (SVF) is the non-adipocyte part of AT including leukocytes, progenitor cells, and other immune cells[20,21,22]. Understandably, these cells influence each other in homeostasis and disease.

Adipose tissue is a metabolic organ that stores lipids as triglycerides(TAGs), but it also provides energy in the period of starvation by lipolysis. The adipose tissue is distributed in two compartments in our body , subcutaneous and visceral, and the latter is usually associated with metabolic diseases, especially with type 2 DM or cardiovascular disease [23,24].

Adipokines are molecules produced by AT and different depots of AT can produce a variety of these molecules. Structure and function of adipokines are diverse: some of them are hormones (leptin, adiponectin, etc), growth factors (IGF, VEGF, FGF etc.) or cytokines (IL-6,TNFa)[25] . Adipokines are important regulators of insulin signaling, glucose uptake, fatty acid oxidation etc. and cytokines control inflammation or its resolution along with regulating angiogenesis in AT[26], thus contributing to immune cell recruitment during inflammation.

1.2.1. White adipose tissue

White adipose tissue(WAT) is the most abundantly present AT in our body[27]. WAT is composed of large adipocytes with a single lipid droplet and lesser number of mitochondria than brown adipocytes[27]. As mentioned earlier, WAT has subcutaneous and visceral depots in humans which is also recapitulated in rodents. Mice and rats are useful models to study human adipose tissue because they pose roughly similar visceral (mesenteric, perirenal and gonadal) and subcutaneous (inguinal and axillary) depots[28]. The systemic effects of obesity are pronounced in visceral WAT, the reason being free fatty acids(FFAs) generated from lipolysis of visceral WAT are circulated to the liver by the portal venous system[29]. The major functions of WAT are to provide mechanical protection, maintain body temperature, and most importantly, act as a storehouse for fatty acids(FAs) maintaining lipid-energy balance. The FAs stored in WAT can be readily oxidized to produce a large number of ATPs if required[30]. When it comes to the endocrine function, WAT releases most important adipokines like Leptin, Adiponectin, Glucocorticoids, IL-6, TNF-α, PAI-1, MCP-1, FFAs, Adipsin & ASP among others [25,30].

1.2.2. Brown adipose tissue

Brown adipose tissue(BAT) is a special type of AT. Brown adipocytes have their special color due to the high number of mitochondria present on them and multiple fat droplets inside them[19]. Previously it was thought to be important only for newborn babies, however recently using glucose tracers, metabolically engaged BAT has been identified in adults[19,24]. BAT uniquely handles FFAs, by transporting them to mitochondria and oxidizing them by Uncoupling protein 1 (UCP1) thereby producing heat[24]. This process is called non-shivering thermogenesis[24]. Like WAT, BAT is also composed of multiple cell types. While 20-30% of the cells are mature adipocytes, the other portion is constituted by adipose stem cells, preadipocytes, endothelial cells, blood, and neural cells etc.[31]. When in homeostasis, macrophage and other immune cells are present in much lower numbers in BAT as compared to WAT, as revealed by different cell sorting analyses[32,33]. Like WAT, BAT also secretes different molecules known as batokines which can work in paracrine or autocrine way[31,34]. Some of the prominent secreted batotkines are fibroblast growth factor21, IL-6, Slit2-C, VEGF, BMP8b, NRG4, EPRD1, prostaglandin etc.[31,34]. The BAT in the nape of the neck of rodents is surrounded with thin subcutaneous

WAT which has been referred as 'BAT rim' in this dissertation. On the other hand, BAT in the center of the subcutaneous WAT has been referred as 'BAT core'.

1.2.3. Beige/brite adipocytes

The third type of adipocytes is called beige adipocyte or brite. Beigeing or beige adipogenesis is induced by chronic cold exposure, adrenergic activation, long term treatment with peroxisome proliferator–activated receptor γ (PPARγ) agonists [35] ,cGMP agonists like natriuretic peptides (NPs) and inhibitors of phosphodiesterase 5 (PDE5) (sildenafil)[19]. Within WAT depots , beigeing can happen either de novo where progenitor cells directly give rise to beige adipocytes or by proliferation of mature beige adipocyte or phenotypic conversion of mature WAT into brite by reprogramming of the thermogenic process[28,35]. Interestingly, the beige adipogenesis is a temporary mechanism to environmental signals, it gradually loses the morphological and molecular characters after removing the external stimuli and acquires a white like morphology directly by an autophagy mediated mitochondrial clearence[36]. Beige adipose tissue shows reprogramming between white and brown chromatin states with a similar transcriptomic profile like that of WAT, thus representing true plasticity and use epigenetic mechanisms like histone modification to do so[37]. Resident eosinophils are principal recruiter of beige adipocytes[38]. Our understanding, about whether resident AT macrophages influences beigeing by developmental reprogramming, is yet unclear.

1.2.4. Adipocyte size

AT is a highly dynamic organ consisting of adipocytes of different sizes, small or large and their properties have been explored by scientists to know their significance[39]. In the physiological conditions, the adipocytes vary from 20 to 300 µm in diameter, giving a wide range in cell volume within the same depot [39]. This variation comes from the TAG content of the cells; therefore, it is reasonable that the dysmetabolism of adipocytes is somehow dependent on adipocyte size[40,41]. In fact, Fat cell size can be related to many metabolic indicators such as lipid dysmetabolism, ectopic fat accumulation, insulin resistance etc.[41]. Obesity is the result of adipocyte expansion, and the adipocytes expand in two ways in presence of appropriate stimuli, increase in cell size or hypertrophy, and increase in cell number or hyperplasia. Ye and colleagues, in a meta-analysis involving 2348 articles (in Pubmed database till 2021), showed that adipocyte hypertrophy is the 'worse' expansion as it is associated with impaired adipose tissue differentiation potential, rate of adipogenesis, adipose tissue inflammation, and altered adipokine secretion[41]. Understandably, there has

been a need for the measurement of adipocyte size to address the deeper implication of such analysis. Cell diameter, area, and volume of adipocytes are the parameters addressed for quantitative measures[42]. As there is almost no significant research regarding the size of brown or beige adipocytes or the alteration in cell size during the browning of white adipocytes, scientists tend to focus on the significance and measurement of white adipocyte size[39]. Though there are many methods applied in the last few years, there is not one universally agreed method for measuring adipocyte size. Three methods are found to have a superior correlation with metabolic risk: collagenase-isolated cells, histological tissue sections and electronic sizing of osmium-fixed adipocyte[43]. Although scientists have weighed the advantages and disadvantages of the said methods, the histological method has certain pros not noticed earlier [44]. In the histology sections, dead adipocytes can be identified by surrounding crown-like structures and excluded from size measurements, thereby making the calculations more accurate[44]. There is also a certain discussion about the small adipocyte appearance. McLaughlin and colleagues found that there is clearly an association between small adipocytes with a diameter of 20-50μm with insulin-resistant patients[45]. However, the limiting factor in considering the significance of the 'small adipocytes' is the lack of universal agreement regarding the median size and presence of different percentages of them in different studies.

1.2.5 Adipose tissue macrophage (ATM)

Adipose tissue macrophages (ATMs) are perhaps the most important second cellular population in adipose tissue after adipocytes. In homeostasis, macrophages are 5-10% of AT microenvironment[46.47]. ATMs are the key component of immune response in AT and studies using different mouse models showed it can comprise up to 40-50% of the stromal vascular fraction in obesity[46,48,49]. Sharma and colleagues obtained transcriptomes from 2,740 and 1,697 $CD45^+$ cells from gonadal white adipose tissue(gWAT) from mice fed normal or high-fat diets, respectively, and categorized them into 17 clusters, of which major 7 clusters corresponded to macrophages/monocytes. The majority of the macrophage clusters showed a spectrum of related activation state[50]. This finding proves the predominance of macrophage in AT over other immune cells. As discussed earlier macrophages are developmentally diverse and ATMs are not exceptions. Studies from primitive gWAT in neonatal mice shows $LYVE1^+$resident macrophages present in one day after birth when gWAT starts to form[51]. Contrary to the longstanding belief that resident macrophages derives from monocytes, separate ontogeny has now been proposed and established by several researchers for resident macrophages[11, 13, 14, 51, 52]. Recently, three different macrophage populations have

been described depending on Tim4 and CD11c expression, two Tim4- populations depleted in$CCR2^{-/-}$ mice showing their monocyte-dependence and one $Tim4^{+}$ population using a fate mapping model based on the macrophage-specific expression of the colony-stimulating factor-1 receptor gene confirming their embryonic origin[53]. Morphologically, ATMs also form some histological niche in the AT microenvironment. The $LYVE^{+}$ tissue-resident macrophages in AT are said to be associated with vasculature and late depleted by monocyte derived macrophages[16]. In addition, studies identified one or two CD63+ monocyte-derived ATM subpopulations based on differential expression of MHCII, CD11c, and CX3CR1. $CX3CR1^{hi}$ $MHCII^{hi}$ were found predominantly associated with nerve bundles[16]. The ATMs do not merely reside in AT microenvironment, they also significantly influence the development and function of AT. If the embryonic ATMs are removed by excision of primitive gWAT in D4, that hinders the development of mature AT in adult mice[54]. It suggests the influence of the resident macrophages in gWAT formation. For the brown adipose tissue, ATMs expressing $Cx3Cr^{1+}$ and $MHCII^{+}$ are identified to influence physiological functions[55]. All these studies prove that heterogeneity in macrophage subpopulation in AT exists even in homeostasis and may show a plethora of changes in presence of stress or stimuli. Ultimately, those changes are either prognostically or diagnostically associated with metabolic syndrome.

1.2.6 importance of ATM for BAT & WAT function

In normal white adipose tissue, macrophages are responsible for three main functions such as efferocytosis, lipid buffering and influencing adipogenesis[56]. Cellular turnover in AT is described annually from 10% to 70% by different observers[28, 57, 58] but total fat cell numbers are tightly regulated requiring an efficient mechanism to remove the dead adipocytes to maintain an anti-inflammatory state[56]. The ATMs take this opportunity to scavenge dead adipocytes to maintain balance. In mice WAT, ATMs remove or store the excess amount of lipolyzed lipid products, monitoring the level of lipid release in blood as evidenced by rapid accumulation of ATMs in fasting or pharmacologically induced lipolysis and depletion of them while weight loss[59]. It is further supported by the presence of Lysosomal acid lipase(Lipa) in ATMs which is required for hydrolysis of TAGs and cholesterol esters and its deficiency leads to AT atrophy and severe hepatic steatosis. The expression of Lipa in ATMs rescues the complication and thus concludes the need of ATMs to maintain lipid metabolism in AT homeostasis[60,61,62].

Interestingly, for BAT macrophages are implicated for cold induced metabolic adaptiveness. Studies on $IL4R\alpha^{L/L}LysM^{Cre}$ mice show susceptibility to cold induced hypothermia because of

inactivation of specific macrophage population[63]. Also, macrophages help in browning of WAT and beige fat production to counteract onset of obesity[64]. Resident macrophages produce PDGFcc and Pvf3 which mediate storage of lipid in adipocytes by hypertrophy of the fat cells by sensing increased food intake[53]. Therefore, macrophage have wide and often contradictory influence over AT function.

The importance on macrophage on adipogenesis will be discussed further in detail in a following section.

1.2.7 ATM biology in metabolic imbalance

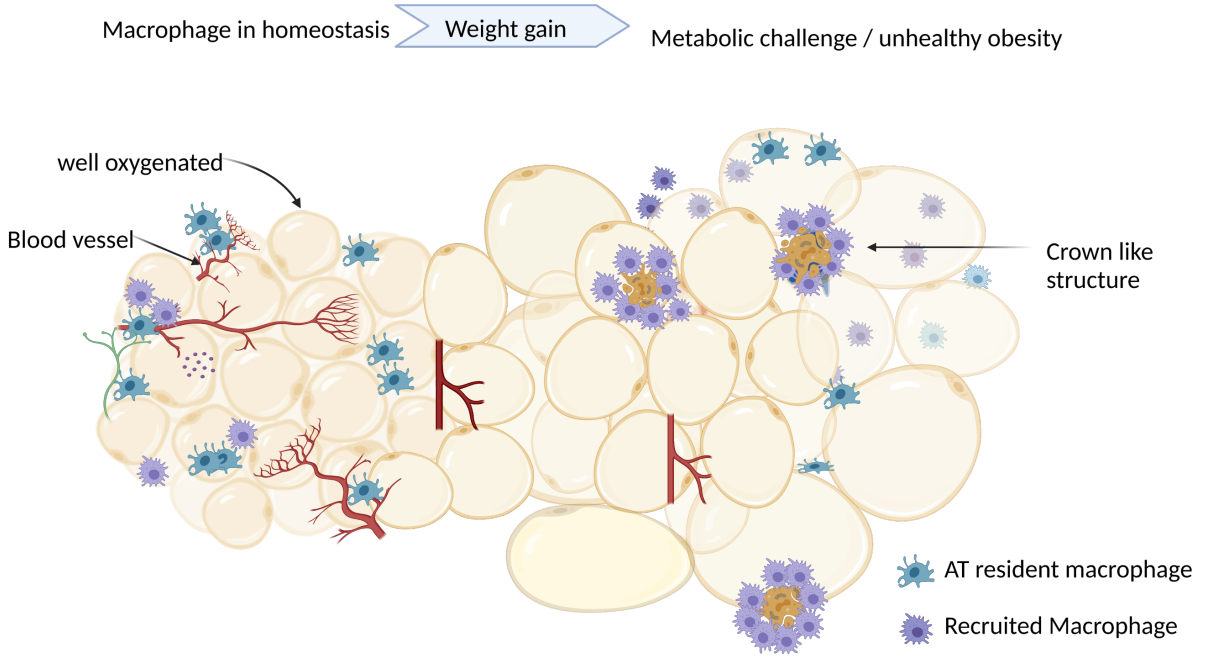

Figure 4: Adipose tissue microenvironment in health and disease

It is understandable ATMs will be the main drivers of adipose tissue inflammation in metabolic challenges as it control the AT homeostasis. It has been 20 years since the macrophage infiltration in obese AT has been first described[47, 65]. However, the complete dissection of the ATM population and attributing each and every event in metabolic crisis to them is yet incomplete. Obesity is a state of chronic low-grade inflammation or metainflammation. There is an expansion of specific macrophage subpopulations in obese AT which promotes inflammation and insulin resistance[66]. These ATMs can take up to 40-50% of the obese adipose tissue[46, 48, 49, 66] and secrete increased amounts of

proinflammatory cytokines[66] specially TNF-α and IL-1ß which acts as both paracrine and endocrine manner[67]. As the visceral adipose tissue drains the FFAs to the liver, the deranged AT environment directly contributes to hepatic insulin resistance[66].

The inflammatory macrophage subpopulation also releases MCP-1 in the visceral AT leading to more and more macrophage recruitment[68,69]. Since long time and even until now, macrophages are described in the M1-M2 spectrum ,where M1 is exploiting glycolysis and M2 takes OXPHOS for primary metabolic pathway. But it is no longer valid as single cell & single nuclear RNA-sequencing data could delineate multiple macrophage phenotypes in between M1 and M2 spectrum [70]. As there are many subsets described by different studies, it will be rational to look through the glasses of Ontogeny for ultimately precise the list. Indeed, BM chimeras suggested that many of these obesity related ATMs are of monocytic origin[47, 71]. Also, there is increased blood monocytes in obese children supports the association[68]. In obese AT, ATMs accumulate around the dead adipocytes to form crown-like structures(CLS) which is the histological hallmark of macrophage infiltration in AT microenvironment[72,73]. While in lean mice the incidence of CLS is rare, it can increase up to 30-fold in obese mice[72]. HFD induced obese mice showed endothelial dysfunction. The increased need for expanding AT leads to hypoxia and reduced adiponectin secretion, thereby further accelerating the endothelial dysfunction[74]. These events lead to massive adipocyte death and debris, provoking NOD like receptors through damage associated molecular pattern[75]. On the other hand, FFAs secreted by adipocytes induce TLR2 & TLR4 receptors and promote CCL2 secretion and monocyte derived ATM recruitment[76]. NOD like receptor activates the NLRP3 inflammasome and all these together activate the reactive oxygen species (ROS) which establish chronic inflammation. Monocyte derived macrophages are marked by CD11c, CD63, CD9 and TREM2 expression among others[77].

1.2.8. Adipogenic precursor cells(APCs)

The cellular basis of adipocyte differentiation is called adipogenesis[78]. AT develops in a spatiotemporal manner, whereby each individual subcutaneous or visceral tissue develops in different fetal stages[79]. Still the precise origin of adipogenesis is unclear, but line tracing studies have shown subcutaneous and intra-abdominal fat originates from separate mesenchymal lineages[80]. Not only that, even in the same depot, adipocytes arising from different lineages may exist[81]. In the first postnatal years AT grows by both hypertrophy and hyperplasia[82]. The ability of emergence of new adipocytes and expansion of AT is critical for

tissue homeostasis and perhaps systemic metabolism[79]. Friedman and colleagues isolated APCs from murine SVFs which are characterized by lack of endothelial or hematopoietic marker ($CD31^{-}$, $CD45^{-}$) and expression of all common mesenchymal stem cell markers ($CD29^{+}$, $Sca1^{+}$, $CD34^{+}$) with an additional marker CD24 expression status[83]. Accordingly, APCs could be either CD24 positive or negative, but to what extent adipocytes originate from each of them was still not clear[80].

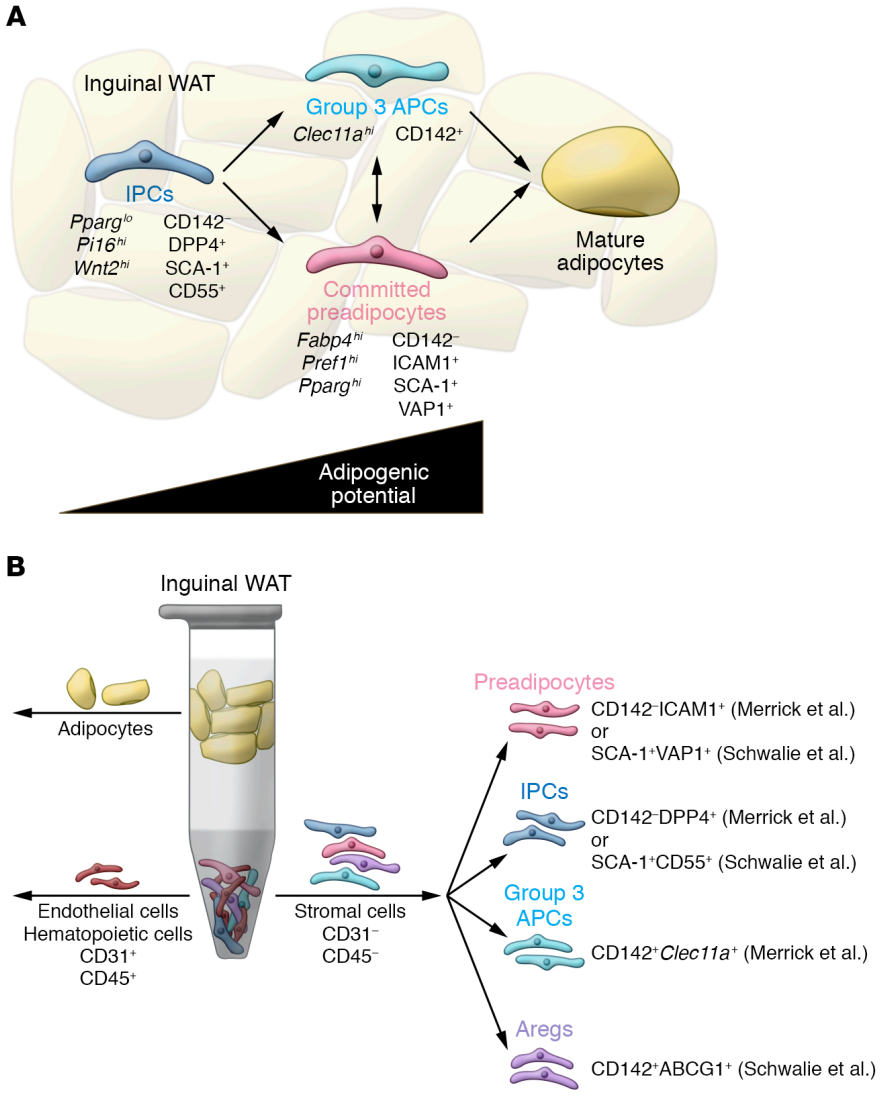

Fig5: Different adipogenic precursor cells (Visvanath &Gupta, 2019)

In this pursuit, it was shown by Merrick and colleagues that a primitive stem cell population expressing DPP4(CD26) exists [84]. FACS strategy isolated a more committed highly adipogenic preadipocytes expressing ICAM(CD54) and an additional pre-adipocytic precursors which are $CD142^{+}$ [78,84]. Brown adipose tissue development is different from WAT and closer to myogenic precursors. Fate mapping studies in mice show that brown adipocytes

in anterior depots develop from $En1^+$ cells at E8.5-E9.5 and in dorsal depots from paraxial mesoderm[79]. They also develop from $Myf5^+$ and $Pax7^+$ myogenic precursors like cells[79].

1.2.9. Interaction of adipogenic precursor cells with macrophages

Macrophage influences adipogenesis as a part of its functions. Emerging Studies are exploring the mechanisms which are still not completely understood and several hypotheses have been proposed. It is seen that $CD9^+$ macrophages are found in the fibrotic extracellular matrix (ECM) of obese AT, generated under the influence PDGFR expressing adipogenic precursors and these senescent macrophages inhibits adipogenesis[85]. On the other hand tissue resident macrophages help in adipose tissue to expand by hypertrophy in obesity[53]. Two facts taken together, it seems only plausible that as macrophages inhibit the new adipocyte generation so AT cannot expand by hyperplasia and takes the mean of hypertrophy, however, it is an area of active exploration.

1.3. Maternal Obesity

1.3.1.Maternal metabolic health in pregnancy

Often maternal health is ignored in pregnancy, especially in developing countries. With the rise of obesity as a pandemic, there is also an increased prevalence of overweight and obesity in women of reproductive age having 14.6 million obese pregnant mothers all over the world in 2014[86]. Metabolic instability with increased BMI can give rise to many maternal complications in pregnancy, such as gestational diabetes, hypertension, pre-eclampsia etc[87]. Not only that, maternal metabolic ill-health can extend its effects further by transmitting bad metabolic signatures to the next generation.

1.3.2 Maternal obesity and offspring health

Dr. David Barker was the first to propose the developmental origins of health and disease (DOHaD) theory[88]. Though Barker's theory was based on maternal undernutrition, any form of malnutrition during pregnancy, either lack or overnutrition can be regarded as maternal metabolic stress that can affect fetal programming adversely, increasing the chance of getting metabolic disease in the later life of offspring[88,89]. Fortunately, researchers have started to

focus more in this previously ignored area in the past few years. Several studies show sex-dependent propensity of the metabolic disease in the male offspring [90,91]. It can be due to the hormonal influence of estrogen protecting female offspring to some extent as adipose tissue is a sexually dimorphic tissue influenced by sex hormones[92]. Studies showed an increased expression of inflammatory markers in the AT of offspring of obese mothers such as overactivation of NF-kB and JNK signaling and infiltration of macrophages .Those offspring had a decreased level of insulin signaling protein [93]. It has been also suggested that obesogenic diet of mother may lead to transplacental passage of maternal microbiome to fetus creating an immunologically challenging environment, which in terms creates 'inflamed ' fetal brain and abrupts homeostasis[94]. The liver lipidomic profile of the offspring from obese moms showed distinct changes in male and female offspring[91, 95]. This distinction has also been cited as one of the reasons of male offspring susceptibility to the effects of maternal obesity[91].Overall literature review shows link of maternal obesity to offspring metabolic health, but precise mechanism for transmission of metabolic diseases to the next generation remains to be elucidated.

1.4 Adipose tissue microenvironment influencers

1.4.1. Adipose tissue microenvironment & HIF-1α

Obesity is not that simple, and one of the reasons is complex interaction between multiple stakeholders of AT microenvironment(ATME). Obese ATME is known to be hypoxic, and exact reason for the same has not been pinpointed, at least it can be assumed multifactorial. Initially the hypertrophy resulted from rapidly expanding adipocytes plays the role[96]. The postprandial blood flow fails to rise for obese subjects[97] and the diameter of the hypertrophic adipocytes are often >100 μm, which is larger than the normal diffusion distance, and PO_2 can be near zero from even in 100 μm distance from the vasculature[98]. The capillary density is low in obese adipose tissue of humans compared to lean subjects which contributes to hypoxia[99].

Major two members of the ATME are macrophages and adipocytes which interact intimately and their crosstalk is associated with secretion of cytokines, adipokines, FFAs etc. in obesity. FFAs are particularly important (specially the saturated fatty acids) which can directly activate TLR2-TLR4 , and cause NLRP3 inflammasome mediated activation of IL-1ß[100,101,102]. These inflammatory signals attract more recruitment of monocyte derived macrophages which accumulate around the dead adipocytes forming CLSs. In later stages of obesity, the CLS becomes a major site of hypoxia [103]. On the other hand, FFAs are responsible for increased oxygen consumption through uncoupling[104]. In the tissue microenvironment, HIF-1α is the

master regulator of hypoxic response , so naturally HIF-1α is activated in both adipocytes and macrophages in obese ATME[105,106,107]. Surprisingly, not only HIF-1α is activated in truly hypoxic ATME, but also by pseudohypoxia. Lipopolysachharide induced (LPS) macrophages can activate HIF-1α in normoxia (pseudohypoxia) [108]. This is particularly important in case of obesity, because of a shift towards glycolysis and the pentose-phosphate pathway. The activated HIF-1α is required for full expression of many glycolytic gene encoding GLUT1, lactate dehydrogenase-A (LDH-A), hexokinase, phosphofructokinase, pyruvate kinase, and GAPDH[109]. Alongside, the kreb cycle intermediates like succinate, fumarate, malate are also accumulated[110]. Succinate competes with αKG to inhibit prolyl hydroxylase (PHD) or do so by generation of ROS by reverse electron transport from complex I in mitochondria leading to constant stabilization and accumulation of HIF-1α [111,112]. As mentioned already, IL-1ß is one HIF-1α's target and promotes proinflammatory ATME. PKM2(Pyruvate Kinase M2) is also activated by LPS macrophages and binds with HIF-1α in the nucleus to activate downstream transcription[110].

1.4.2 Metabolic adaptation of ATME by HIF-1α

As described earlier, the obese ATME sets the stage for chronic HIF-1α activation. Hypoxia-inducible factor 1 (HIF-1) is a heterodimeric DNA binding complex and also called as the master regulator of oxygen homeostasis. It has two subunits: alpha subunit - hypoxia-inducible and beta subunit, oxygen non-responsive[113] . While in normoxia, HIF-1α is quickly degraded by prolyl hydroxylation which is suppressed in hypoxia leading to HIF-1α forming dimer with HIF-1ß. This dimer binds with hypoxia response elements in promoter or enhancer sequences of the target genes . Among others, critical HIF-1α-binding sites are found in genes encoding the glycolytic enzymes phosphoglycerate kinase-1 and LDH[113]. The hypoxic cells prefer to use the less energy efficient metabolism leading to pyruvate to lactic acid formation[113]. Secondly, HIF-1α inhibits insulin signaling in adipocytes leading to insulin resistance[114]. Thirdly, HIF-1α downregulates oxidative phosphorylation (OXPHOS) in mitochondria, reducing oxygen-dependent energy production by cells. It also diverts the Tricarboxylic acid (TCA) cycle intermediates like glucose, fatty acids and glutamine , thereby inhibiting it[115]. Moreover, HIF-1α activates glutamine-dependent lipid synthesis , ultimately leading to accumulation of lipid droplets in different organs[116]. All these effects together modulate the AT towards the pathophysiology of insulin resistance, diabetes mellitus and cancer. The KEGG signaling pathway for HIF-1α in Mus musculus (Fig 6) shows all connected metabolic and oxidative pathways which is also recapitulated in human. (https://www.genome.jp).

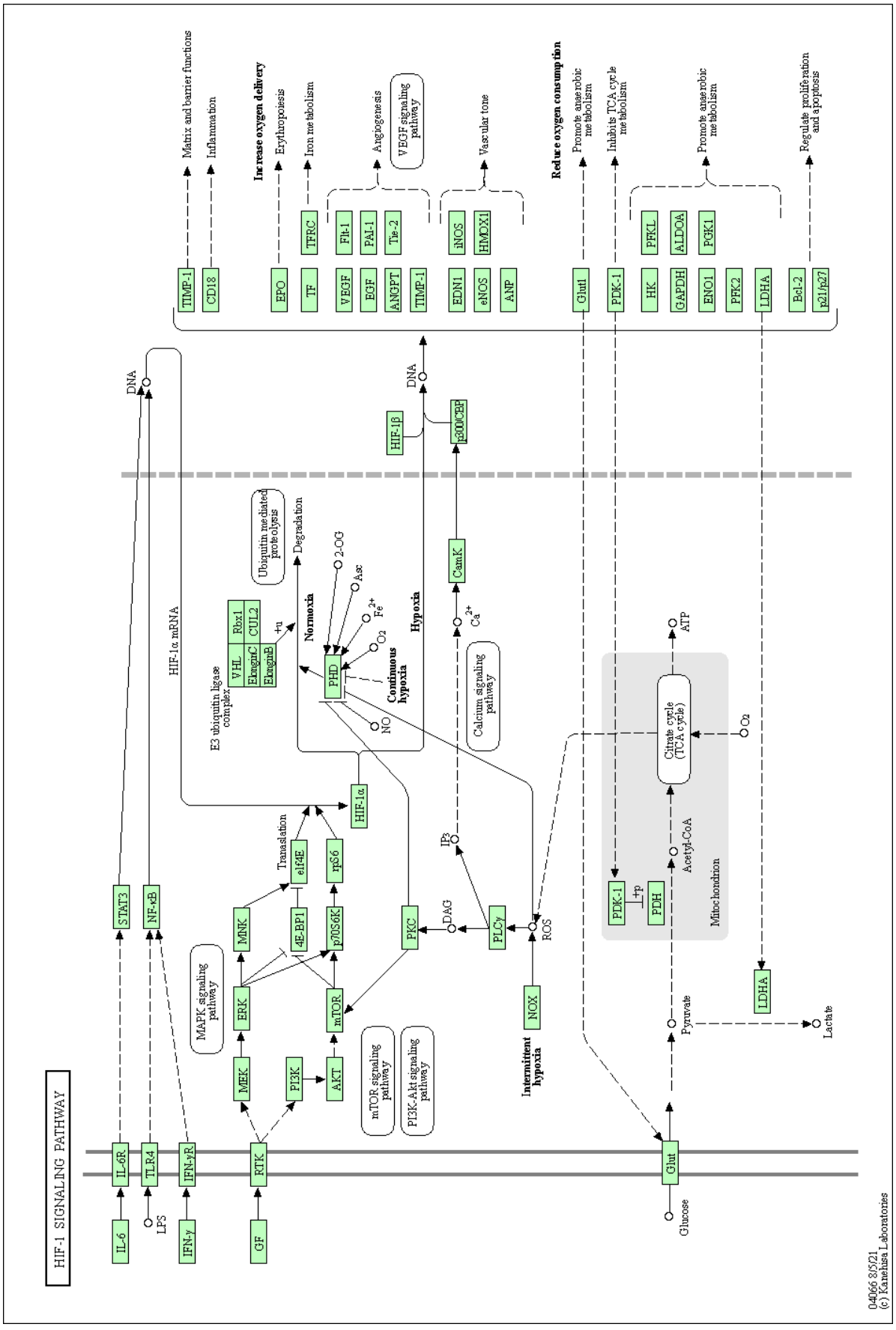

Figure 6: KEGG map showing HIF-1α signaling pathway and metabolic adaptation in Mus musculus (Source : https://www.kegg.jp/pathway/mmu04066)

1.4.3. MYD88 signaling pathway and its interaction with HIF-1α

Specific downstream events in HIF-1α signaling in ATME during obesity are not well studied. In C57BL/6J mice IRAK-M shows robust upregulation in presence of HIF-1α activation in AT along with impaired glucose tolerance and AT fibrosis[117]. On the other hand, study showed hypoxia-induced expression of HIF-1α in fibroblasts stimulated the TLR/MyD88/NF-κB signaling pathway and promoted the expression of some inflammatory factors such as IL-6 in Keloid [118]. These findings suggest HIF-1α interacts with TLR-MYD88-IRAK pathway intimately and in a complex way depending on tissue specificity and disease pathway. Recently it was found that IL-1R can induce MYD88-IRAK-2-PHB/OPA1 signaling directly contributing to the metabolism in obese AT suppressing OXPHOS and fatty acid ß-oxidation[119]. The String database shows the interaction between HIF-1α and MYD88 (Mus musculus) and other interacting nodes(Fig7).

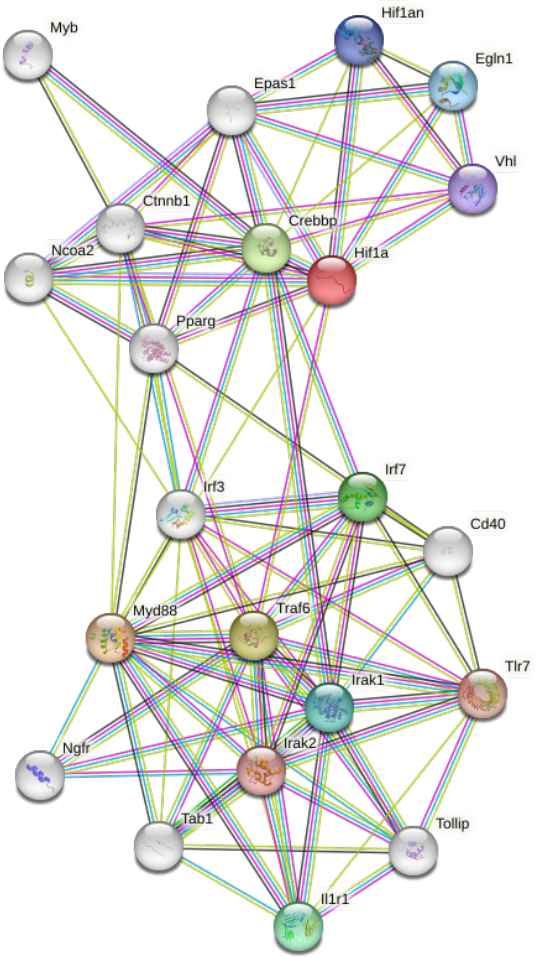

Fig7: HIF-1α & MYD88 interaction(Mus musculus) with predicted functional partners in STRING protein interaction network (Szklarczyk D et al 2023, source: https://version-11-5.string-db.org)

The STRING (*Search Tool for the Retrieval of Interacting Genes/Proteins*) database is a biological database developed by a consortium of academic institutions including European molecular biology laboratory (EMBL), Technical University of Dresden, Swiss institute of Bioinformatics, Novo nordisk foundation center Protein research etc., which is a web source for known and precited protein-protein interaction, helping researchers to find predictable associations. Both the said proteins are enriched for positive regulation of cytokine production, smooth muscle proliferation and IL-1 mediated signaling pathway and abnormal macrophage physiology.

Isolated, it is shown that lack of MYD88 protected from adipose inflammation caused by gut microbiota ablation from HFD and protected from metabolic syndrome[120]. MYD88 in the intestinal epithelium acts as a sensor changing the host metabolism in a diet dependent manner leading to the development of obesity[121]. Hypothalamic inflammation induced by obesity is also affected by MYD88 signaling where MYD88 expression is upregulated on long term HFD and astrocyte specific KO of MYD88 improves the metabolic derangement[122]. All these studies clearly establish the importance of exploring MYD88 signaling in obesity especially in two circumstances, such as in case of HIF-1α activation or hypoxic ATME , and while investigating the role of gut microbiota in development of metabolic diseases. However, until now, we could not find a study which looked into direct and joint influences of HIF-1α and MYD88 activated macrophages in remodeling ATME of the offspring from obese dams.

2. Aims of the study

Previous study from our group showed that maternal obesity can cause developmental programming of Kupffer cells which are the tissue resident macrophages in the liver. Also, they observed an upregulation of Hif-1α gene in the glycolytic pathway when the mother had HFD. (Nóra Reka Balzar et al, unpublished data 2023). However, whether the effects are part of a larger fetal multiorgan reprogramming due to developmental switch, is largely unknown. Liver and adipose tissue being two complementary metabolic organs, it is rational to explore if the effects seen in offspring liver are to be recapitulated in AT. Also, whether HIF1α activation is an isolated event in mother's obesity alone, or has a deeper transmitted systemic effect to the offspring remains to be explored. Thus, three major research questions arose :

1. Do the ATMs in the offspring of obese mothers show developmental diversity?
2. Do these ATMs remodel the AT in those offspring ?
3. Does activation of specific immune signals cause reprogramming of offspring's AT?

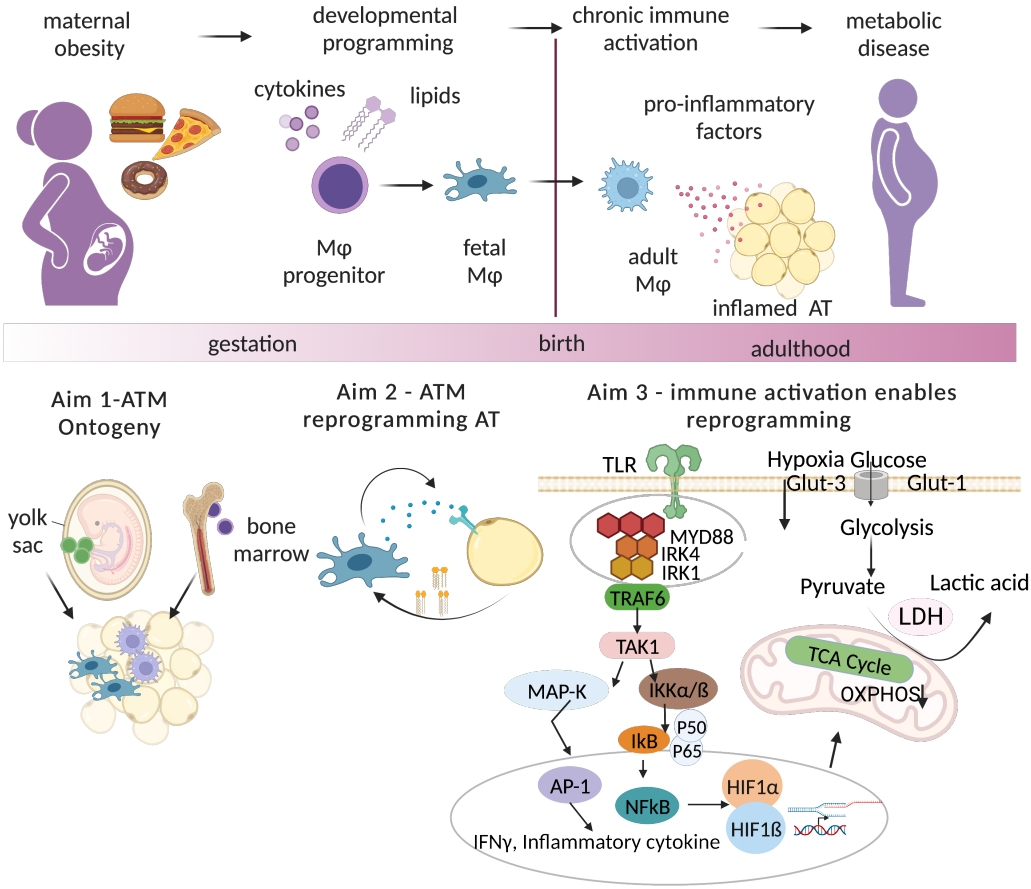

Fig8: Aims of the current study. AT= adipose tissue, ATM= adipose tissue macrophages, TLR= toll like receptor, Mφ= resident macrophage, GLUT = glucose transporter, LDH=.lactate dehydrogenase, MYD88= myeloid differentiation primary response protein 88, IRK= interleukin-1 receptor-associated kinase, TRAF=tumor necrosis factor receptor associated factor, TAK1=TGF-ß activated kinase 1, IKK= MAP K= mitogen-activated protein kinase,AP-1=adaptor protein -1, NFkB=Nuclear Factor Kappa B, IFNγ= Interferon gamma, HIF-1=Hypoxia induced factor1, TCA Cycle= Tricarboxylic acid cycle.

3. Material and methods

3.1. Chemicals and compounds

Key resources used in the project are listed below, more essential details are accompanied in the relevant sections.

Table1: List of antibodies for investigating macrophage heterogeneity in mice gWAT by Flow cytometer:

Heterogeneity Panel for ATMs					
Primary Antibodies					
Antigen	**Conjugate**	**Clone**	**Dilution**	**Source**	**Catalogue#**
CD45	APC-Cy7	30-F11	1:400	BioLegend	103116
CD11b	PE/Cy7	M1/70	1:800	BioLegend	101216
Tim-4	AF647	RMT4-54	1:400	BioLegend	130008
F4/80	BV421	BM8	1:400	BioLegend	123132
CD11c	BV605	N418	1:200	BioLegend	117333
Ly-6C	BV510	HK1.4	1:200	BioLegend	128033
Ly-6G	PE	1A8	1:400	BioLegend	127607
NKp46(CD335)	PE	29A1.4	1:200	BioLegend	137604
TCR ß	PE	H57-597	1:200	BioLegend	109208
CD19	PE	1D3/CD19	1:400	BioLegend	152408
Siglec-F/CD170	PE	S170007L	1:100	BioLegend	155506
MHCII	AF700	L243	1:400	BioLegend	307626
Cx3CR1	PE-Dazzle^{TM} 594	SA011F11	1:200	BioLegend	149014
CD63	PerCP-Cy5.5	NVG-2	1:100	BioLegend	143912
CD206 (MMR)	BV711	C068C2	1:200	BioLegend	141727
VCAM-1/CD106	AF488	MVCAM.A	1:100	BioLegend	105710
CD9	Biotin	MZ3	1:400	BioLegend	124804
CD16/32	-	93	1:100	BioLegend	101302

Secondary Antibody					
Antigen	**Conjugate**	**Clone**	**Dilution**	**Source**	**Catalogue#**
Streptavidin	BV785	-	1:200	BioLegend	405249

Table2: List of antibodies for investigating adipogenic precursor cells in Flow cytometer:

Adipogenic precursor heterogeneity panel					
Primary antibodies					
Antigen	**Conjugate**	**Clone**	**Dilution**	**Source**	**Catalogue#**
CD55 (DAF)	APC	RIKO-3	1:800	BioLegend	131812
VAP1	AF700	7-88	1:800	Abcam	ab81673
SCA-1	BV510	D7	1:200	BioLegend	108129
CD29(Intrgein ß-1)	PerCp Cy5.5-efluor 710	HMb1-1	1:200	ThermoFisher	46-0291-82
CD26 (DPP4)	PE/Cy7	H194-112	1:400	BioLegend	137810
CD54 (ICAM)	APC/fire™ 750	YN1/1.7.4	1:800	BioLegend	116126
CD142	PE	-	1:100	Sino Biological	50413-RP01-100
CD45	Biotin	30-F11	1:200	BioLegend	103104
CD31	Biotin	MEC13.3	1:200	BioLegend	102504
TER119-Erythroid cells	Biotin	TER119	1:200	BioLegend	116204

Secondary Antibody					
Antigen	**Conjugate**	**Clone**	**Dilution**	**Source**	**Catalogue#**
Streptavidin	BV785	-	1:200	BioLegend	405249

Table3: List of antibodies for spatiotemporal localization of macrophage subsets in PhenoCycler:

Multiplex Immunohistochemistry panel for macrophage adipocyte spatiotemporal relationship					
Primary antibodies, Barcodes and Receptors for Phenocyler(CODEX)					
Target	**Reactivity**	**Clone**	**Sample type**	**Barcode**	**Receptors**
CD11c	Mouse	N418	FFPE	BX030	Cy5
CD140a(PDGFRa)	Mouse	APA5	FFPE	BX004	AF488
CD31	Mouse	MEC13.3	FFPE	BX002	Atto550
Ly6C	Mouse	HK1.4	FFPE	*BX040*	AF488
Ly6G	Mouse	1A8	FFPE	BX024	Cy5
MHCII	Mouse	M5/114.15.2	FFPE	BX014	Atto550
UCP1	Mouse	EPR20381	FFPE	*BX031*	AF750
Perilipin	Mouse	Polyclonal	FFPE	*BX023*	Atto550
CD45	Mouse	I3/2.3	FFPE	*BX019*	AF488
IBA1	Mouse	Polyclonal	FFPE	*BX017*	Atto550
Tim4	Mouse	RMT4-54	FFPE	BX007	AF488
F4/80	Mouse	BM8	FFPE	BX006	Cy5

Table4: List of chemicals and solutions:

Chemicals and solutions		
Item	**Vendor**	**Catalogue#**
Bovine Serum Albumin (BSA)	Sigma-Aldrich	A9647-500G
EDTA (Ethylenediaminetetraacetic acid)	Sigma-Aldrich	E9884-500G
DPBS (10x) without Ca^{++}, Mg^{++}	PAN-Biotech	P04-53500
Rat serum	Bio-Rad	C13SD
DRAQ7	BioLegend	424001
Dream Taq™-Green PCR Mastermix	Thermo Fisher Scientific	K1082
Sodium hydroxide	Merck	1.06498.1000
TRIS-Hydrochloride	AppliChem Panreac	50012105
DNA ladder	New England Biolabs	N3231S
16% Formaldehyde , methanol free	Thermo Fisher Scientific	11586711
Propidium iodide	Thermo Fisher Scientific	BMS500PI
Collagenase from Clostridium histolyticum, Type II	Sigma -aldrich	C6885-1G
RPE Conjugation Kit	Biorad	LNK02
Alexa Fluor® 700 Conjugation Kit (Fast) – Lightning-Link®	Abcam	ab269824
Guava ICF	Luminex	4200-0140
Calcium chloride(Hydrated)	Merck	2382

Table 5. List of main buffers:

Buffers	
Buffer name	**Components**
1XPhosphate buffered saline (PBS)	10xPBS diluted with Bides water (1:10)
WAT Buffer	BSA 0.5% diluted in 1x PBS
FACS Buffer	BSA 0.5% & EDTA 2mM diluted in 1x PBS

Table 6. List of non-reagent materials:

Non-reagent plastic and other materials		
Item	**Vendor**	
Weighing boats	VWR	611-0093P
96 well plate	Fischer Scientific	15227905
70 µm and 100µm strainers	VWR	732-2758, 59
50 ml falcon	VWR	734-0448

15 ml falcon	VWR	734-0451
10 ml pipette	VWR	KAVA632434116723
1.5 ml eppendorf tubes	Eppendorf	0030125150
2 ml eppendrof tube	Fischer Scientific	10038760
Insulin syringe	BD	11575

Table 7. List of main equipment:

Equipment used for the project		
Equipment	**Manufacturer**	**Description**
Accu Check Aviva	Roche	Glucometer
FACSymphony A5	Becton, Dickinson Biosciences	Flow cytometer
Guava easyCyte	Luminex	Flow cytometer
5810R Centrifuge	Eppendorf	Centrifuge
AXIO Lab.A1	Zeiss	Microscope
Zeiss Axioscan Z.1	Zeiss	Slide scanner
Analysis computer(8 core processor)	Zeiss	Computer
Brunswick innova	Eppendorf	Incubator-shaker

3.2. Building maternal obesity model using mice

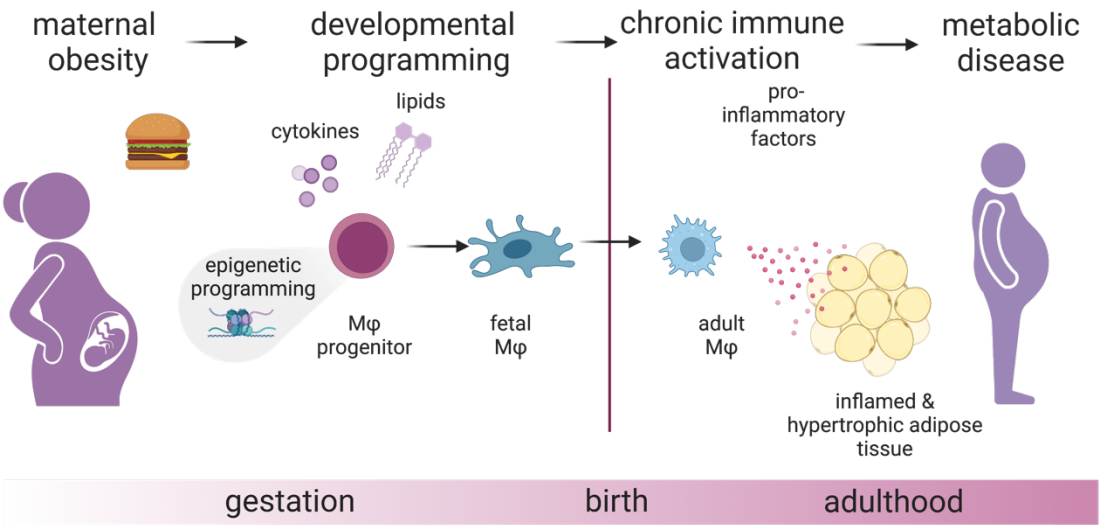

Fig9. Maternal obesity model

In the diet induced maternal obesity model, the mother had a high fat diet before and during pregnancy and the macrophages underwent developmental programming in the fetal stage. So, reprogrammed macrophage in the fetus obtains a chronic immune activated status facilitating a chronic low-grade inflammation in AT. Also, the reprogrammed resident-

macrophages facilitate adipose tissue hypertrophy paving the way for hypoxia and the interaction recruits more macrophage from the system to make a vicious cycle. Mouse model was used to build a close to real-life scenario in the lab, as mouse has similar distribution of fat depots as humans, as well as a well-established model for studying human pathology.

3.2.1 Mouse lines

C57BL/6JRccHsd mice

Our initial experiment involved building the maternal obesity model using C57BL/6JRccHsd mice. These mice were obtained from Envigo GmbH. All mice were maintained and bred in the animal facility in Specific Pathogen Free (SPF) area, LIMES-GRC, LIMES institute, Bonn. The mice had free access to food (Altromin Rod 16A or 18A) and autoclaved water. Female mice were weaned at 3 weeks of age and transferred to the Tierversuche Verstehen Room (TVR) and then treated with special diet. The special diet consists of 8 weeks of either control (CD: 13kJ% fat, 11%Sucrose) or high fat diet (HFD: 60kJ% fat (Lard)). Then they were mated overnight with C57BL/6JRccHsd male mice on a control diet. Breeding always took place in a male´s cage, and possible mating was investigated through plug-checking the next day (between 8:00 am and 9:00 am). Upon observation of a plug, the day of vaginal plug formation was estimated as E0.5. Pregnant mice were separated and after birth half of the HFD mom's pups were cross fostered with a lactating CD mom. At an age of 2 weeks after birth, sex determination and ear punches for marking were done. After

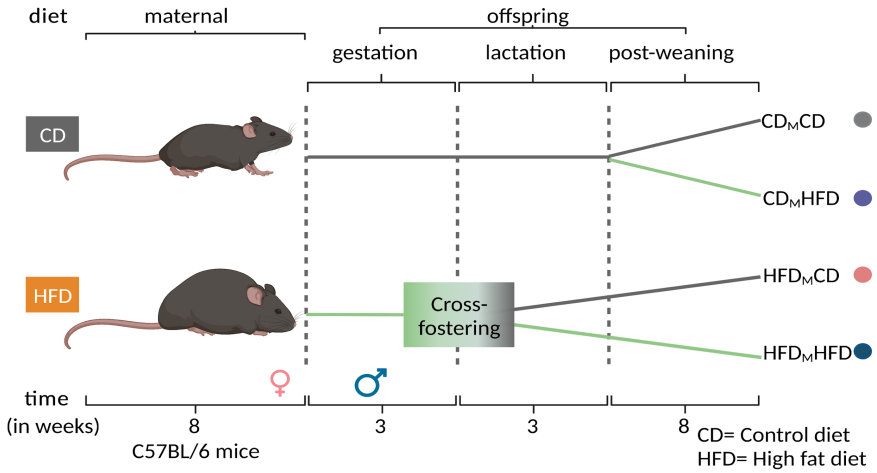

Fig10: Schematic showing maternal obesity model in C57BL/6JRccHsd mice.

weaning of the pups they were housed in separate cages. Male pups were fed with CD or HFD for 8 weeks and were subjected to sacrifice for organ harvesting at 11 weeks of age. Depending on the dams' and pups' diet, four groups were obtained:

CDmCD (CDm = maternal control diet , pup's control diet) ,
CDmHFD (CDm = maternal control diet , pup's high fat diet),
HFDmCD (HFDm = maternal high fat diet , pup's control diet)
HFDmHFD (HFDm = maternal high-fat diet , pup's high-fat diet).

HIF-1α conditional KO mice

Similar to C57BL/6 mice, the HIF-1α mice were also kept in SPF and bred to generate female and male breeders. At 3 weeks of age, females were transferred to the TVR. They were fed with either CD or HFD for 8 weeks. Afterwards, they were mated overnight with a $LysM^{Cre/+}Hif1\alpha^{flox/flox}$ male mice and plug checking was done in next morning. Upon observation of a plug, the day of vaginal plug formation was estimated as E0.5. For few mice, if plug-check was negative, females were checked for body weight. If there was no change of body weight, they were kept for one more night for mating. Usually gestation was observed for 18-20 days, a pregnant mouse was separated by second week of gestation to a clean new cage and after birth, number of pups were noted. That is how either wild type or conditional knockout offspring were generated. The pups were cross fostered in a similar manner described earlier. Sex determination and marking with ear punches were performed in 2 weeks of age. At an age of 3 weeks, weaned mice were separated by sex, and housed in separate cages. Male pups underwent either CD or HFD and now depending maternal and pup's diet and genotype, there were 8 different group :

1.CDmCD (CDm = maternal control diet, CD= pup's control diet), $LysM^{Cre/+}Hif1\alpha^{flox/flox}$
2.CDmCD (CDm = maternal control diet,CD= pup's control diet), $LysM^{+/+}Hif1\alpha^{flox/flox}$
3.CDmHFD (CDm = maternal control diet, HFD= pup's high fat diet), $LysM^{Cre/+}Hif1\alpha^{flox/flox}$
4.CDmHFD (CDm = maternal control diet, HFD= pup's high fat diet), $LysM^{+/+}Hif1\alpha^{flox/flox}$
5.HFDmCD (HFDm = maternal high fat diet,CD= pup's control diet), $LysM^{Cre/+}Hif1\alpha^{flox/flox}$
6.HFDmCD (HFDm = maternal high fat diet, CD=pup's control diet), $LysM^{+/+}Hif1\alpha^{flox/flox}$
7.HFDmHFD (HFDm = maternal high-fat diet, HFD= pup's high fat diet) $LysM^{Cre/+}Hif1\alpha^{flox/flox}$
8.HFDmHFD (HFDm = maternal high-fat diet, HFD=pup's high fat diet) $LysM^{+/+}Hif1\alpha^{flox/fl}$

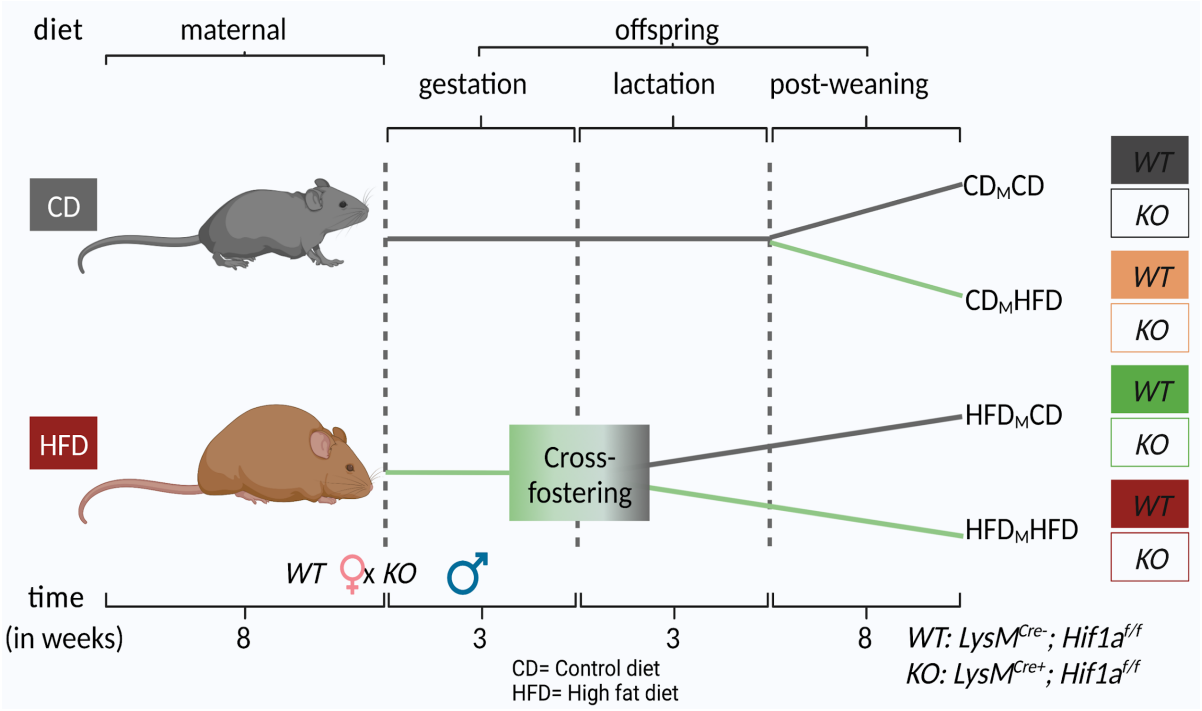

Fig11: Schematic showing maternal obesity model in HIF1α mice.

MYD88 conditional KO mice

MYD88 mice was generate in a similar manner of HIF1α mice. Post 8 weeks diet, they were mated with a RANK$^{Cre/+}$MYD88$^{flox/flox}$ male mice to generate either wild type or conditional knockout offspring. The pups were cross fostered in a similar manner. After weaning at 3 weeks, pups underwent either CD or HFD and similar to Hif1α mice and there were 8 different group:

1.CDmCD (CDm = maternal control diet ,CD= pup's control diet) , Rank$^{Cre/+}$MYD88$^{flox/flox}$
2.CDmCD (CDm = maternal control diet ,CD= pup's control diet) , Rank$^{+/+}$MYD88$^{flox/flox}$
3. CDmHFD (CDm = maternal control diet,HFD=pup's high fat diet), Rank$^{Cre/+}$MYD88$^{flox/flox}$
4. CDmHFD (CDm = maternal control diet, HFD=pup's high fat diet), Rank$^{+/+}$MYD88$^{flox/flox}$
5. HFDmCD (HFDm = maternal high fat diet ,CD= pup's control diet), Rank$^{Cre/+}$MYD88$^{flox/flox}$ 6.
6.HFDmCD (HFDm = maternal high fat diet ,CD= pup's control diet), Rank$^{+/+}$MYD88$^{flox/flox}$

7.HFDmHFD (HFDm=maternal high-fat diet,HFD=pup's high fat diet), Rank$^{Cre/+}$MYD88$^{flox/flox}$

8.HFDmHFD (HFDm=maternal high-fat diet,HFD=pup's high fat diet), Rank$^{+/+}$MYD88$^{flox/flox}$

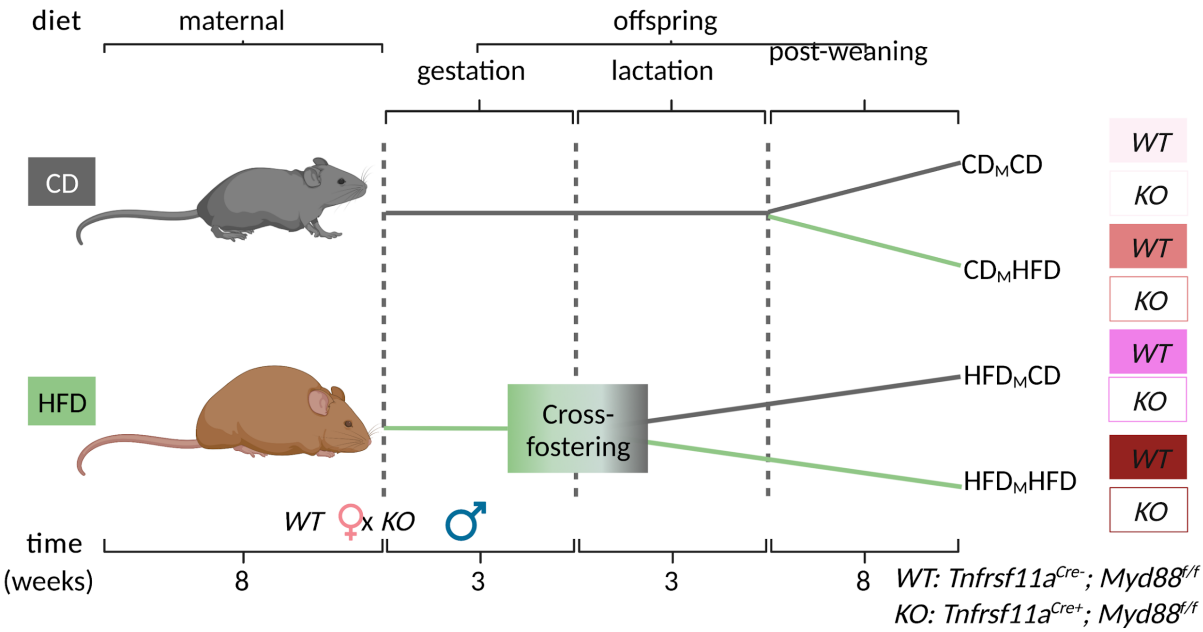

Fig12: Schematic showing maternal obesity model in MYD88 mice.

For all mouse models, going forward, the CDmCD pups would be referred as control pups, HFDmCD pups would be referred as maternal obese pups and HFDmHFD & CDmHFD both would be referred as obese pups throughout this dissertation for ease of discussion.

Table 8. Transgenic mouse lines and references:

Mouse line	Background	Designated international nomenclature	Generated by	References	MGI
HIF-1α	C57BL/6J	B6.129-*Hif1α*^{tm3Rsjo}/J	Randall Johnson	Ryan HE et al 2000 (123)	MGI:106918
LysM^{Cre}	C57BL/6J	B6.129P2-*Lyz2*$^{tm1(cre)Ifo}$/J	Irmgard Foerster	Clausen BE et al 1999 (124)	MGI:1934631
Rank^{Cre};	C57BL/6J	Tnfrsf11a$^{tm1(EGFP/Cre)Ykob}$	Y. Kobayashi	Maeda et al. 2012 (126)	MGI:108005
MyD88	C57BL/6J	B6.129P2(SJL)-Myd88$^{tm1.1Defr}$ /J	AnthonyL. DeFranco,	Hou.B et al. 2008 (125)	MGI:5316980

3.2.2. Genotyping

A small part of adult mouse tissue (ear tag or tail) used for genotyping. It was dissolved in 200µl of 50 mM NaOH for 20-30 min at 95°C. To this, 20µl of 1M TRIS HCl (pH of 8) was added. Later, 1µl of supernatant was taken and added to 0.5µl of each of the forward and reverse primers, 5µl DreamTaq ™ Green PCR Master-Mix and rest of the volume of H_2O to make a total volume = 10µl. After the PCR program ran, samples were applied to a 1.5% agarose gel in 1x TBE buffer and separated by electrophoresis at 120V for 30 min. The DNA was stained with Sybr safe/green and visualized by UV light.

Table 9: List of Primers for genotyping:

Gene	Primer:	Sequence (5'—3')
LysM ^{Cre}	Altern. Cre	CTG TCA CTT GGT CGT GGC AG
	MLys1- Common (oIMR3067)	CTT GGG CTG CCA GAA TTT CTC
	MLys2-Wild type(oIMR3068)	TTA CAG TCG GCC AGG CTG AC
Rank^{Cre}	RANK- Cre_For	TGA AGG GTG ACA TCA TCG TGG T
	RANK- Cre_mut_Rev	ACT TCT CCA TGG TAG CCT CC
	RANK- Cre_wt_Rev	TAT GGG GGT GGG GTG ATA C
HIF-1$\alpha^{f/f}$	HIF-1α_Forward	TCG ATG TGT ATG GGT GTT TTG
	HIF-1α_Reverse	GAA AAC TGT CTG TAA CTT CAT TTC C
	HIF_forward_old	gCA gTT Aag AgC ACT AgT Tg
	HIF_reverese_old	ggA gCT ATC TCT CTA gAC C
Myd88$^{f/f}$	MYD88_mutant_For	CCA CCC TTG ATG ACC CCC TA
	MYD88_wt_For	GTT GTG TGT GTC CGA CCG T
	MYD88_Reverse	GTC AGA AAC AAC CAC CAC CAT GC

Table 10:PCR program for Genotyping:

Steps	***Temparature***	***Time***
Initial denaturation	95°C	3 min
Denaturation	95°C	30sec
Annealing	60°C	30sec
Elongation	72°C	30sec
Extension	72°C	5 min

Denaturation, primer annealing and elongation (steps 2-4) are to be repeated for 34 cycles.

Exception: For LysM^{Cre} and Rank^{Cre}, initial denaturation is set for 30 sec instead of 3 min and annealing is at 55 °C and 51 °C respectively. For both, the elongation is run for 68°C ,60 sec and extension is at 68°C, 5 min.

3.2.3. Animal Housing

Mice were group-housed with one to five mice per individually ventilated cages (IVCs, TECNIPLAST) with free access to autoclaved tap water and food .The mice were kept under SPF conditions. Later the prospective mothers were transferred to the TVR for treatment with special diets. The light/dark cycle was 12/12 h and temperature was constantly kept at 21°C with 55% relative humidity. All animal studies were performed according to German animal welfare laws. Experiments were performed according to institutional animal welfare guidelines (LIMES-GRC) and were previously approved by by the Landesamt fr Natur, Umwelt und Verbraucherschutz (LANUV) Nordrhein-Westfalen, Germany, number of permision : Lizenz ID “[S] 2019.A146- Entwicklung Immunsystem bei Diäten.

3.3. Insulin and glucose tolerance tests (ITT & GTT)

The glucose tolerance test measures the clearance of an intraperitoneally(IP) injected glucose load from the body. It is used to detect disturbances in glucose metabolism that can be linked to human conditions such as diabetes or metabolic syndrome. Insulin tolerance test measures the sensitivity of insulin-responsive tissues in the rodent. This is determined by measurement of glucose remaining in the circulation over time after a bolus IP insulin injection. Insulin and glucose tolerance tests were carried out according to the guideline of International Mouse Phenotyping Consortium. Initially, the tests were carried on prospective mothers and mothers with abnormal GTT and ITT were subjected to further diet and mating. Later, the male offspring were subjected to the tests at 9th-10th weeks of their age as only these mice were used for further experiments. Quality Control of the glucometer was performed routinely as outlined in the vendor manual.

3.3.1 Materials

1. CD -LF Control diet ‘E15748-047’ (250g/cage/week - calculated with 5 mice/cage)
2. HFD - DIO HF diet Lard ‘E15742-347’ (120g/cage/week - calculated with 5 mice/cage)

3. 9-10th weeks old male HIF1-α mice
4. Animal protocol
5. Blood sugar measurment machine + sticks :Accu Check Aviva (# 06114963)
6. Fine and sharp scissor
7. Actrapid Penfill 100 IU/ml Insulin human
8. 20% Glucose stock Solution
9. Octenisept Wound-Desinfection spray
10. Insulin Syringe VWR #613-4897
11. Sterile 1-use NaCl 0.9% in 5ml containers

3.3.2. Glucose Tolerance Test

The mice were fasted for 6 hours drinking water ad libitum by putting them in a new clean cage without food or feces. Mice body weights were measured. The desired dose of glucose is 2mg of glucose/g of mouse body mass administered by intraperitoneal (IP) injection. The amount of glucose was calculated using formula: 10 x body weight (g) from 20% stock solution. The mice were transferred to experiment room within the mouse facility(TV-OP)one hour before the measurement to acclimate. To perform the first measurement , a small cut was made on the mouse tail , the first drop was discarded. A small drop of blood (5-10µl) was placed on the test strip of the blood glucometer. This was recorded as the baseline glucose level (t = 0). The glucose was injected IP followed by blood glucose levels measured at 15, 30, 60. and 120 minutes (t = 15, t = 30, t= 60 and t = 120). The insulin tolerance tests were performed 3-7 days after the GTT to provide the mice adequate time to recover.

3.3.3. Insulin Tolerance Test

The mice were fasted 6 hours, drinking water ad libitum. Mice body weight were measured and the exact amount of insulin to inject 0.75 IU of insulin/kg of mouse bodyweight were calculated. Insulin in saline solution (sterile NaCl 0.9%) was used for injection. The stock solution was prepared by diluting 100 IU human insulin (Actrapid) in sterile saline 1:400 (9,975mL of saline and 25 µL of 100 IU Insulin). The solution was mixed by vortexing and sterilized by passing it through a 0.2-µm filter into a sterile 15-mL Falcon tube. The insulin volume could be calculated by the formula : 3 x body weight (g). For HFD mice, including having > 40gm body weight, the dose could be increased upto 2unit per kg. To perform the

first measurement, a small cut is made on the mouse tail or the scab wound from GTT were displaced. A small drop of blood (10 µl) is placed on the test strip of the blood glucose meter. This is the baseline glucose level (t = 0). The required amount of insulin is injected and a timer is started for 15 min. Subsequently blood glucose levels were measured at 15, 30, 60 and 120 minutes (t = 15, t = 30, t = 60 and t = 120). Data from mice with experimental hypoglycaemia were excluded.

3.4 Surgical procedure for organ harvesting

3.4.1 Surgical Procedure

The mice were weighed and according to the body mass, anesthesia was prepared.To make balanced anesthesia, ac ombination of Ketamine and Xylazine were used (Ketamine - 100mg/Kg: Xylazine 20mg/kg in Sodium chloride (5:1:4)). The anesthesia were injected intraperitoneally. Usually by 8-10 minutes mice were anaesthetized , it was checked with toe pinch. Mouse abdominal surface was cleaned with ethanol and opened along linea alba. Diaphragm was cut to expose the heart and blood was collected from the heart . From the total amount, 200µl was taken in a 15 ml falcon, which was later filled with a 3 ml RBC lysis buffer for flow cytometry. Rest of the blood was put into the serum tube (500µl) and lysis was blocked and was kept frozen for metabolomics. Heart perfusion was performed to get rid of red blood cells. Different fat depots were identified in the mouse. Gonadal WAT, core of BAT and BAT-RIM WAT was collected.

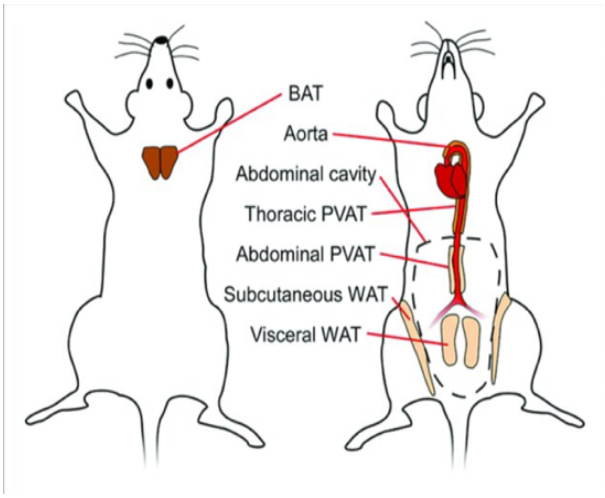

Fig13: Simplified illustration off different adipose tissue depots in mice. BAT, brown adipose tissue; WAT, white adipose tissue; PVAT, perivascular adipose tissue. (Ref Hildebrand et al 2018, Frontiers in Physiology)

3.5. Methods for Flow cytometry

3.5.1 Isolation of stromal vascular fraction (SVF) from WAT & BAT

Flow cytometry was used to analyze ATMs and APC population in the stromal vascular fragment at the single cell level.

- Adipose tissues were weighted (~0.3 g) and collected in 2ml cold PBS with 0.5% BSA (WAT buffer), in weighing boats. The weighing boats were preferred over 6 well plates to make transfer and washing easier due to the stickiness of AT.
- AT were cut into small pieces using Fine Scissors – Tough Cut" (F.S.T Item No. 14058-9) and transferred in 50ml falcon tubes. Boats were washed with 1ml PBS to collect the remaining tissue to the corresponding 50 ml falcon tubes.
- Digestion mix was prepared using Collagenase II (sigma,#C6885-1g) mixed with 4mg/mL in PBS with 0.5% BSA and $CaCl_2$ 5mmol/l. 3 mL of Collagenase II mix per tube were added (final concentration for the collagenase 2 mg/mL
- The mix was incubated for 20 min in the incubator-shaker under agitation 200 rpm at 37°C
- 10 mL ice cold PBS (0.5% BSA) was added per tube and pipetted up and down several times with the 10ml pipette and transferred to a new falcon tube through a 100 µm strainer.
- The tubes were spun for 10 min at 500*g*, supernatants were removed and the pellets were resuspended in 50µl of Fc-Block (CD16-CD32) (1/100) and rat serum (2%) in FACS buffer and incubated for 10 minutes. The total volume was brought to 200 µl by adding FACS buffer. A 10 µL aliquot of the cell suspension was taken for cell counting in Guava.
- Rest was plated into 96-well plate, centrifuged to get a pellet . 20µL of 1^{st} antibody mix was added and incubated 30min on ice. The 100 µL of FACS Buffer added and spun 5 min at 400g, plate flipped, resuspended cells in 20 µL of 2^{nd} Ab mix
- Again, the plate was incubated in ice for 30 min, then 100 µl of FACS buffer was added to each and spun 5 min at 400g, plate flipped, pellet was resuspended in final volume of 100µl FACS buffer

3.5.2. Analysis of flow cytometry data for cell quantification

For detecting antigen expression by different macrophage populations, antibody mixes were freshly prepared on the day of experiment. The stained cells were resuspended in 100 µl of FACS buffer as described above and stained with Hoechst or DRAQ7 as live/dead staining. The final dilution of live/dead staining was 1:10000 for Hoechst or 1:1000 for DRAQ7. 20000-50000 CD45+ cells were recorded using FACSymphony™ A5 (BD Biosciences) cytometer for analysis of macrophage subsets. The recorded data is collected in .fcs format and analyzed by FlowJo™ v.10.8.1. software from Becton, Dickinson and Company. The population of interest was analyzed and the quantification of macrophage subsets was done using the following gating strategy to quantify different cell types (Fig14). The count of each cell type was recorded and plotted for quantification and using R programming language, the flow data was further analyzed for cellular clustering for unique macrophage subsets.

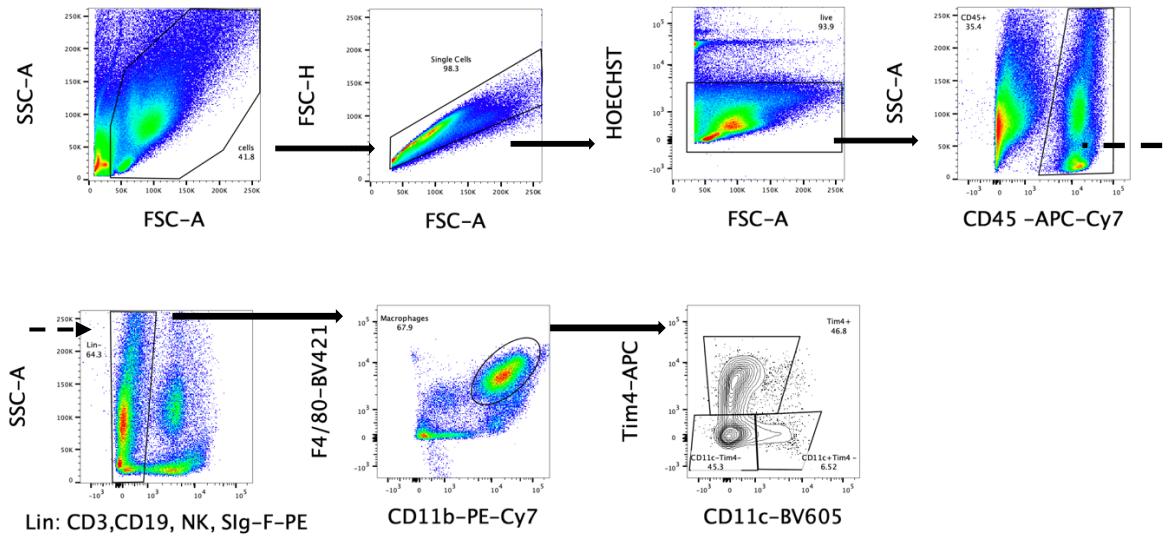

Fig14 : Gating strategy used for flow cytometry analysis of ATM subsets, (gWAT is represented here, the same gating strategy was used for BAT). Lin is CD3, CD19, NKp46, and Siglec F.

3.5.3 Analysis of flow-cytometry data for heterogeneity of macrophage subsets:

The $CD45^+$ cells were gated and downsampled using downsample plug-in (v.3.3.1) in the FlowJo software v.10.8.1 to reach a fixed cell number. The downsampled population was imported and

analyzed by R in RStudio 2022.02.1. The importing and processing of data was done using the CATALYST package (v. 1.18.1)[127] , which was installed through the Bioconductor package (v 3.14). Data visualization was done using the UMAP algorithm[128], and the clustering of data was done using FlowSOM[129] clustering and ConsensusClusterPlus metaclustering[130]. CATALYST package uses a simple wrapper to combine the FlowSOM and ConsensusClusterPlus clustering. Using FlowSOM, the wrapper first did high-resolution clustering and later on using ConsensusClusterPlus metaclustering, a lower resolution of clustering using the previous clusters were obtained. In the first step of the wrapper, the data was initially clustered into the multiplication of two dimensions: Xdim x Ydim, which would provide n groups. In the second step, the wrapper metaclustered the populations into a minimum of 2 through a maximum of k clusters. The resulted clusters were manually inspected for expression of different markers and clusters of interests were chosen and merged to form final clusters that would represent macrophage and their heterogeneity.

3.5.4 Isolation of adipogenic precursors (APCs)

For isolation of adipogenic precursors, the same procedure is followed except with different panel and different gating strategy (Fig15). 1-2.5 million total cells were needed to record for identifying all three APC subsets in AT described in figure 5A.

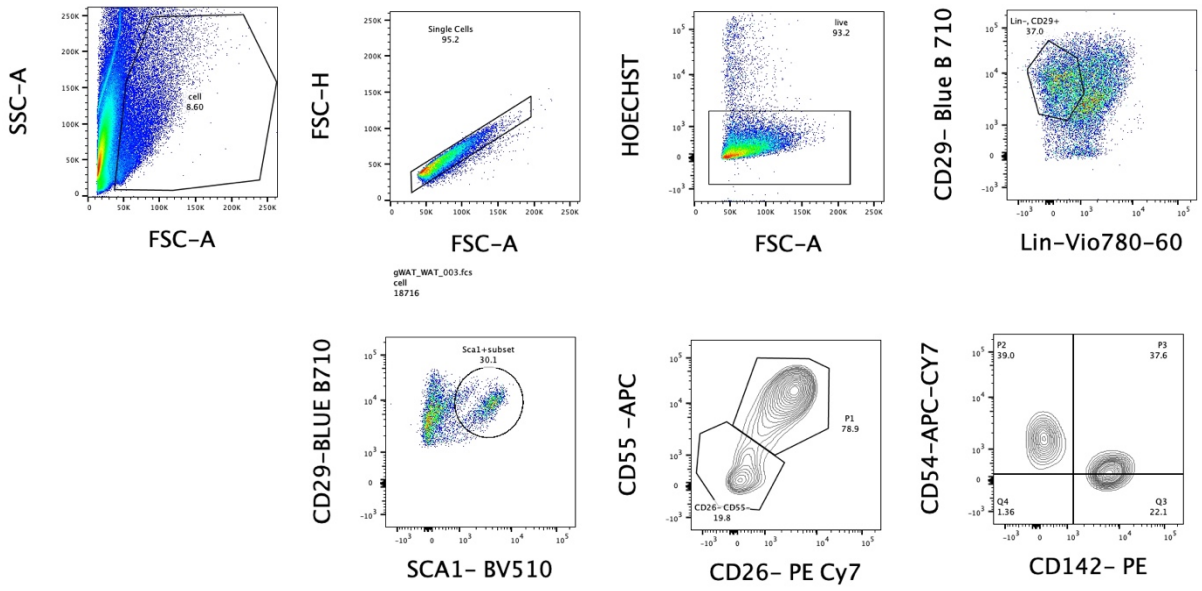

Fig15: Gating strategy used for flow analysis of APCs in gWAT

3.6 Cell counting by GUAVA

For cell counting in adipose tissue, a dilution of 1:100 was used. Propidium Iodide was added in a concentration of 1:100 or 1:200 to the diluted cells for live/ dead staining. In the GUAVA machine InCyte v3.1software was used to measure the cells. The "Worklist Editor" function was used for inputs of dilution factor, cell suspension volume, time and numbers to be recorded. Each well was named specifically for identifying the output later. AT specific organ-setting was used for counting and the analysis was saved from group stat.

3.7. Lipidomics

The lipidomic analysis was performed on gWAT of HIF-1α mice in collaboration with Dr Jelena Zurkovic, AG Thiele.

3.7.1. Materials

- Chloroform, Methanol, water, isopropanol (all MS Grade), internal standard mix.
- Hamilton syringes for IS.
- original Eppendorf tubes.
- glass bottles.
- All solvents were HPLC grade or LC-MS grade purchased from VWR International GmbH (Darmstadt, Germany) and Merck KGaA (Darmstadt, Germany).
- gonadal (visceral) white adipose tissue was collected from mice during organ harvesting and flash frozen in -80 degree. 2 mg (exact weight of each sample was determined) was further processed for lipidomic analysis

3.7.2: Procedure

- The internal standard mix was prepared. E.g.
  for 5 Samples: 2.1 ml methanol, 2.5 ml chloroform**,** 500 µl internal standard mix and 50µl of TAG_IS/sample
- Spray buffer was prepared: 16 ml isopropanol, 10 ml methanol, 1720 µl water, 280 µl 1 M NH4Ac in water

- AT was cut into small pieces (between 1 and 2mg!!) and final weight was noted.

- Quickly 1000 µl Extraction Mix was added and sonicated for 30 min in the bath sonicator and spun at 20000 g for 2 min
- 15 µl of the supernatant was transferred into new Eppi, 200 µl chloroform and 800 µl 1% acetic acid in water was added . It was shaken manually for 5 sec and spun for 2 min at 20000 g
- The entire lower phase (using a chloroform-rinsed yellow pipet tip) was transferred into a fresh Eppi and evaporated in the speed vac (45°C, 15 min) , avoiding over-drying.
- 1000 µl spray buffer was added and it was sonicated in the bath for 5 min . The samples were now ready for MS

3.7.3. Lipidomic analysis

All samples were separately infused at 10 µl/min into a Thermo Q Exactive Plus spectrometer equipped with the HESI II ion source for shotgun lipidomics. MS1 spectra (resolution 280 000) were recorded in 100 m/z windows from 250 to 1200 m/z (positive mode) followed by recording MS/MS spectra (resolution 70 000) by data independent acquisition in 1 m/z windows from 250 to 1200 (positive mode). Raw files were converted to .mzml files and imported into and analyzed by LipidXplorer software using custom mfql files to identify sample lipids and internal standards. For further data processing, absolute amounts were calculated using the internal standard intensities. After the analysis, .mzml files were subjected statistical analyses were conducted in the R environment (version 4.2)[131]. To ensure high-quality data, lipids with over 25 percent zero or missing values across samples were excluded from the analysis, resulting in the filtering of 31 percent of the lipids. The data were then log-transformed to reduce the effect of heteroscedasticity. By taking the logarithm of the data, the scale of the values is compressed, reducing the impact of extreme values and bringing the data closer to a normal distribution.Next, the data were normalized using the median normalization method, by which the median value of the lipids abundance measurements across all samples are being equalized. Median normalization has several advantages over other normalization methods. First, it is robust to outliers. Second, it does not require any assumptions about the distribution of the data, and third, median normalization does not change the shape of the data distribution, preserving any biological signal in the data. After data normalization, the remaining missing values were imputed using the KNN method from the R package imputeLCMD[132].

For the analysis of the lipid-classes, the abundances of individual lipids that correspond to the same lipid-class were combined, in order to estimate the overall abundance of that lipid-class. This was done using the Tukey's median polish method. Finally, the statistical test was performed using the R package limma[133]. To account for multiple testing, P-values were adjusted and false discovery rates (FDR) were calculated using the Benjamini-Hochberg method for each statistical contrast. For multivariate analysis (PCA), the FactoMineR package was used[134] and complex heatmaps codepackage in R was used to create the heatmaps[135] showing lipid class distribution in different conditions in HIF-1α mice.

3.8. Methods for pathological examination

3.8.1. Materials

- Mouse adipose tissue
- 4% PFA
- PBS
- 70% ethanol
- 15 ml falcons
- Scalpel and petri dish
- Pasteur pipette

3.8.2.Sample preparation

During surgical procedure a portion of gWAT and BAT were procured for histology without damaging the tissue integrity. It was kept 24 hours for fixation in the cold room in a rotator. After 24h in PFA 4% , the tissues were washed with PBS for 3 times and placed into a 15ml falcon tube, labelled with mouse number, genotype, experiment date. Then the tissues were put into 70% ethanol and submitted to the core facility. The tissue underwent serial steps of dehydration in ethanol and in xylene for clearing followed by embedding into paraffin to prepare the block. Then the section is cut in a Leica microtome and the slides are subjected to staining.

3.8.3. Hematoxylin/Eosin staining (H&E)

Reagents:

Mayer's Hematoxylin

2% Eosin

For H&E staining, first the paraffinized slides were deparaffinized by running in xylene and serial concentration of ethanol followed by water. The section is then subjected to Mayer's hematoxylin for 2.5 min followed by differentiation and bluing (3-5 min). Excess background stain was washed and then eosin was added for 5 min, rinsed and was subjected to ascending alcohol concentration, xylene and then was covesliped. The staining was performed in a batch in Leica ST5020 stainer.

3.9 Digital pathology application

The importance of adipocyte hypertrophy has been described in the earlier sections. To measure the size of adipocytes in homeostasis and metabolic syndrome, digital pathology was used. The slides are numbered and catalogued according to diet and genotype and scanned in Zeiss Axioscan Z1. The scanned slides are then stored and analyzed by a special algorithm.

3.9.1.Equipment specifications: ZEISS Axioscan.Z.1 slide scanner

Requirements :

- Standard microscopy slides (**76 x 26 mm**) with rectangular coverslips(**50 x 24 mm**) or: big microscopy slides (**76 x 52 mm**) with rectangular coverslips (**75 x 50 mm**)
- Coverslip thickness **0.17 mm** (high precision coverslips are recommended)
- Bottom of the microscopy slide has to be perfectly flat (e.g. free of any tape or label).
- No cracks in microscopy slides or coverslips.
- Coverslips must not protrude the microscopy slide.

Software: Zeiss Zen 2.x

3.9.3. scanning procedure

The Zeiss Axio scanner was used to scan the H&E stained slides in the microscope core facility. The scanner is accessed with Zen3.1 software. Slides were loaded to the scanner with the help of loading station, Slides' positions were determined by naming sheet which is

an excel sheet to identify the slide position in the scanner. First the preview scan was performed followed by identifying the correct tissues by tissue detection wizard. The regions of interest (ROI) was needed to be drawn manually for each slide due to absence of a specific shape for adipose tissue unlike some solid organs. After the detection, scanning was done by the machine.

3.9.3 storage

The scanned slides were stored in isi2 storage drive or the BTC cloud offered by the core facility.

3.9.4 Image analysis

The image analysis was done on scanned H&E stained slides to measure the adipocyte size. The (Fiji is just) ImageJ application was downloaded and the AdipoQ plugin developed by our collaborator Jan Hansen was installed in ImageJ. The software is opensource and can be find in Github: https://github.com/hansenjn/AdipoQ . The plugin has 2 parts , AdipoQ preparator and AdipoQ analyzer. First the scanned image from a slide was opened in (Fiji is just) ImageJ and one with the best resolution was selected for analysis from multiple resolution images. The image was then saved in .tiff format and AdipoQ_Preparator plugin version 0.0.1 was opened. Where ALL is written, SLIDESCANNER can be entered (Fig16) to select the largest pictures with the best resolution automatically if not already selected manually. The images were prepared by the software to give an AQP file which was inspected and corrected manually. Here all gross errors, such as holes in the tissue, blood vessels, areas of necrosis, part of nonadipocyte such as epididymis etc. were removed manually. An area with intact morphology of adipocytes with relevant histological features was selected as the region of intertest. This is saved as a new picture, e.g. AQPn. The AQPn image was analysed by AdipoQ Analyzer. Channel 1 was chosen, as this is segmented Channel for adipocyte size calculation. Additionally, “Quantify crown-like structures” was also selected. Analysed data was extracted in excel and plotted in GraphPad prism 9.5.1 for statistical analysis. The data was correlated with the morphological findings found by light microscopy and only the data confirmed by morphology was regarded for interpretation.

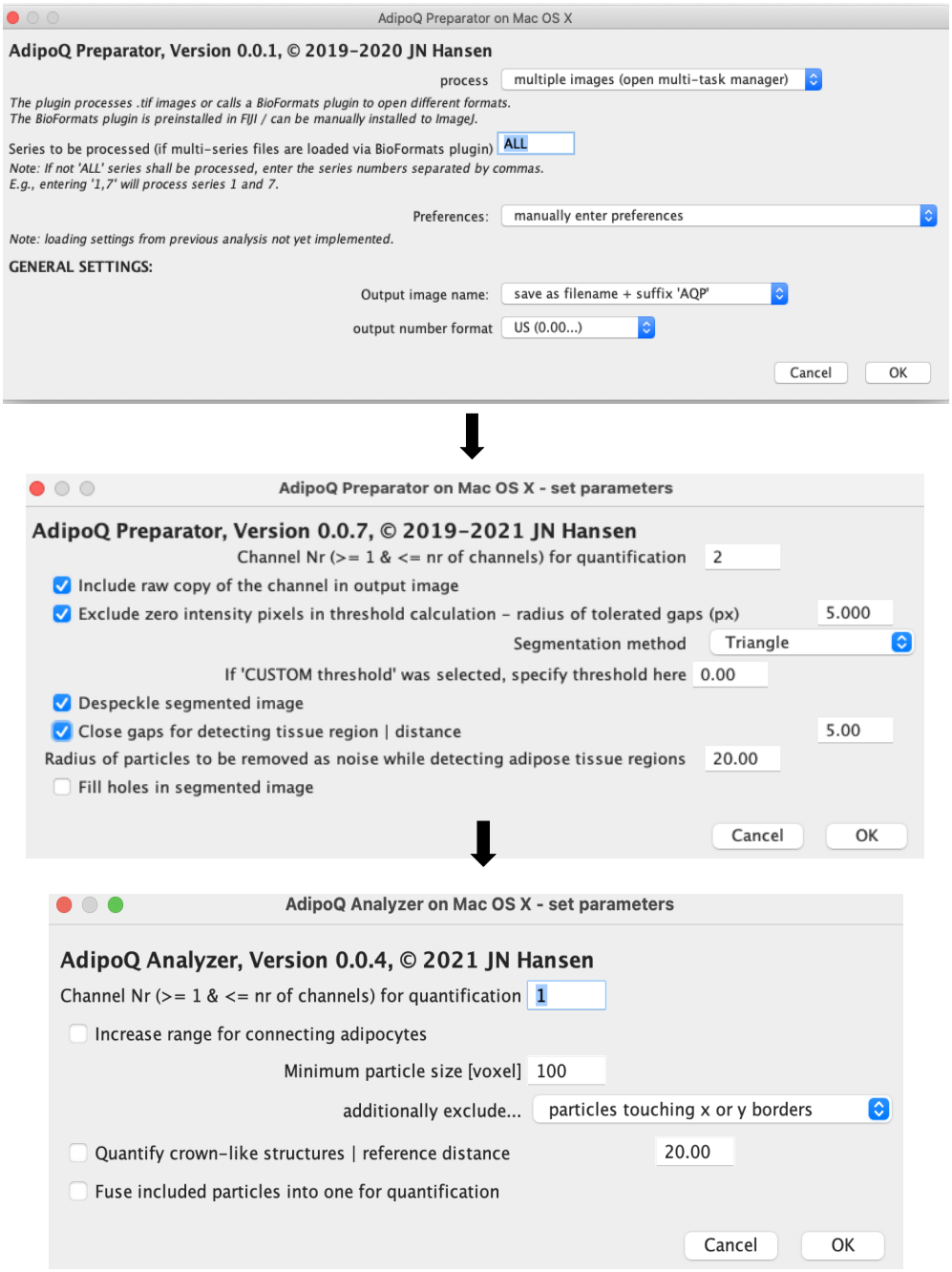

Fig16: Step by step analysis of adipocyte size in gWAT in different dietary conditions using AdipoQ plugin in ImageJ

3.10. Multiplexing by CODEX

Multiplexing by immunofluorescence was tried as an advanced technique to check spatiotemporal mapping in adipose tissue microenvironment. It was performed in collaboration with Dr David Bejarano from AG Schlitzer. The slide preparation was done and provided to the collaborator for the technical steps in the multiplex machine, so detailed description of the methods is not included here. A brief description of the method is as follows:

3.10.1 Special Reagents

Antibodies (barcodable in CODEX)
CODEX (Phenocycler) Barcode
Dye labelled reporter

3.10.2 Equipment

In CODEX (now PhenoCycler), Formalin- Fixed Paraffin-Embedded (FFPE) tissue can be used. The PhenoCycler antibodies are conjugated to distinct PhenoCycler Barcodes (BX000-unique oligonucleotides). There is a corresponding dye-labeled Reporter (RX000) conjugated to a Barcode to visualize the antibody. PhenoCycler screened antibodies are actually a list of antibody clones which can be successfully conjugated to PhenoCycler barcodes. The clones are commercially available from regular antibody vendors and can be conjugated by a conjugation kit. PhenoCycler barcodes and the associated conjugation protocol are available from Akoya Biosciences. For each imaging cycle, three PhenoCycler Reporters, each with a spectrally-distinct dye, are applied to the stained tissue to assay the corresponding Antibody Barcode. The barcode tagged antibody thus can be identified and imaged. The associated CODEX software suite can be used for analysis.

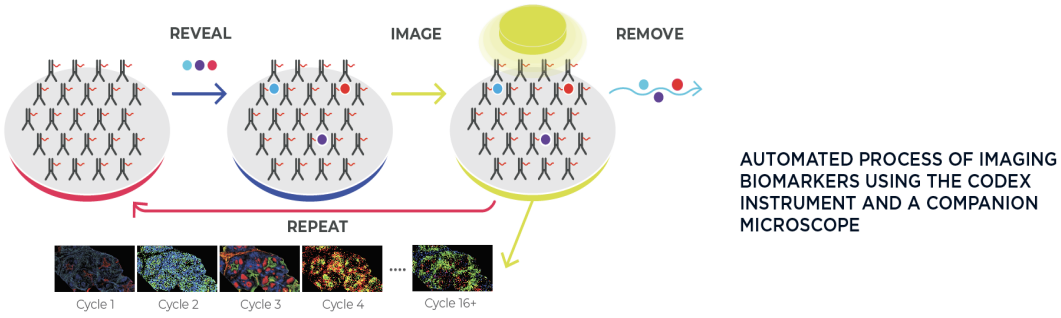

Fig17 : Principle of multiplex immunohistochemistry by Phenocycler (CODEX)

3.10.3 Procedure

The mice FFPE sections were cut in a desired thickness (10µm) and put in a specialized coverslip provided by the collaborators. A panel was prepared to get maximum information from a single tissue section. First the tissue section was stained with the whole antibody panel

where each antibody is conjugated with a barcode. In each cycle, 3 fluorescent reporters were added , they were bound to the complementary barcodes and upon excitation by light source they fluoresced. The software then directed the microscope to take pictures of the tissue, followed by removal of these 3 reporters. Then the cycle was repeated until the desired panel was completed. The resulting image could show the full panel for spatio-temporal relationship.

3.11. Statistical analysis methods

Statistical analysis was performed using Graph Pad Prism 9.5.1. As there were predominantly more than two sets of data, one-way ANOVA was used followed by Dunn–Šidák's multiple comparison tests and Dunnett's multiple comparison tests. Occasionally, when compared between two groups, *Unpaired T tes*t was used. The following format was used for P values

Symbol	Meaning
ns	$P > 0.05$
*	$P \leq 0.05$
**	$P \leq 0.01$
***	$P \leq 0.001$
****	$P \leq 0.0001$

N equals to the number of mice or adipocyte size or CLS-intensity or cell count on a case-by-case basis, depending on a particular experiment. Detailed statistical specifications are described in the corresponding figure-legend.

4. Results

4.1. Maternal obesity influences offspring's health in C57BL/6JRccHsd mice

To understand the effects of maternal obesity, unbiased expression of adipose tissue macrophages were evaluated. The results showed a definitive change in the profile of pups from dams with high fat diet induced obesity, compared to the control.

4.1.1. Body weight and organ weights in C57BL/6JRccHsd mice in different dietary groups

To evaluate the physiological changes, the body weights of the offspring were measured over time, precisely on each week during scoring to see weight gain over time. Final end body-weight was noted during sacrificing the animal and organ harvesting. During organ harvesting the individual whole organ weight was also measured for gWAT and BAT. The comparative analysis of body weight and whole organ weight (gWAT) among different dietary groups are shown in Fig 18(a b,& c). As initially brown adipose tissue was not collected, the n numbers are limited for the same. There is a significant increase of body weight for obese and maternal obese groups, which is also reflected in organ weight for gWAT. There is non-significant changes in BAT-organ weight in obese group compared to control.

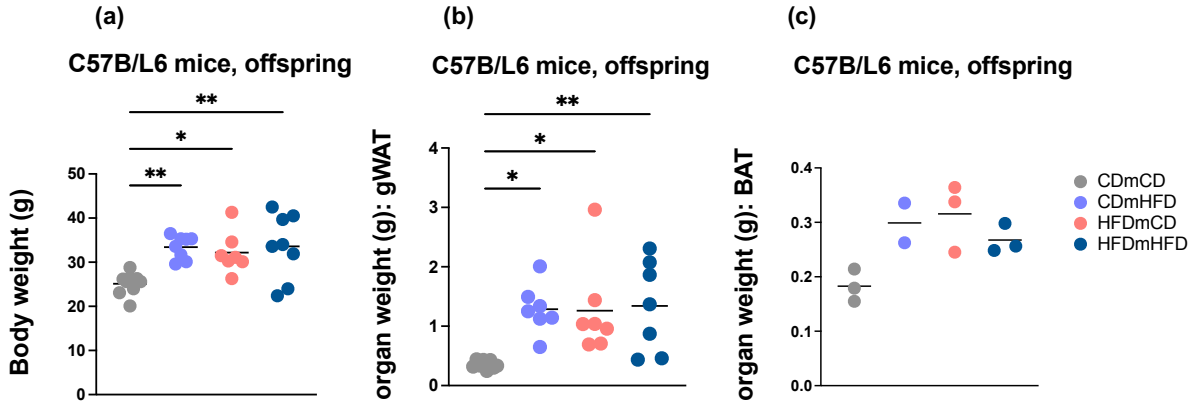

Fig18. Comparative analysis of body weights and organ weights in C57BL/6J animals from different dietary group. (a) Body weights, n=7 (b) whole organ weight of gWAT , n=7 & (c) whole organ weight of BAT , n=2-3 in control (grey) vs obese (purple & blue) and maternal obese groups (red). Each dot represents one mouse, p values obtained by one-way ANOVA with Sidak's multiple comparison unless otherwise indicated, * - p <0.05 , ** - p < 0.01, * - p< 0.001.**

4.1.2. Quantification of macrophage subsets in gWAT of C57BL/6 mice by flow cytometry

As we argue that, the developmental programming by maternal obesity leads to chronic immune activation in the fetal adipose microenvironment, favoring a proinflammatory condition, it is important to document the cellular landscape of chronic inflammation as a proof of our theory. Macrophage being the predominant cell type of chronic inflammation in general and AT inflammation in particular , the ATM landscape was delineated by flow cytometry analysis. The specific antigenic profile pinpoints the macrophage phenotypes associated with specific conditions like obese or maternal obese, compared to control. The flow cytometry result showed three different macrophage populations in the adipose tissue of WT animals based on our antigen panel. We found Tim4+ tissue resident macrophages and Tim4- recruited macrophages. Within recruited monocyte derived macrophages, two sub-populations were noted based on CD11c positivity: Tim4-CD11c- and Tim4-CD11c+ macrophage populations. While the Tim4+ recruited macrophage always maintain their niche in AT, , there was an influx of both subpopulations of Tim4- macrophages (Fig19) in AT of pups when either dams or pups or both were subjected to HFD.

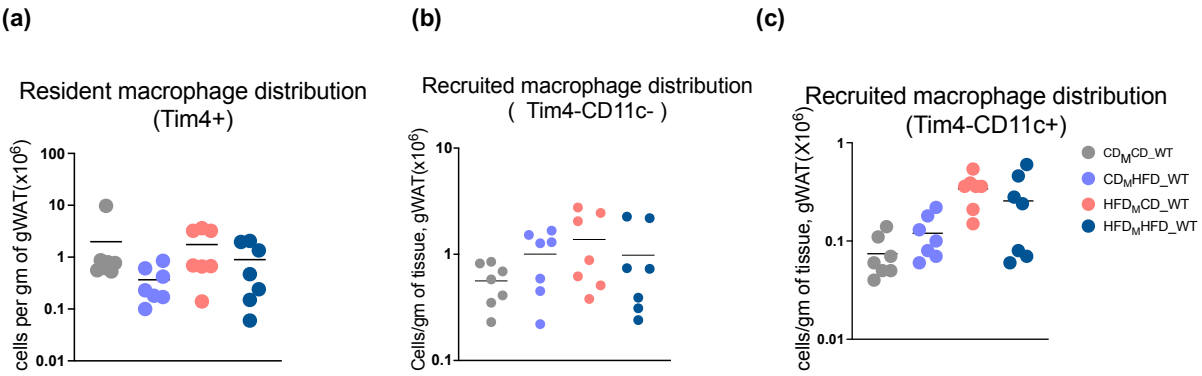

Fig19 : Quantification of flow cytometry data for resident and recruited macrophage populations in gWAT in 11 weeks old C57Bl/6J mice in different dietary groups. Mice were fed with 13 kJ% low sugar, high fiber control diet or 60 kJ% fat(Lard) diet, (n=7) . (a) Tim4+ Tissue resident ATMs (b) Tim4-CD11c- recruited ATMs (c)Tim4-CD11c+ recruited ATMs. Each dot represents one mouse, p values obtained by one-way ANOVA with Sidak's multiple comparison unless otherwise indicated, p value > 0.05 is nonsignificant.

4.1.3. Visualization of macrophage subsets in gWAT of C57BL/6 mice by UMAP analysis

As gating and compensation in flow cytometry can be user dependent, clustering analysis is a good way of unsupervised learning for identifying cellular subsets in flow cytometry data. Though originally used for genomic data analysis, clustering analysis has gained popularity for analysis of tissue as well. Unsupervised learning means the object classification is independent of any prior knowledge, so it can show the presence of unique gene or cellular subset in a multidimensional data. For this, dimension reduction technique UMAP (Uniform Manifold Approximation and Projection) was used, which helps to see high dimensional data in 2D or 3D format. Among different machine learning algorithm for clustering, UMAP is preferred because it is faster, and cluster the data points and their relative proximities. When analyzing the data from C57BL/6J mice, Initially the macrophage populations showed 10 different clusters based minor differential expression of MHCII and CD11c, with 2 nonsignificant clusters. After merging the clusters with very close antigenic profiles, ultimately 5 clusters (CL) were found: 2 Tim4- recruited and 3 Tim4+resident sub-set (Fig20)

Table 11: Macrophage subsets in C57BL/6JRccHsd mice

Phenotype name	Antigenic profile
RecMac 1	$Tim4^{-}$ $CD11c^{+}$ $MHCII^{+}$
RecMac 2	$Tim4^{-}$ $CD11c^{-}$ $MHCII^{+}$
ResMac 1	$Tim4^{+}$ $CD11c^{+}$ $MHCII^{-}$
ResMac 2	$Tim4^{+}$ $CD11c^{+}$ $MHCII^{+}$
ResMac 3	$Tim4^{+}$ $CD11c^{-}$ $MHCII^{+}$

UMAP in WT mice did not show any other significant subset. It also aligns with the flow cytometry quantification data of Tim4+ resident and Tim4- recruited macrophage subsets. The resident macrophages maintain their numbers in the metabolically challenged condition like maternal obesity with mild influx of $Tim4^{-}CD11c^{-}$ macrophages. This data suggest, there may be additional immune aberration for the complete metabolic shift from steady state to full-blown insulin resistance in maternal obese pups.

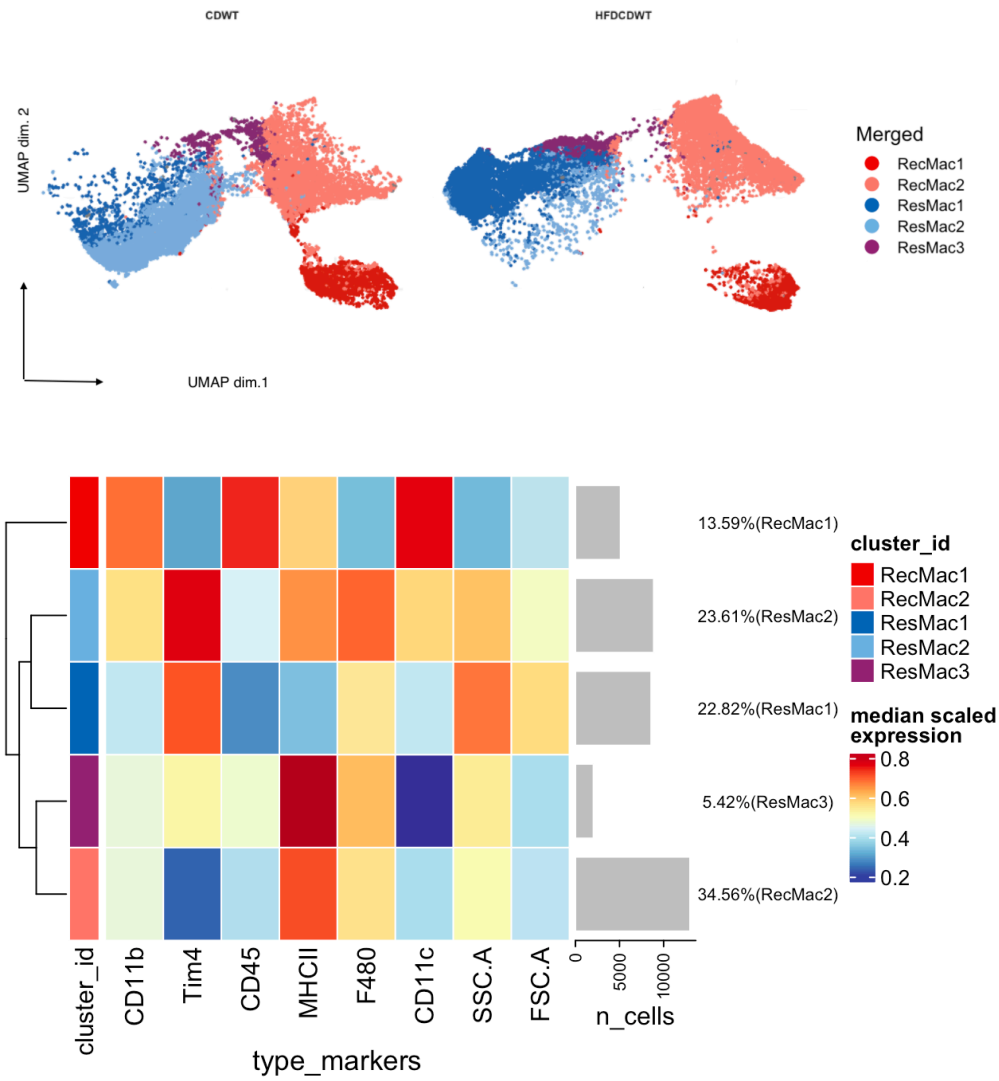

Fig20: Downstream analysis of the flow cytometry data : UMAP visualization of macrophage populations in control vs maternal obese C57BL/6RccHsd mice (after merging the initial clusters).

4.1.4. Morphological aberration in the gWAT of C57BL/6JRccHsd mice

To support the findings of flow cytometry, morphological changes in the different conditions were studied by light microscopy in the formalin fixed mice gWAT using hematoxylin and eosin (H&E) stains (Fig21). The obese adipocytes showed increase in size and the crown-like structures(CLS) were on the making in between adipocytes in hypoxic areas(arrowheads). The tissue microenvironment in adipose tissue shows significant change in metabolic pressure as depicted by changes in adipocyte sizes. As mentioned previously, the adipose tissue expands during metabolic challenge by hypertrophy in

unhealthy obesity. The adipocyte diameter and volume were also measured to conclude the measurement of adipose size. Areas of fibrosis and occasional inflammatory infiltrate were also noted in maternal obese group (Fig22), but no quantitative analysis on that was conducted.

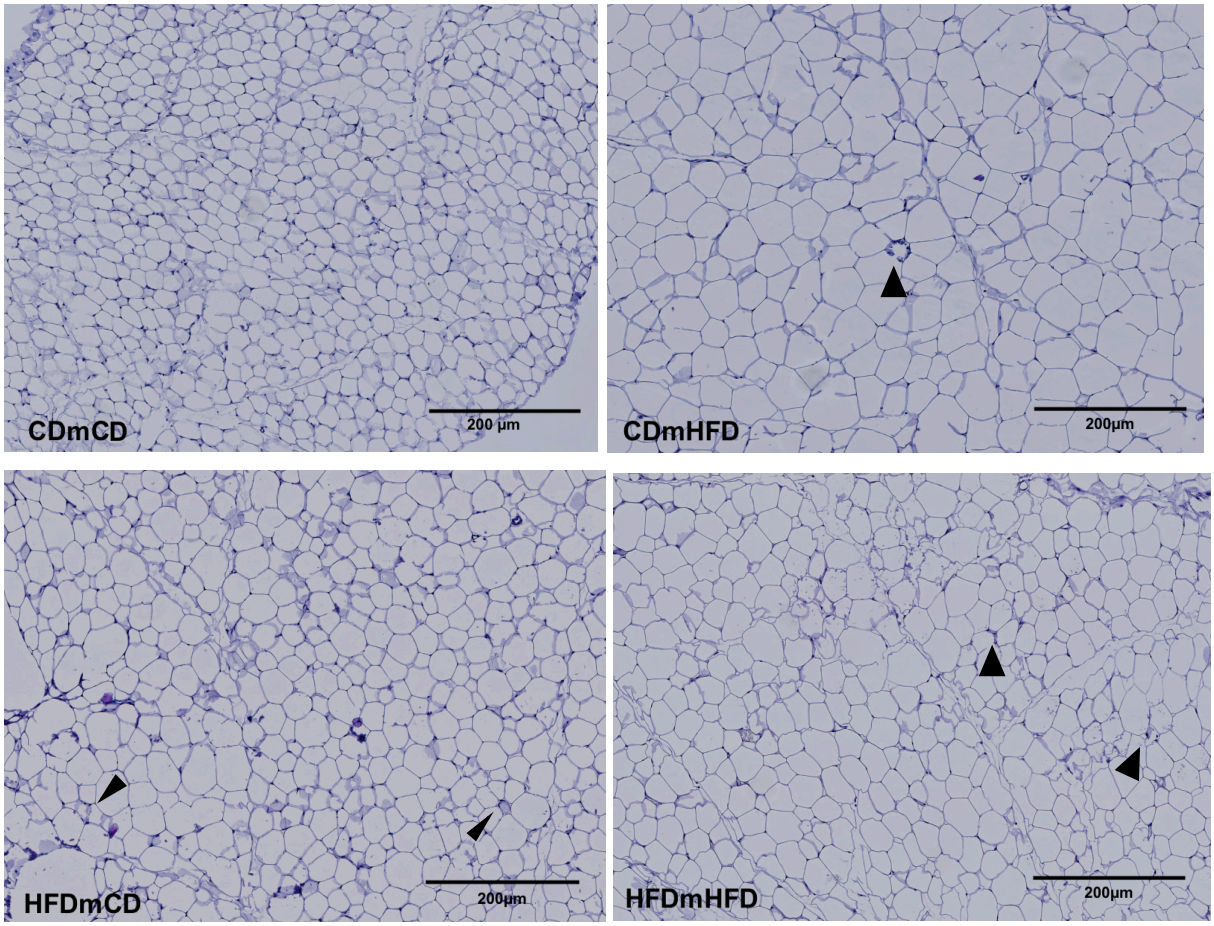

Fig21: H&E staining of paraffin embedded gWAT section from C57Bl/6J offspring mice from different dietary conditions (n=7). Conditions are mentioned over corresponding images.

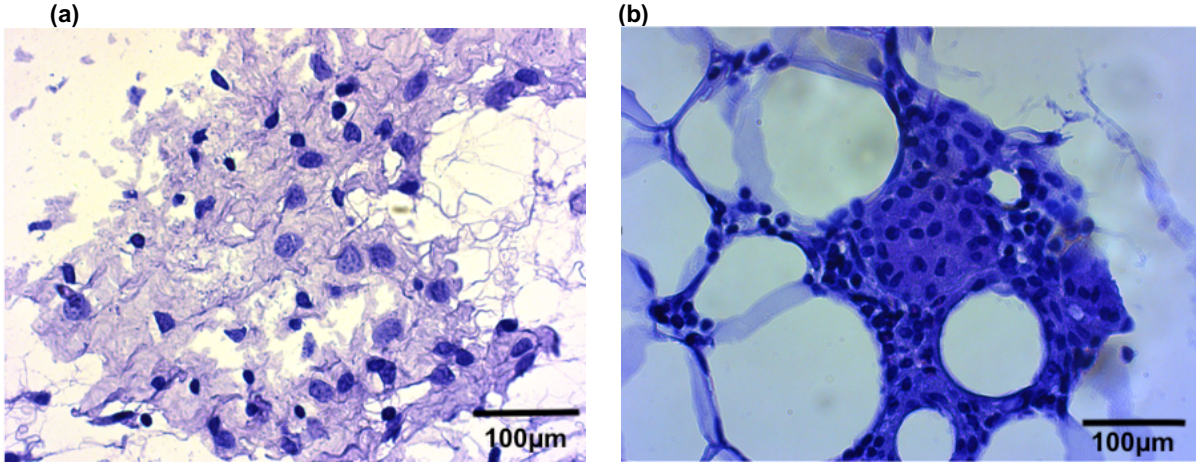

Fig22: Special morphological features noted in maternal obese Adipose tissue by H&E stain (a)Infiltration of macrophages in an apoptotic area. (b) inflammatory infiltrate in peri adipocytic area

Our results show metabolically challenged conditions like maternal obesity or offspring's own obesity causes the expansion of white adipocyte size compared to control. The AdipoQ plugin measures the area (in sq.meter) of adipocytes, however as recent papers suggest to use more than one parameter to describe adipocyte size, comparative study of diameter, volume and area of adipocyte were performed . (Fig23).

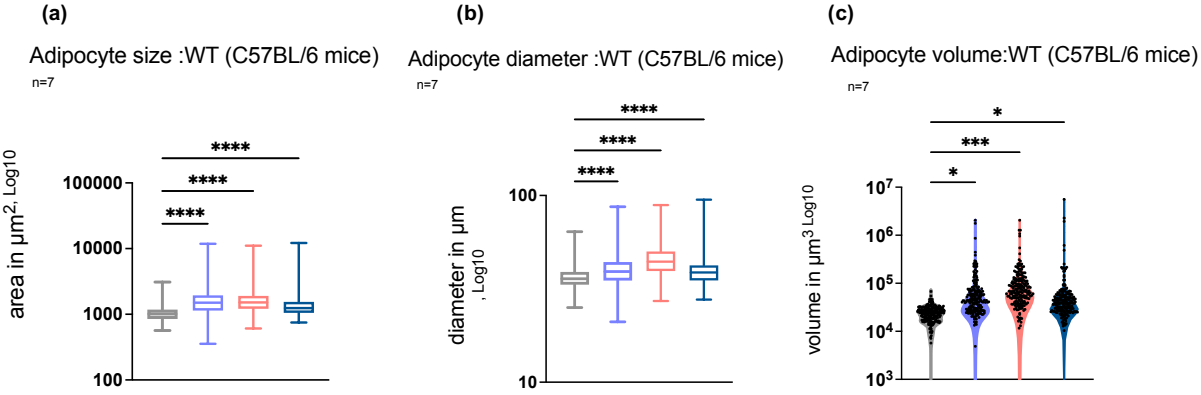

Fig23: Comparison of adipocyte size (area) (a) diameter (b) and volume (c) in different dietary groups in C57Bl/6J mice,(n=7). For quantification , 200 adipocytes from regions of interest are used for each individual tissue. p values obtained by one-way ANOVA with Dunnett's multiple comparison test unless otherwise indicated, * - p <0.05 , ** - p < 0.01, * - p< 0.001.**

4.1.5. Maternal obesity leads to altered AT microenvironment in the offspring

Results shown in the *C57B/L6* mice demonstrated the baseline changes in case of high fat diet induced obesity. The obese offspring show an increased weight gain, more recruited macrophages in the gWAT and increase in adipocyte size when compared to control, these results are all as expected and similar with the findings in literature. Interestingly, our unique result on the maternal obese offspring shows higher infiltration of HSC derived macrophages, significant increase in adipocyte size compared to control animals, and also a slight increase in the body weight like a general obese offspring. These findings clearly indicate maternal obesity leads to an obese-like microenvironment in adipose tissue of the offspring in their adult life in absence of their own environmental stimulus like HFD.

4.2. Pathological HIF-1α signaling in adipose microenvironment paves the way for offspring's metabolic dysfunction

To investigate immunological basis of the AT metabolic challenge, first HIF-1α genetic mouse model was used. This mouse model consists of $LysM^{Cre/+}$; $HIF\text{-}1\alpha^{f/f}$ and Cre negative $HIF\text{-}1\alpha^{f/f}$ littermate controls (hereafter referred as HIF-1α KO and WT mice). Adipose tissue undergoes hypertrophy during unfavorable metabolic switch leading to lack of adequate blood supply to the sudden increased demand. It paves the way for hypoxic tissue microenvironment. Macrophages have a tropism for hypoxia and they infiltrate hypoxic regions to take part in the immune-adipose interaction[136,137]. HIF-1α is directly induced by hypoxia in the obese adipose tissue and undegraded HIF-1α directly controls multiple enzymes responsible for metabolic switch toward anaerobic glycolysis[113]. Moreover, activated HIF-1α shuts the TCA cycles causing decreased OXPHOS and increase ROS[113]. However, it has not been established, if HIF-1α can reprogram fetal macrophages under influence of maternal obesity and therefore, the rational was that knocking out HIF-1α in ATMs would prevent the adverse metabolic changes of the progeny's AT.

4.2.1. Body weight and organ weights in HIF-1α mice in different dietary groups

Similar to the WT animals, to evaluate the physiological changes, the body weight of the offspring was measured for HIF-1α animals. Also weight gain over time in WT vs KO are recorded (Fig24d). Unlike WT mice, the body weight or whole organ weight for gWAT of maternal obese animals does not increase significantly when compared to control. The other obese groups show significant weight gain compared to the control group. To understand why this happened, I looked into the macrophage landscape in AT.

The BAT organ weights are not significantly affected in changes of dietary conditions. Interestingly , though maternal obese animals weigh similar to lean animals, their tissue microenvironment looked far from similar.

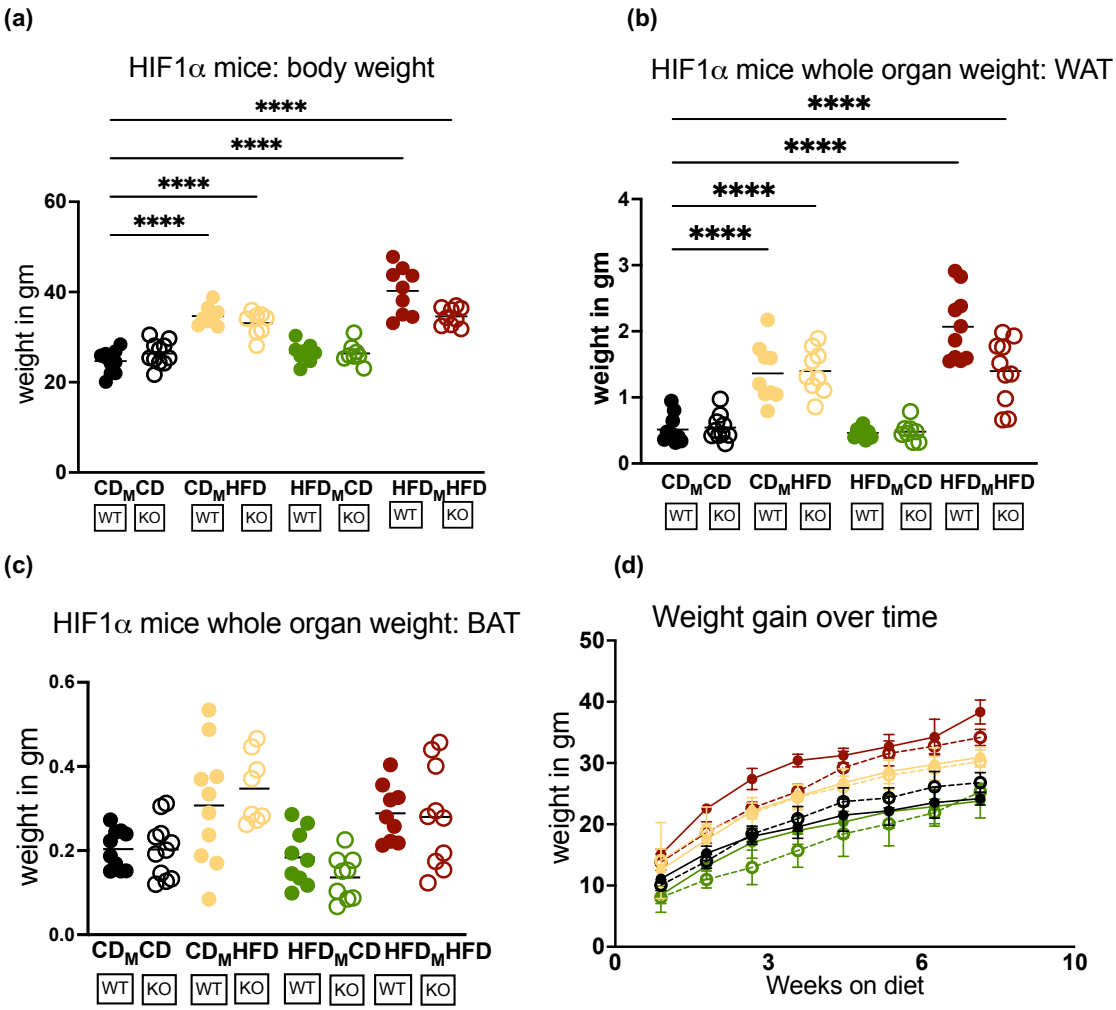

Fig24: Comparison of body weight and organ weight of HIF-1α animals from different dietary groups a) Body weight n=8-11. (b) whole organ weight of g WAT , n=8-11 & (c) whole organ weight of BAT , n=8-11 in control (black) vs obese (yellow & brown) and maternal obese groups (green) . (d) sequential weight gain over time in HIF-1α animals. Each dot represents one mouse, p values obtained by one-way ANOVA with Sidak's multiple comparison unless otherwise indicated, * - p <0.05 , ** - p< 0.0001.**

4.2.2. Insulin and glucose tolerance tests

One of the obvious effects of obesity noted in both murine and human is insulin resistance. To register the insulin intolerance in various HFD induced obesity in mother and/or pups , the results of Glucose tolerance tests (GTTs) and insulin tolerance tests(ITTs) were analyzed. (Fig25). Obese animals show higher blood glucose level which was improved in case of conditional KO of HIF-1α. Blood glucose was only marginally increased in case of maternal obese offspring compared to control. Higher n numbers for this test will be required in future

to show the statistically significant results in maternal obese animals. When compared within a dietary group, KO animals showed lower blood glucose compared to WT in maternal obese and obese groups.

(a)

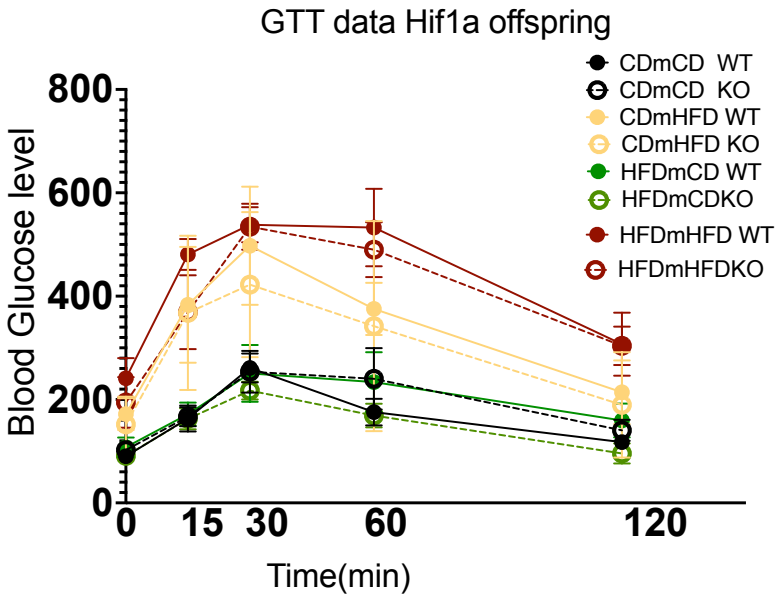

(b)

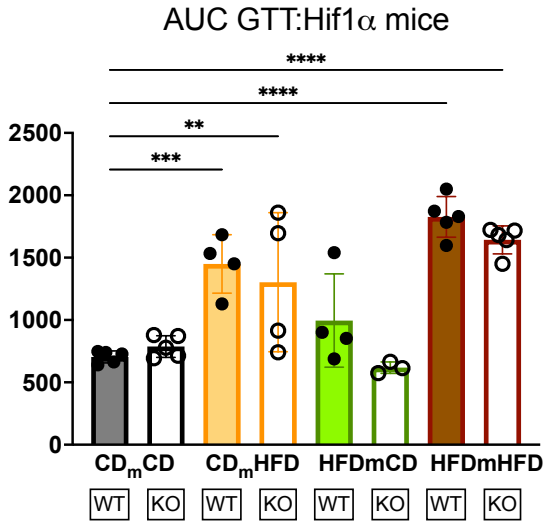

Fig25:, Glucose tolerance test on 11-week-old HIF-1α mice in different dietary groups. The diet and conditions are indicated in the figure a. Response with time each dot represents the mean ±SD (a). The area under the curve(AUC) was measured (n=3-5) with each dot representing one area under the curve from one mouse(b).

For the insulin tolerance test, mice were fasted 6 hours to avoid any hypoglycemia. In case of hypoglycemia occurred, the results from such animals have been excluded. There marginal

difference between maternal obese and control WT animals in insulin sensitivity(Fig26). The observed changes are subtle. That is why comparing WT &KO mice within a dietary group also gives meaningful insight. After injection of insulin, the blood glucose level drop towards normal in maternal obese KO animals compared to WT. The effect is fairly less pronounced when the offspring of an obese dam is fed with HFD too. In absence of maternal HFD, the initial responsiveness (15 min) to insulin is almost comparable in WT & KO offspring, with later time points KO animal shows better sensitivity before returning back to normal level (FigS1b).

(a)

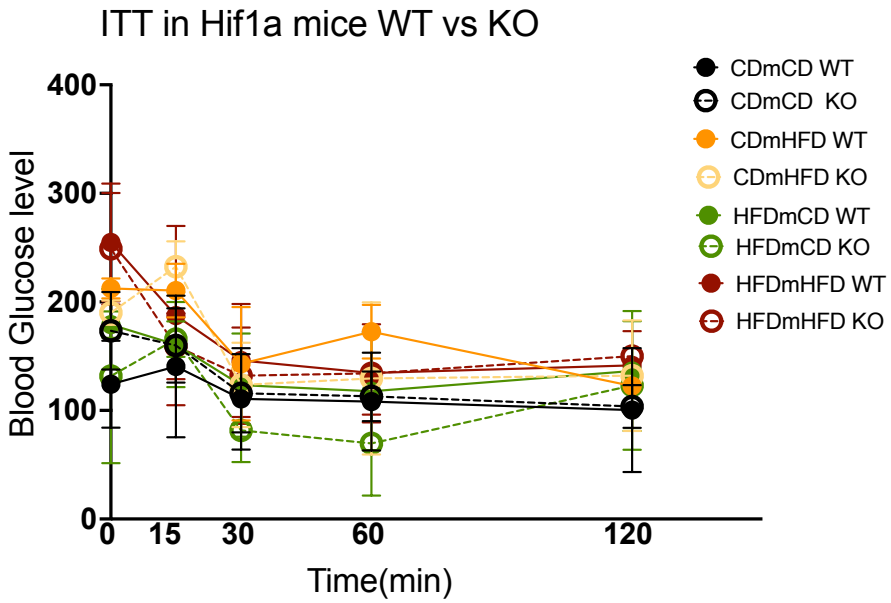

(b)

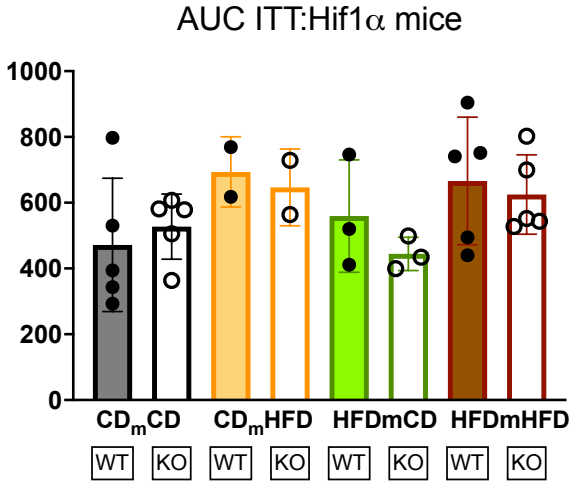

Fig26: Insulin tolerance test on 11-week-old HIF-1α mice in different dietary groups. The diet and conditions are indicated the figure a. Response with time ach dot represents the mean ±SD (a). The area under the curve (AUC)was measured (n=2-5) with each dot representing one area under the curve from one mouse(b).

4.2.3. UMAP visualization of the flow cytometry data in pursuit of unique macrophage subset in HIF-1α mice

On the basis of the information obtained from C57BL/6J mice, first attempt was to unbiasedly cluster on flow cytometry data using UMAP and FlowSom clustering in R studio to find out the presence of unique clusters in the gWAT of HIF-1α mice. FlowSOM is an algorithm that speeds the analysis of cytometry data and can identify clusters that might be otherwise missed with Self-Organizing Maps (SOMs) that considers the behaving of all antigenic markers on all cells. First UMAP shows revealed 18 different clusters (Fig27) based on the antigenic markers available on the macrophage panel (Table1) which consists of 3 resident macrophage clusters and 5 recruited macrophage clusters, 2 DC clusters and 2 monocyte clusters and one undifferentiated cluster. Interestingly, all 3 resident macrophage subsets seen in C57BL/6J mice could also be seen here , though the percentage of ResMac 1& 3 are negligible. Moreover, broadly recruited macrophages showed Tim4 negativity, however differentiation using CD11c was somewhat blurred. Also Mono2 cluster showed proximity to Mono1 but lack Ly6c or CD63 positivity and could be a part of recruited subset. All these issues arose due to undertaking the analysis with all 8 dietary groups together and batch effects due to different experiment dates . To avoid such batch effects, only KO animals from specific dietary condition and their littermate controls (WT) from the same day were compared in further clustering (Fig 28,29).

Table 12: Macrophage subsets in gWAT in HIF-1α mice by UMAP

Populations	Markers expressed
ResMac 1	$Tim4^{+}$ $CD206^{+}$ $CD11c^{+}$ $MHCII^{-}$: CL 4
ResMac 2	$Tim4^{+}$ $CD206^{+}$ $CD11c^{+}$ $MHCII^{+}$: CL2,
ResMac 3	$Tim4^{+}$ $CD206^{-}$ $CD11c^{-}$ $MHCII^{+}$: CL3
RecMac1	Tim4-CD11c+ $MHCII^{hi}$ CD206- Cx3cr1-CD63-CD9+ Lyc6- : CL7
RecMac2	Tim4-$CD11c^{low}$ $MHCII^{hi}$ CD206+Cx3cr1+CD63+CD9+Lyc6+ :CL1
Mono1	Tim4-CD11c+CD11b+ MHCII-Cx3cr+CD63+CD9+ $Lyc6^{hi}$: CL5
?Mono2	Tim4-CD11c- MHCII-Cx3cr1+CD63-$CD9^{lo}$ Lyc6- : CL11
RecMac3	Tim4-CD11c+$MHCII^{hi}$ CD206-Cx3cr1+CD63+CD9- Lyc6- : CL8
RecMac4	Tim4-CD11c+$MHCII^{hi}$ Cx3cr1-CD63-CD9- Lyc6- : CL15
?RecMac5	$Tim4^{lo}$ CD11c+ MHCII+ CD206+Cxcr1-$CD63^{lo}$ $CD9^{hi}$ Ly6c+ : CL14
DC	CD45+MHCII+ CD11C+ : CLs17,18
Undifferentiated	CD45+ : CL 13
Nonsignificant (minimal %)	CLs 6,12, 9, 16, 10

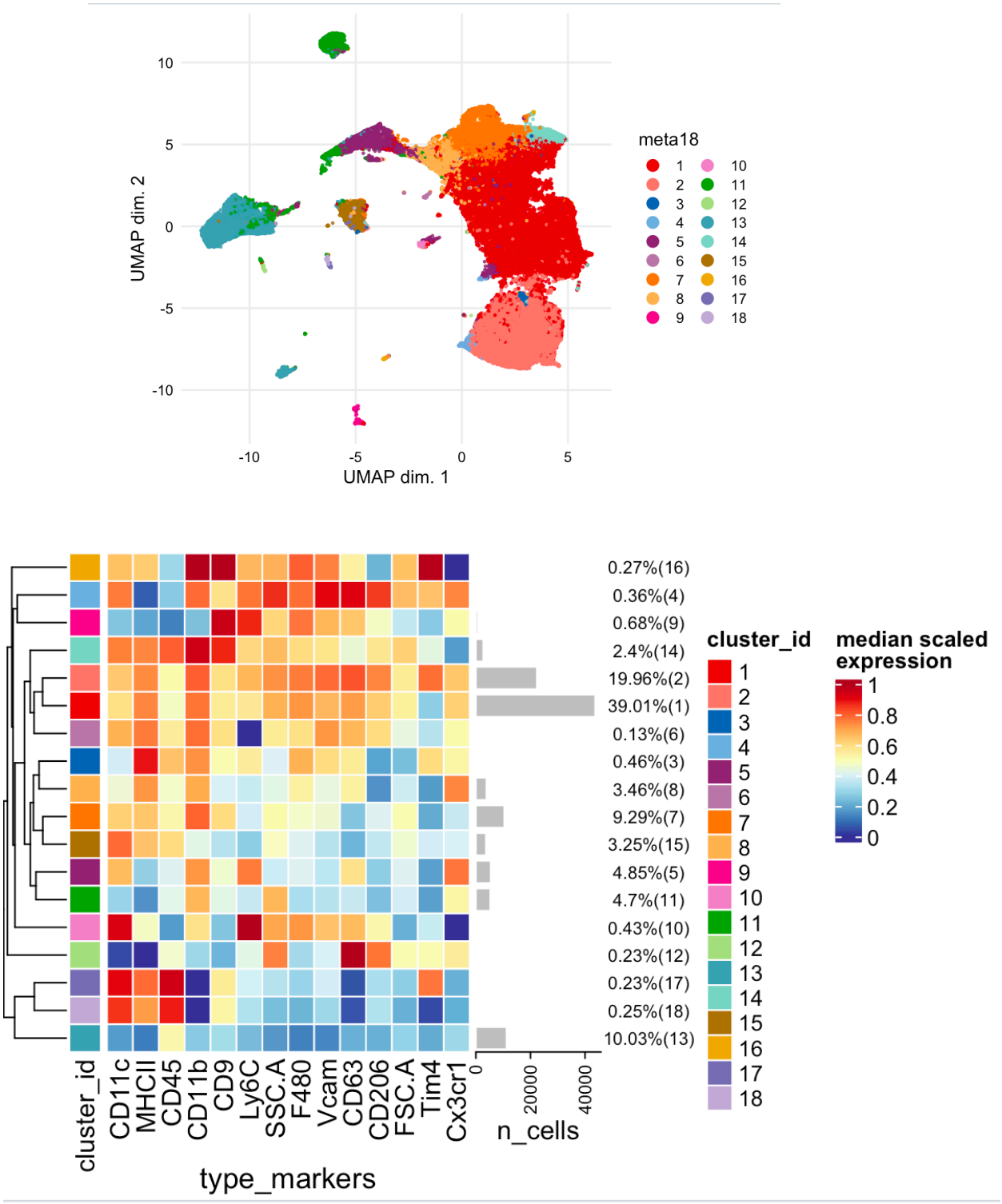

Fig27: UMAP visualization of the flow cytometry data in HIF-1α mice with all dietary groups concatenated

To assess the macrophage subsets in control pups, at first 18 UMAP clusters were obtained. After carefully assessing the antigenic profile, they were merged into two resident macrophage clusters, three recruited macrophage clusters, one monocyte cluster and one dendritic cell

cluster (Fig28). Interestingly, in C57BL/6J mice we saw a ResMac1 population marginally in control mice and enriched in maternal obese mice, which was absent in HIF-1α control mice. The recruited macrophages in HIF-1α mice predominantly were divided by CD11c expression like C57BL/6J mice into 2 groups, $CD11c^{+}$ or $CD11c^{-}$. However within $CD11c^{-}$ cluster, 2 distinct populations were note based on CX3CR1 and LY6C expression. Overall there is no difference in CDWT and CDKO UMAP profile (Fig28). ResMac1 population absent in HIF-1α control mice, came back in HIF-1α maternal obese group (Fig29)

(a)

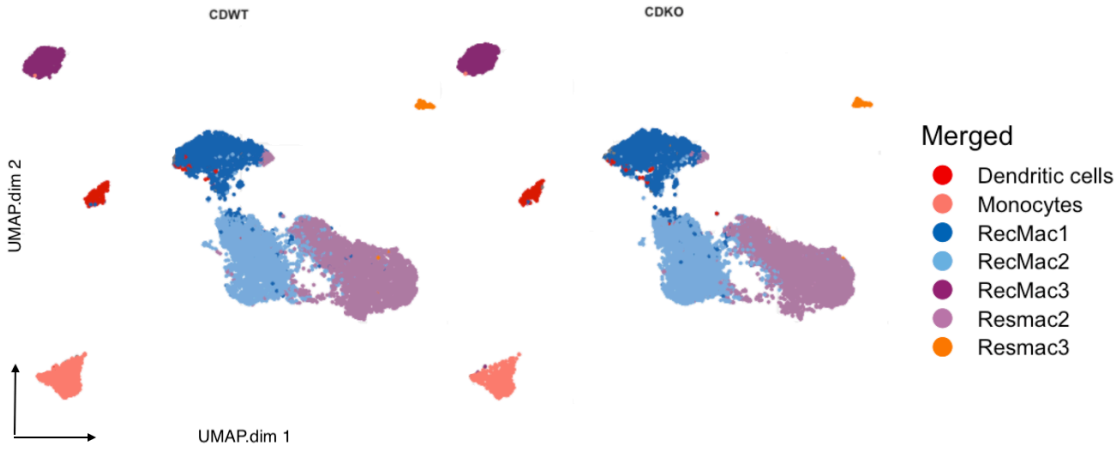

(b)

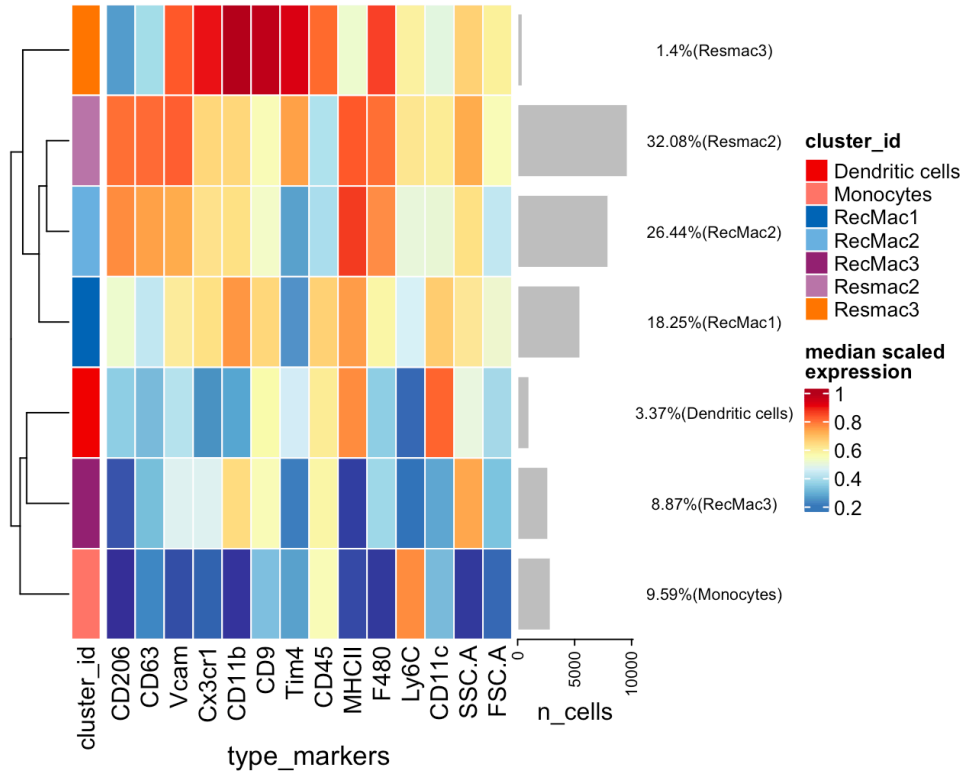

Fig28: UMAP analysis of myeloid population in gWAT of HIF-1α mice, comparison between WT vs KO in control diet group(after merging and excluding granulocytes).

Table 13: Myeloid cell subsets in gWAT in HIF-1α mice, control group (excluding granulocyte)

Populations	Markers expressed
DC	$CD45^+$ $CD11c^+$ $MHCII^+$
Monocytes	$F4/80^+$ $Ly6c^+$ $CD9^+$ $MHCII^+$
ResMac 2	$Tim4^+$ $CD11c^+$ $MHCII^+$:
ResMac 3	$Tim4^+$ $CD11c^-$ $MHCII^+$
RecMac1	$Tim4^-$ $CD11c^+$ $MHCII^+$
RecMac2	$Tim4^-$ $CD11c^-$ $MHCII^+Ly6c^+$ $CX3CR1^-$
RecMac3	$Tim4^-$ $CD11c^-$ $MHCII^+$ $Ly6c^-$ $CX3CR1^+$

To assess the macrophage subsets in maternal obese pups, at first 18 UMAP clusters were obtained. After assessing the antigenic profile, they were merged into three resident macrophage clusters, three recruited macrophage clusters , one monocyte cluster and one dendritic cell cluster (Fig29). The subsets found in C57BL/6J mice (Table 10) were recapitulated in maternal obese pups with all three resident clusters and they preserved their total numbers while minor shift within clusters. The recruited macrophages predominantly were divided by CD11c expression and within $CD11c^-$ cluster, two distinct populations were noted based on CX3CR1 and LY6C expression and one of them were almost completely disappeared in the KO mice (Recmac3) and the other was decreased. The DC, monocyte, and RecMac1 populations showed minor changes.

Table 14: Myeloid subsets in gWAT in HIF-1α mice, maternal obese group (excluding granulocytes)

Populations	Markers expressed
DC	$CD45^+$ $CD11c^+$ $MHCII^+$
Monocytes	$F4/80^+$ $Ly6c^+$ $CD9^+$ $MHCII^+$
ResMac 1	$Tim4^+$ $CD11c^+$ $MHCII^-$
ResMac 2	$Tim4^+$ $CD11c^+$ $MHCII^+$:
ResMac 3	$Tim4^+$ $CD11c^-$ $MHCII^+$
RecMac1	$Tim4^-$ $CD11c^+$ $MHCII^+$
RecMac2	$Tim4^-$ $CD11c^-$ $MHCII^+Ly6c^+$ $CX3CR1^-$
RecMac3	$Tim4^-$ $CD11c^-$ $MHCII^+$ $Ly6c^-$ $CX3CR1^+$

(a)

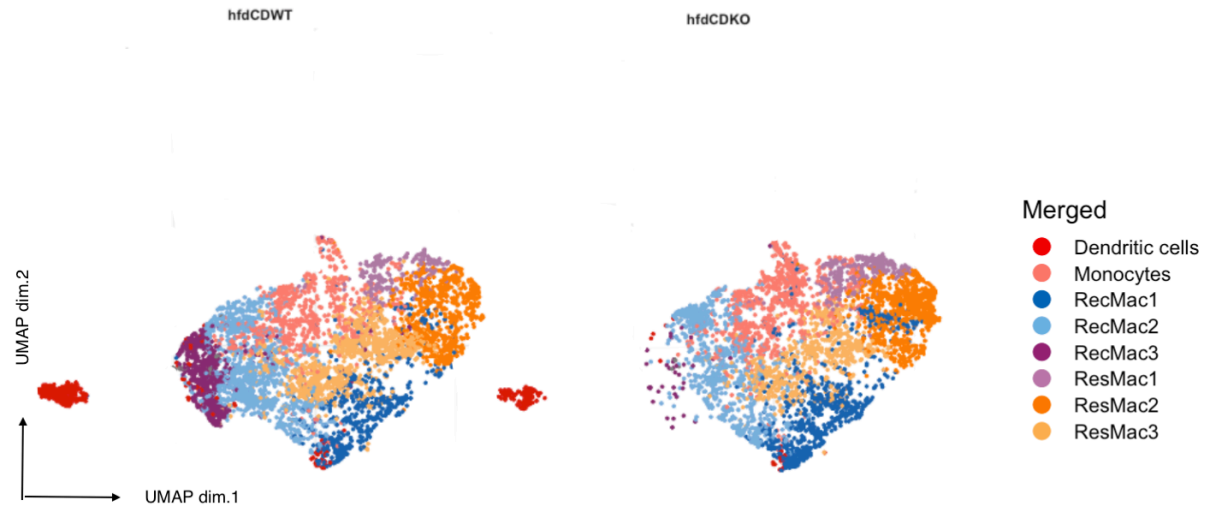

(b)

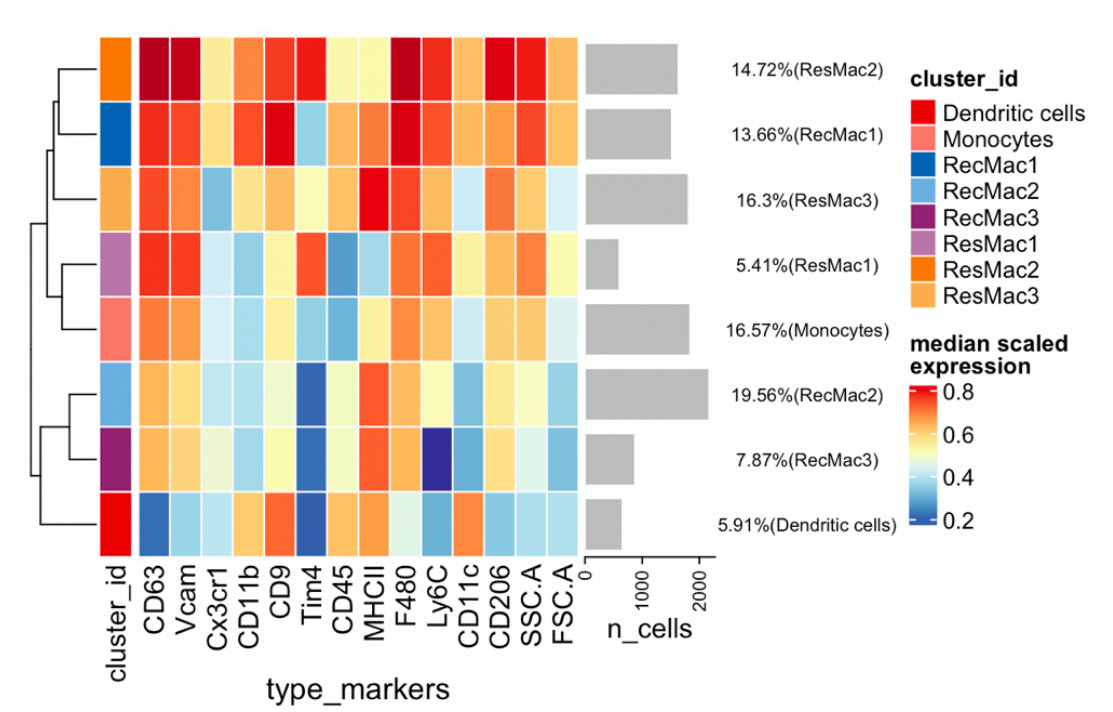

Fig29: UMAP analysis of myeloid population in gWAT of HIF-1α mice , comparison between WT vs KO in maternal obese group (after merging and excluding granulocytes)

4.2.4. Quantification of macrophage subsets in HIF-1α mice by flow cytometry

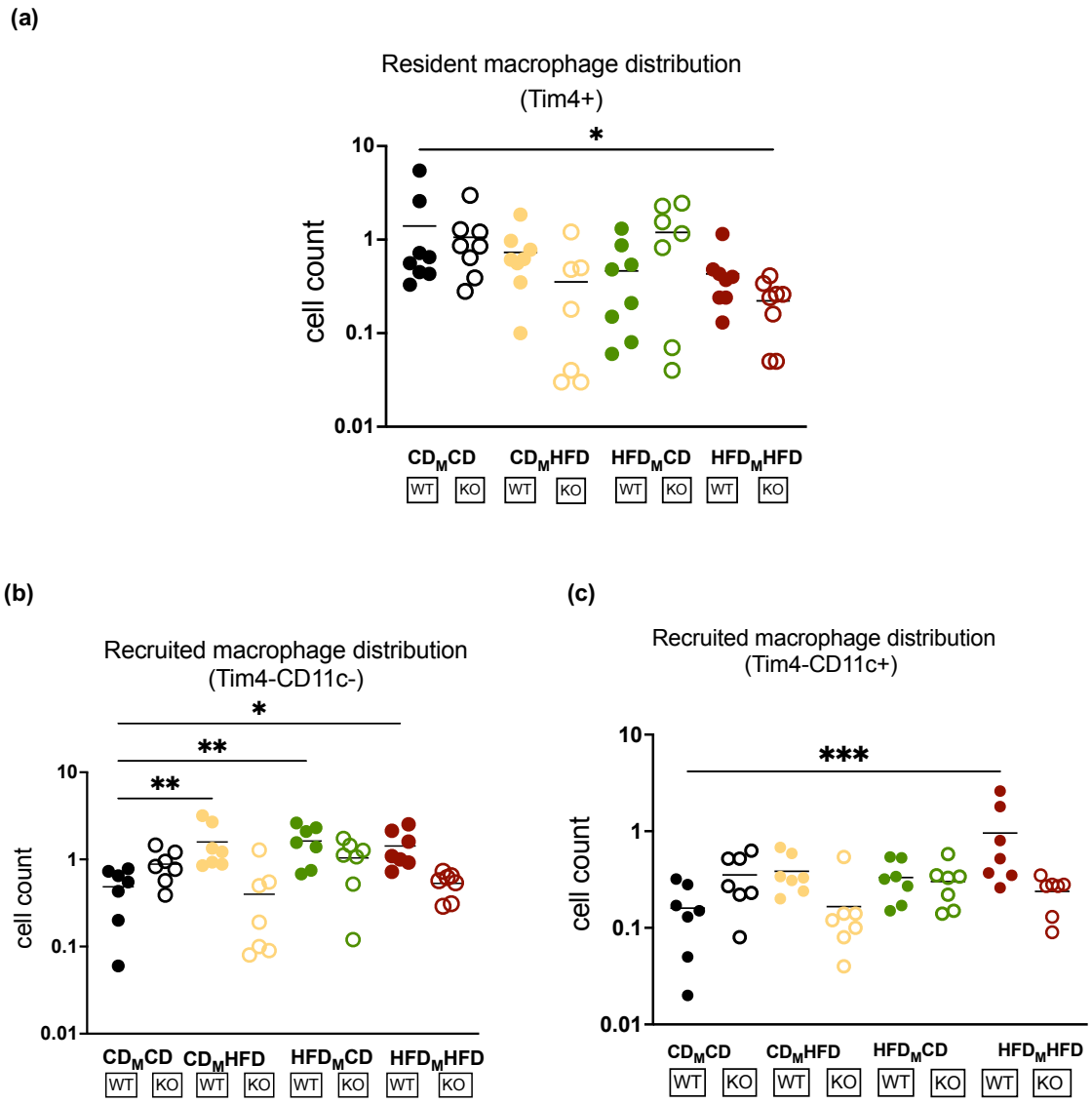

Fig30: Quantification of Flow cytometry data for resident vs recruited macrophages in different dietary groups in gWAT, HIF-1α mice, n=6-8.Distribution of (a) Tim4$^+$ tissue resident macrophages (b) Tim4$^-$ CD11c$^-$ recruited macrophages (c) Tim4$^-$ CD11c$^+$ recruited macrophages. Each dot represents one mouse, p values obtained by one-way ANOVA with Dunnett's multiple comparison unless otherwise indicated, * - p <0.05 , ** - p< 0.01.

With the above unbiased visualization points towards the fact that all resident macrophages in AT are Tim4$^+$. It led to the quantification of the Flow cytometry data from gWAT in HIF-1α

mice towards three main different phenotypes (Fig30) as observed in the C57BL/6J mice. The resident macrophages are marked by the presence of Tim4 positivity while the HSC-derived, monocyte-derived macrophages were $Tim4^{-}$ $CD11c^{+}$ and $Tim4^{-}CD11c^{-}$. The latter group prominently infiltrated the obese and maternal obese adipose tissue and coexisted with adipocyte hypertrophy and more crown-like structure formation, thereby promoting proinflammatory cytokine release and establishing a vicious cycle of chronic low-grade inflammation. Worth noting that, it may appear from figure Fig30a that there is an increase in tissue resident macrophage in the control mice compared to the obese groups. However, it seems so because the percentage of resident macrophage gets diluted in the obese animals with continuous influx of HSC derived macrophages while the total number may remain unaltered.

4.2.5. Morphological changes in adipocytes of HIF-1α KO mice and their quantification

Consistent with the results observed in C57Bl/6J mice, the metabolically challenged conditions like maternal obesity or offspring's own obesity cause the expansion of white adipocyte size compared to control also in HIF-1α mice. The H&E stain of the mice gWAT showed the adipocytes size was increased in obese and maternal obese gWAT compared to control. Interestingly, the adipocyte hypertrophy is rescued by the conditional KO of HIF-1α in macrophage (Fig31). Using 'AdipoQ' plugin to (Fiji is just) ImageJ , adipocyte area, diameter and volume in different dietary conditions were obtained (Fig32). The quantification agrees with the morphological findings showing increased diameter and surface area of adipocytes in maternal obese and obese groups compared to control and this hypertrophy is being rescued by conditional KO of macrophage in adipose tissue morphologically.

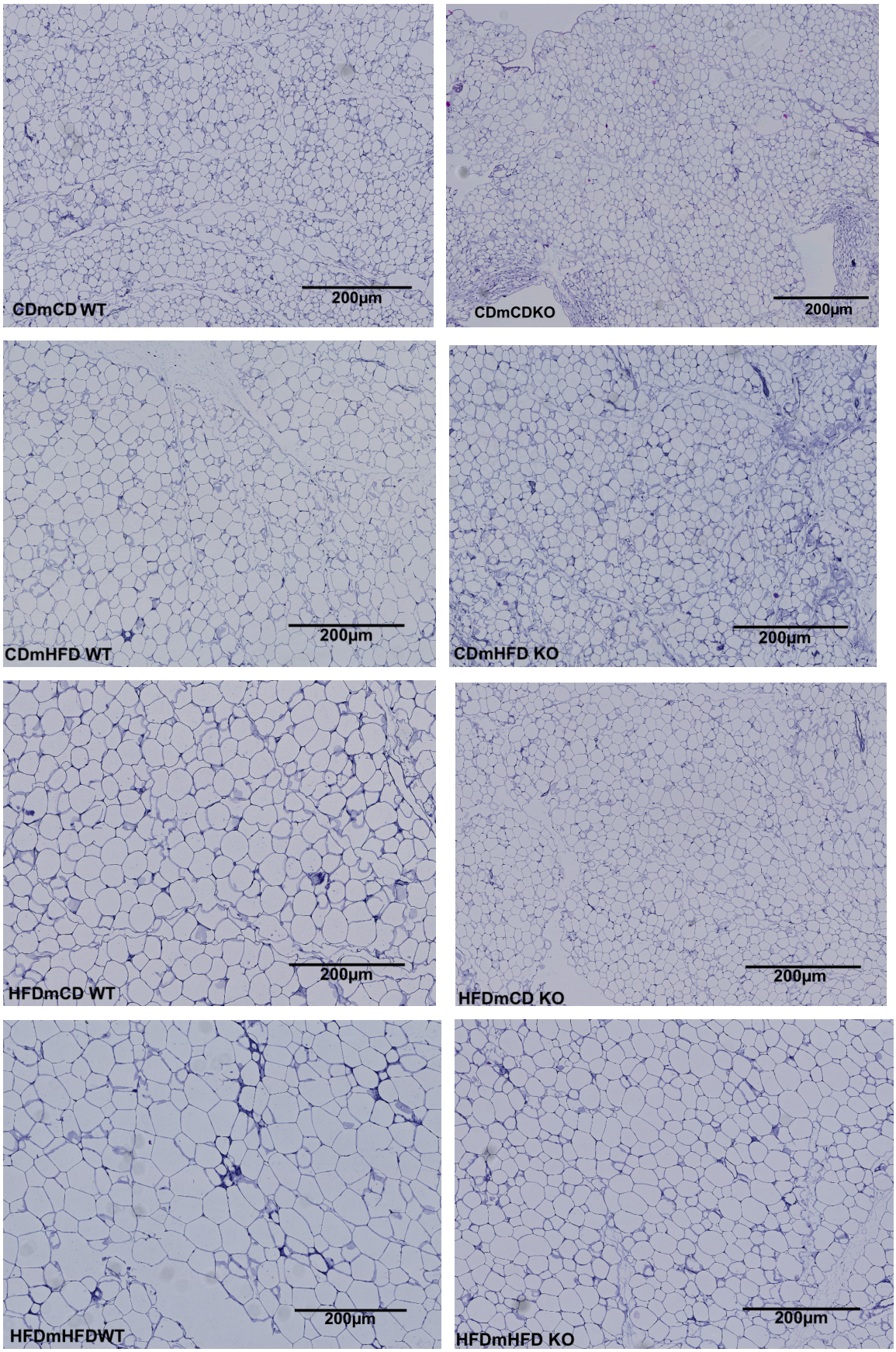

Fig31: H&E staining of paraffin embedded gWAT section from HIF-1α offspring mice from different conditions,(n=7). Different maternal and pups' dietary conditions are indicated on the figures.

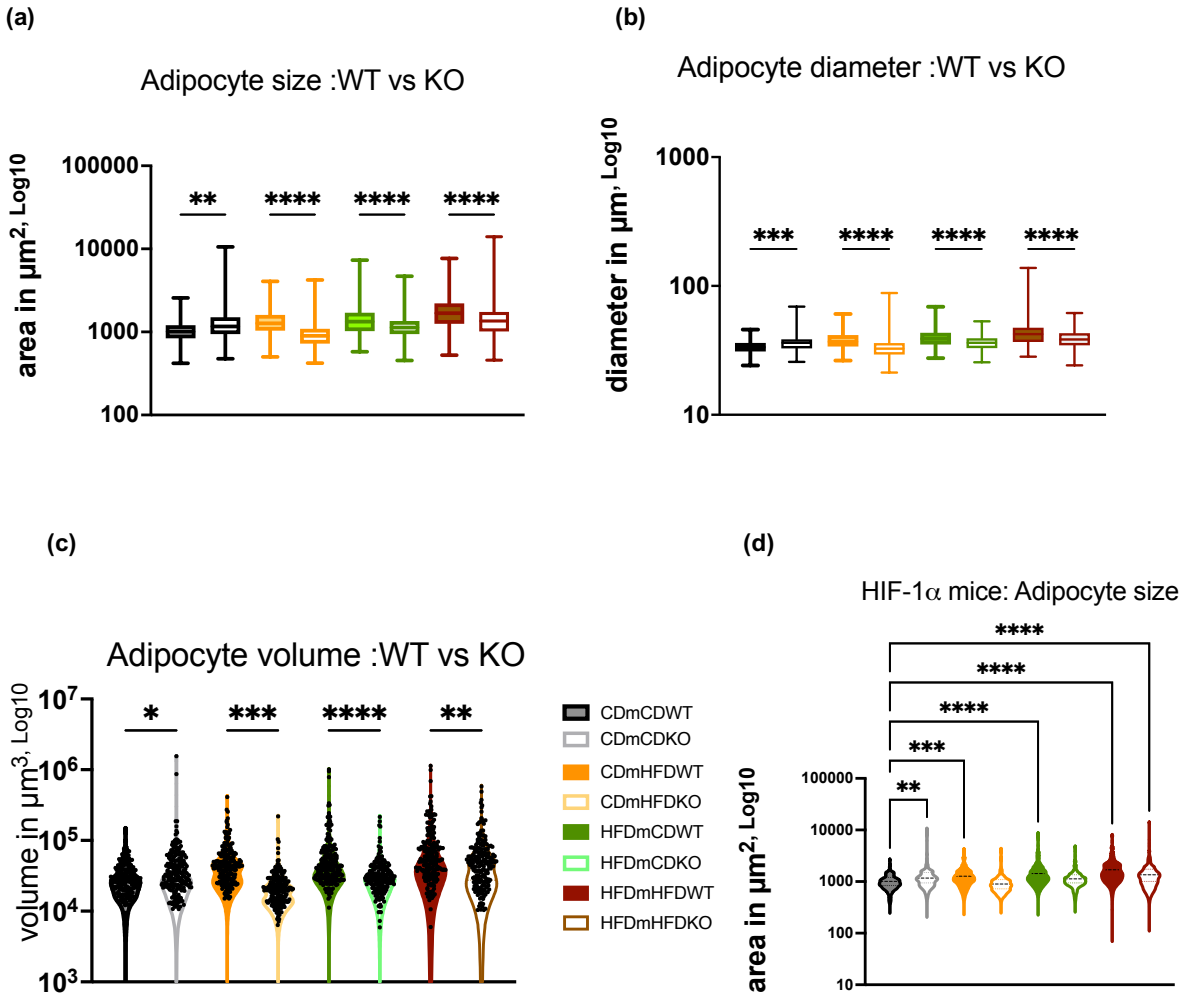

Fig32: Comparison of adipocyte size (area) (a) and diameter (b) volume (c) in different dietary groups in HIF-1α WT and KO mice,(n=7). p values obtained by one-way ANOVA with Sidak's multiple comparison, * - p < 0.05, ** - p <0.01 , *- p <0.001, ****- p <0.0001. For quantification , 200 adipocytes from region of interests were used for each individual tissue. (d) Comparison of adipocyte size between control and different groups are shown.**

Other than the morphological changes in adipocytes, the state of chronic immune activation in AT is hallmarked by formation of crown-like structures(CLS). Fig33 (a,d) shows formation of crown -like structure in the tissue. The CLS intensity was measured using the AdipoQ plugin. CLS intensity is inversely proportional to the formation of CLS, thereby more CLS intensity means less CLS formation and vice versa. To understand it better, the CLS intensity comparison was plotted compared to control and within WT and KO mice(Fig33 b,c). This approach of quantifying CLS is purely exploratory and unique, which needs deeper dive to correlate with each and every individual tissue section with special stains in the future and out of scope of the current project.

(a)

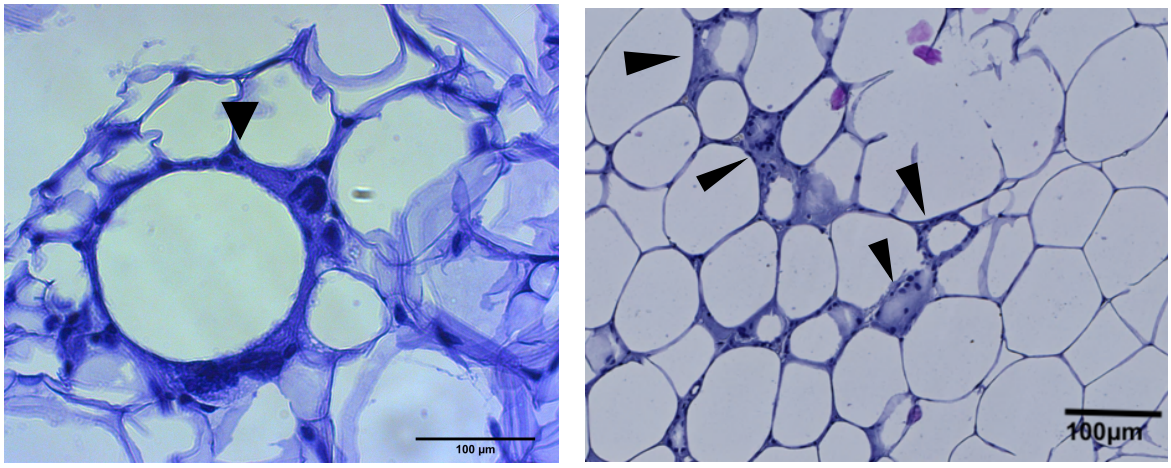
100 μm
100μm

(b)

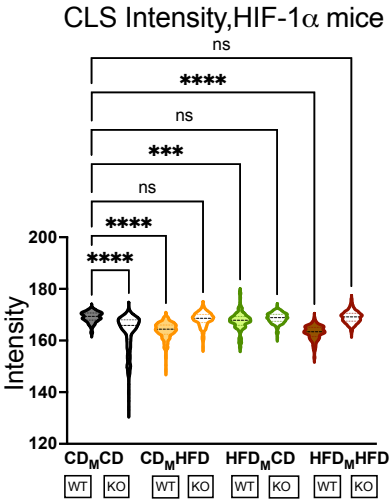
CLS Intensity,HIF-1α mice , control vs others
ns
****
ns
***
ns
****
****
Intensity
200
180
160
140
120
CD_MCD
CD_MHFD
HFD_MCD
HFD_MHFD
WT
KO

(c)

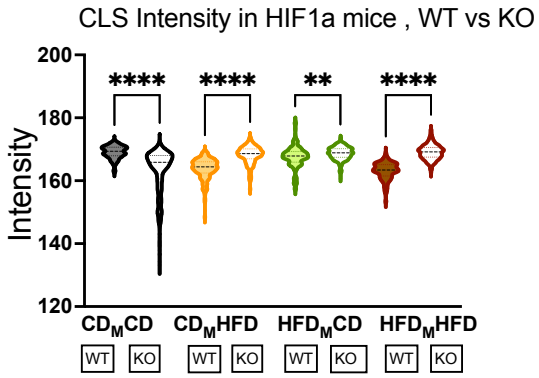
CLS Intensity in HIF1a mice , WT vs KO
Intensity
200
180
160
140
120
****
****
**
****
CD_MCD
CD_MHFD
HFD_MCD
HFD_MHFD
WT
KO

(d)

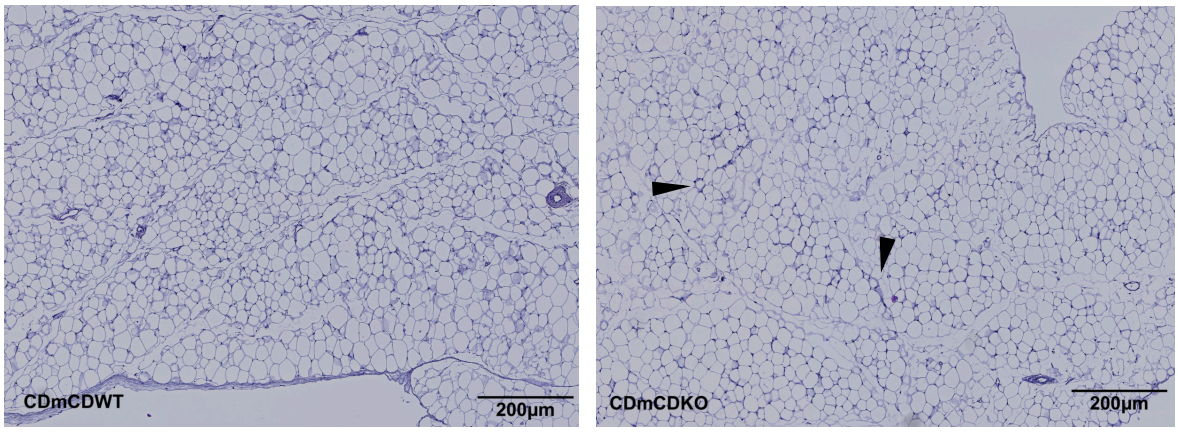
CDmCDWT
200μm
CDmCDKO
200μm

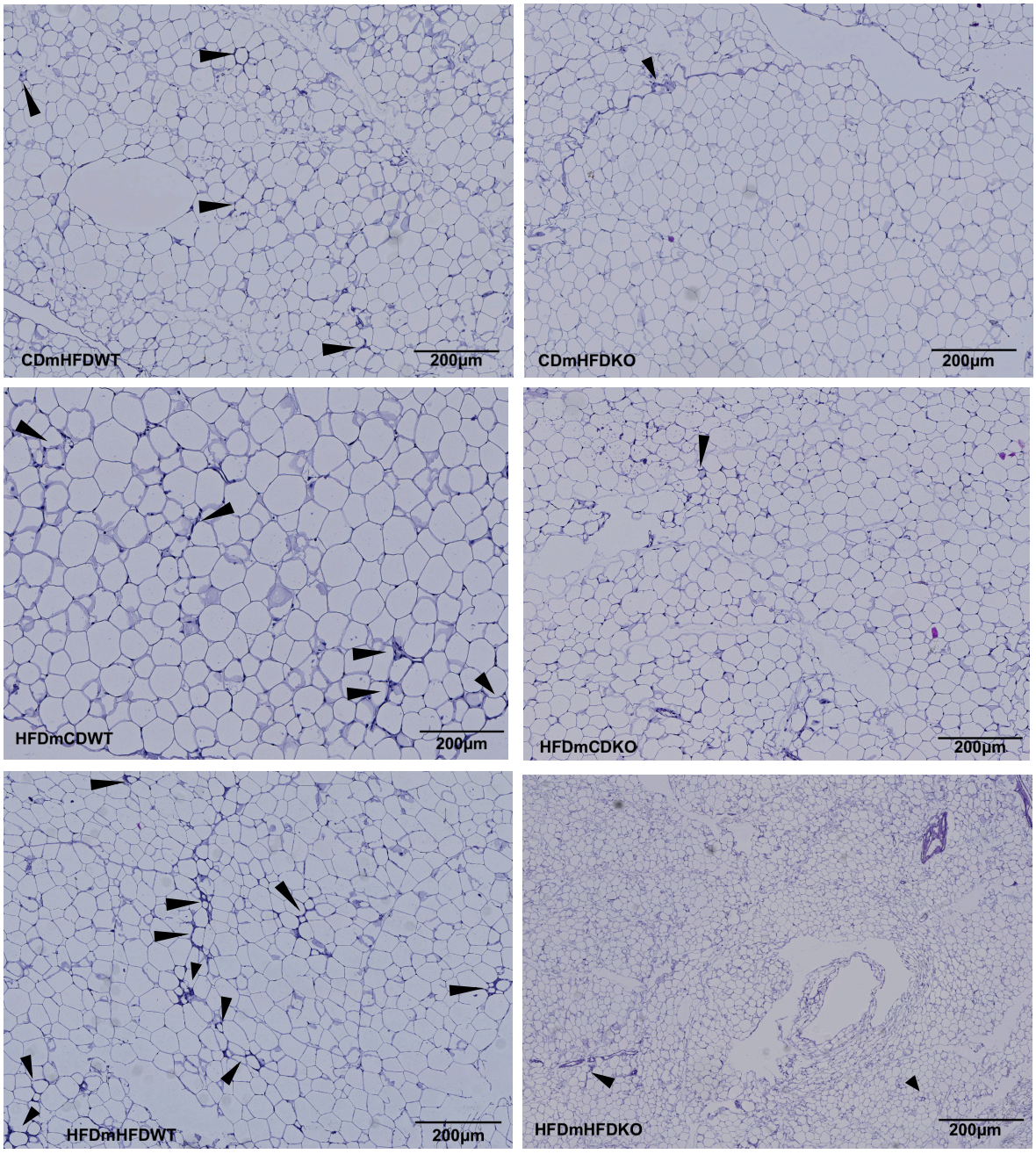

Fig33: Assessment of crown like structures (CLS) in gWAT of HIF-1α mice (a) Crown like structures in gWAT (black arrowheads) and (b) the quantitative analysis of their intensity in different dietary groups between control vs all groups offspring , intensity is inversely proportional to the incidence of CLS. P value was obtained by one-way ANOVA with Dunnett's multiple comparisons test *- p < 0.001 ,**** - p <0.0001 (c) between WT vs KO offspring in between dietary groups, p values obtained by one-way ANOVA with Sidak's s multiple comparisons test,**** - p <0.0001 ns = nonsignificant (d) morphological representation of CLS in different dietary groups**

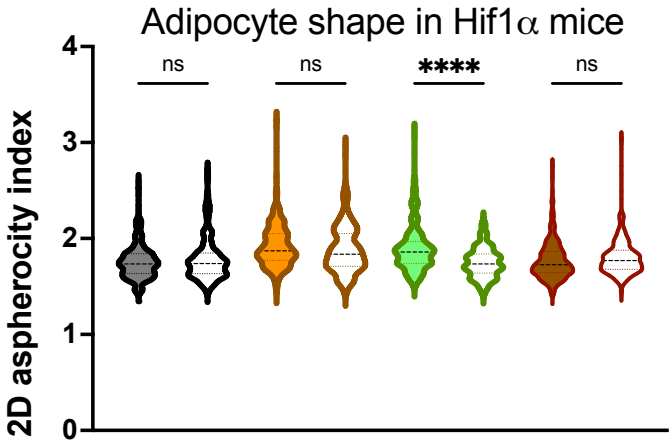

Fig34: Measurement of adipocyte shape in different conditions in HIF-1α mice. Quantitative analysis is done by using 2D aspherocity index, p values obtained by one-way ANOVA with Sidak's multiple comparison, p **- <0.0001 .**

To explore other parameters measured by the AdipoQ plugin, 2D asphericity index was studied to understand the shape of adipocytes in gWAT (Fig34). While the other groups show no difference between WT & KO animals in this index, the maternal obese group shows a significant change which may be due to the variance in lipid droplets' count or property in this group. The biological implication of this result is yet unknown to us which will need further exploration in future by further. Right now, we regard this finding as an observation without a current available interpretation for it .

To observe how BAT is reacting to maternal obesity, the BAT RIM or the thin scWAT surrounding the BAT in the inter-scapular area and the BAT core or the butterfly shaped brown adipose tissue at the nape of neck in 11 weeks old offspring were analyzed. The BAT core and RIM did not show any significant changes like gWAT in flow cytometry analysis (FigS2a,3a). The BAT RIM however, showed interesting features. The BAT-RIM weights were elevated in maternal obese and obese groups compared to control and the KO mice showed lower weight (Fig36a). There was more whitening in that area in obese mice which is consistent with literature. However, uniquely we found that the white adipocytes in maternal obese offspring also underwent hypertrophy,(Fig35, Fig36b,c) though these animals had no significant increase of body or organ weight compared to the littermate control (Fig24a). The quantification of the white adipocytes in BAT RIM of HIF-1α animals recapitulated the results found in their corresponding visceral or gonadal WAT.

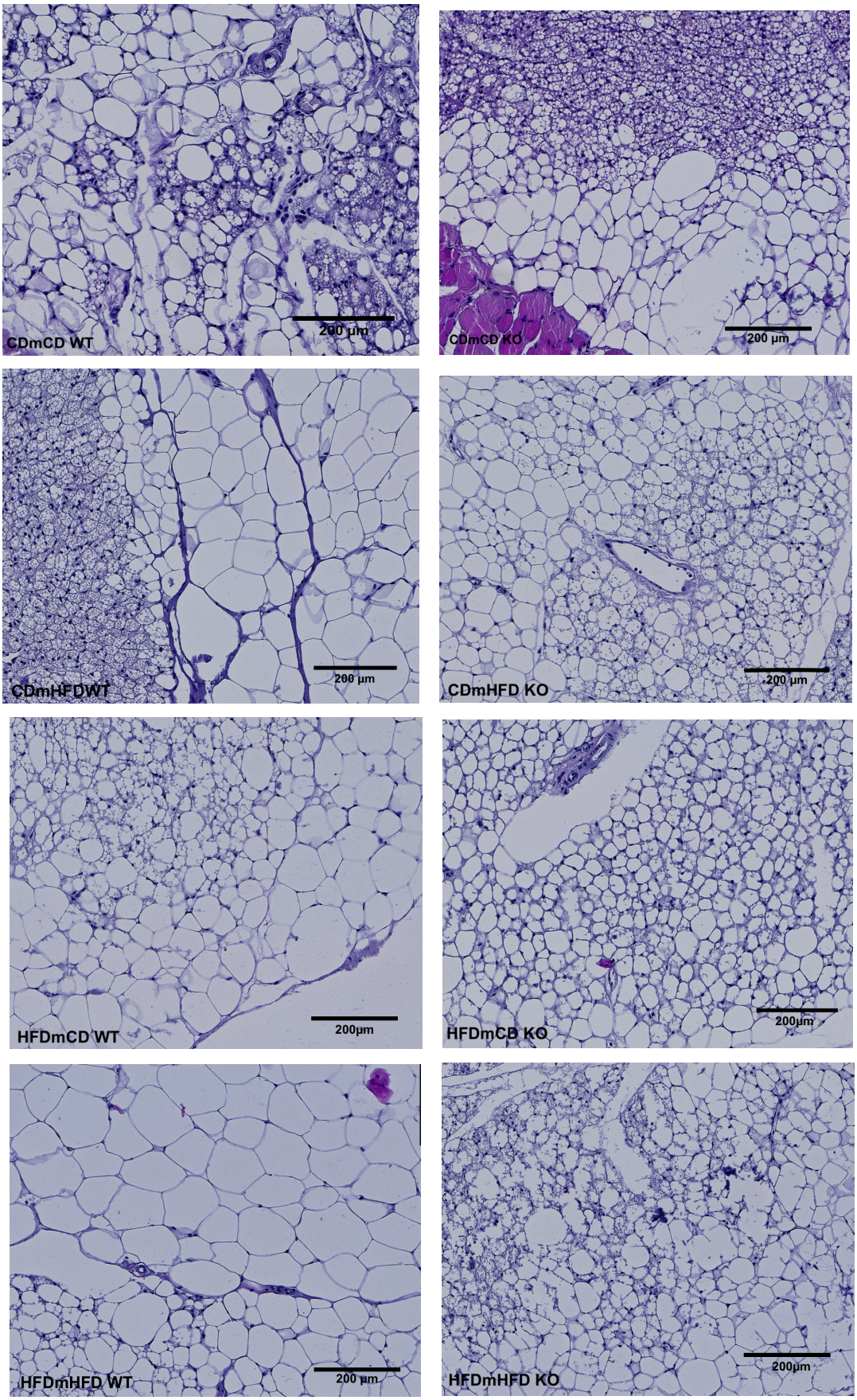

Fig35: Morphological features of BAT-RIM on H&E staining of paraffin embedded section from HIF-1α offspring mice in different dietary conditions (n=6) as indicated on the figure.

(a)

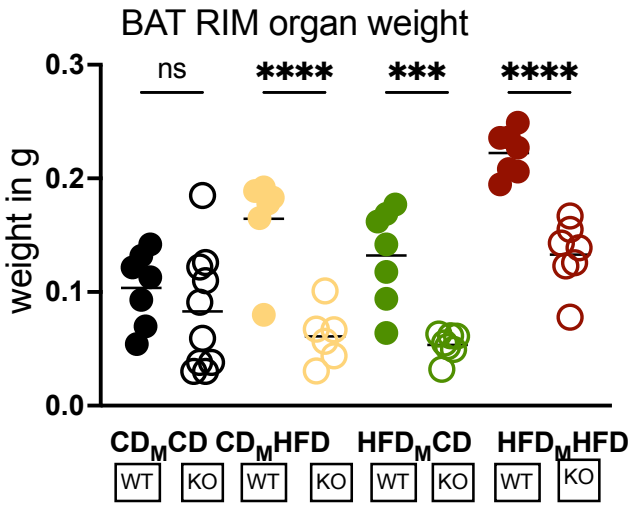

(b)

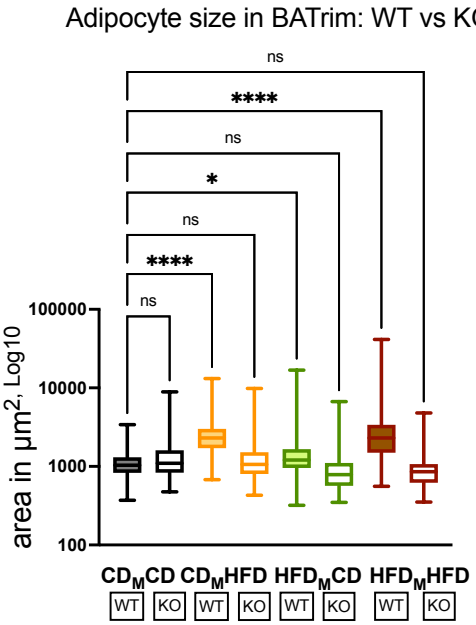

(c)

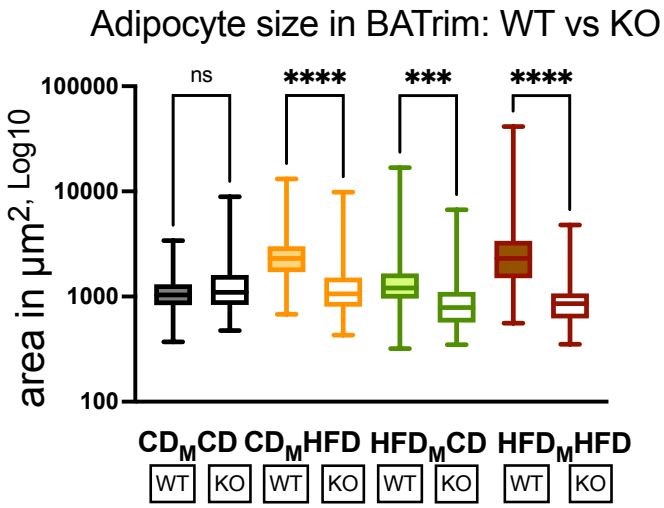

Fig 36: Comparison of organ weight and adipocytes' size of BAT RIM in HIF-1α mice. (a) Relative organ weights of BAT RIM, (b)Comparison of adipocyte size in control vs other groups , p values obtained by one-way ANOVA with Dunnett's multiple comparisons test **- p < 0.01 ,** - p <0.0001 ns = nonsignificant and (c) adipocyte size comparison between WT vs KO within different dietary groups in BAT-RIM, , p values obtained by one-way ANOVA with Sidak's s multiple comparisons test, **** -p <0.0001 ns = nonsignificant n=6**

4.2.6 Results of lipidomics analysis in gWAT of HIF-1α mice

Lipidomic analysis in the gWAT were performed for different dietary groups to find out if any particular lipid classes are significant in case of maternal obese lean offspring or lipid classes found in the maternal obese group are related to any metabolic pathways.

First, the lipid classes obtained from the tissue samples are subjected to quality control(QC) analysis (Fig37). To ensure QC, lipids with over 25 percent zero or missing values across samples were excluded from the analysis, resulting in the filtering of 31 percent of the lipids.

(a)

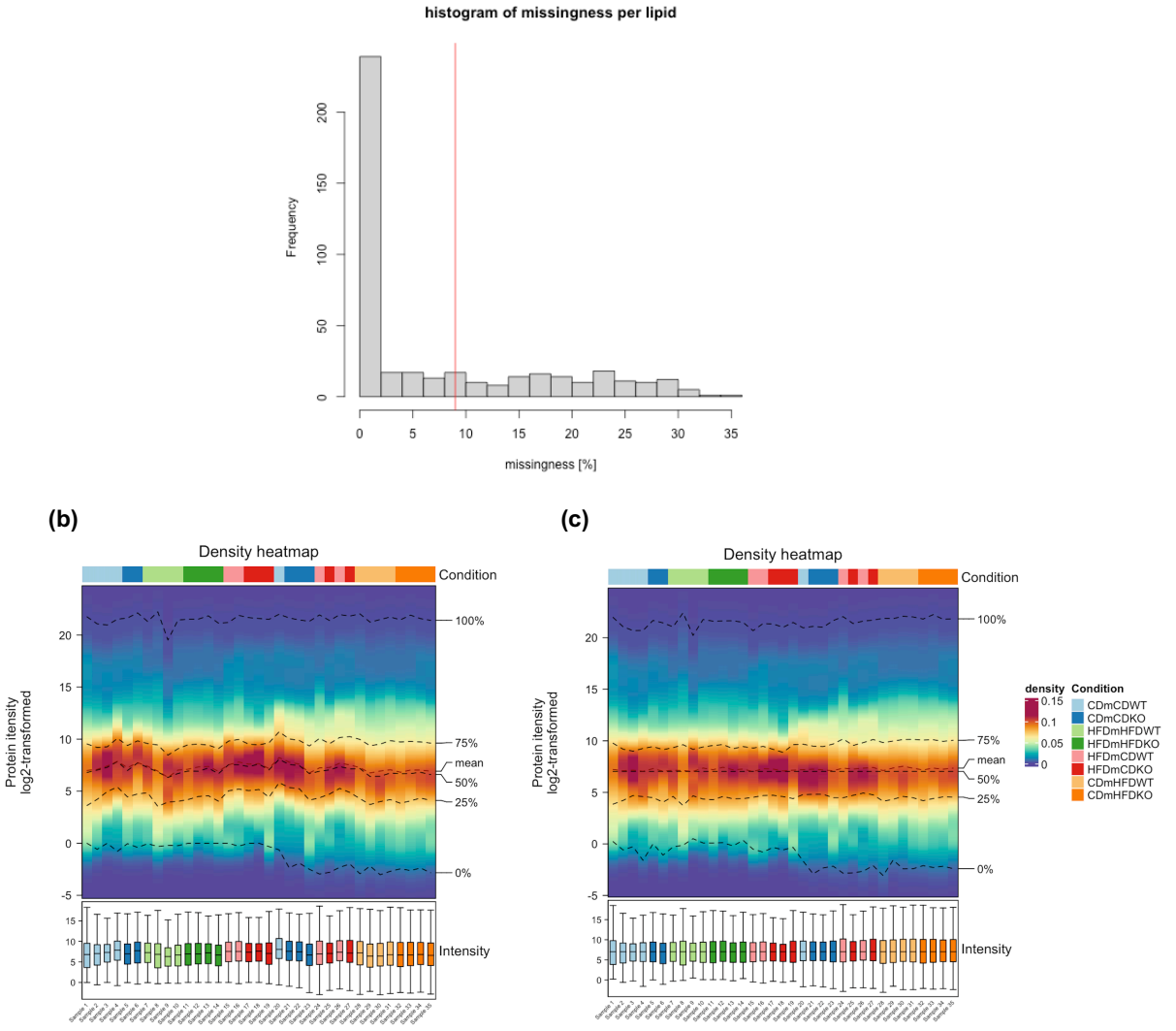

Fig37. Quality control check of lipidomic data (a) Histogram of raw expression of lipids showing the missingness. Density heatmap showing the intensity of samples considered (b)before and (c) after normalization.

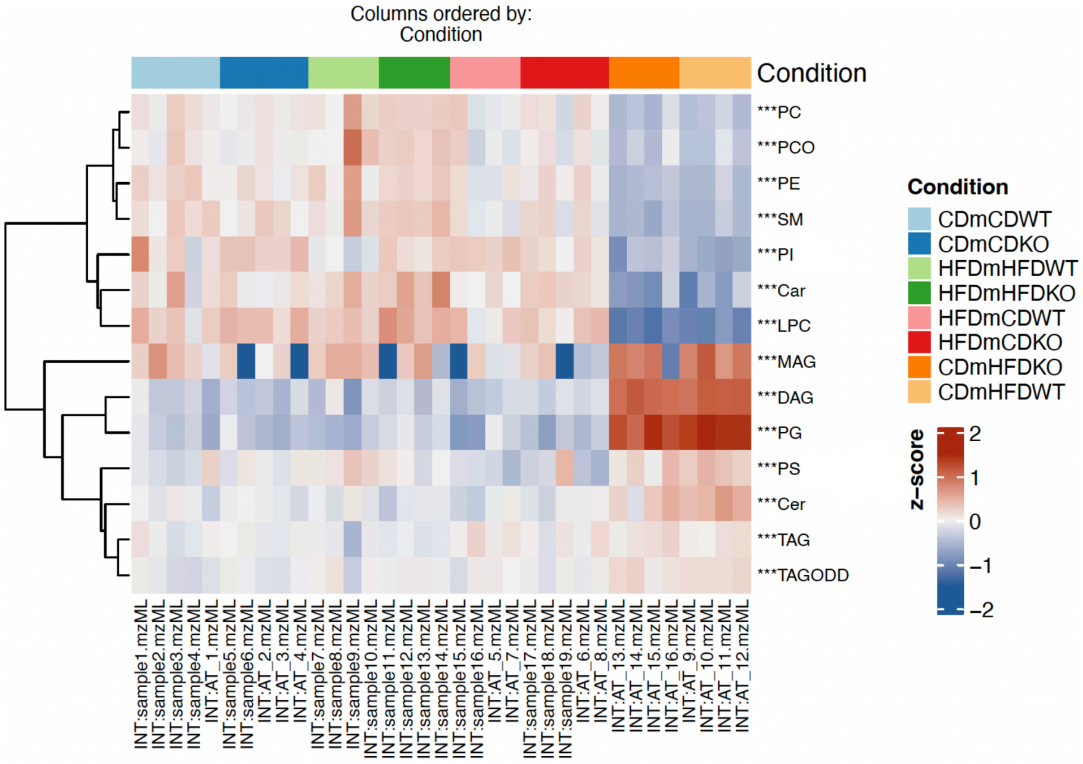

Fig38. Heat map showing abundance of identified lipid classes in gWAT of HIF-1α mice with presence in different dietary conditions in 11 weeks old HIF-1α mice, n=4

First, the lipidome signatures from14 different lipid classes were studied by heatmap to Look for any enrichment found in the groups (Fig38). An enrichment of lipid classes like Monoacylglycerols (MAG), Diacylglycerides (DAG), Phosphatidylglycerols (PG), Triglycerides (TAG), Ceramides (CER) and Phosphatidyserines (PS) was observed in obese pups without maternal HFD. When maternal obese pups were compared with controls, an enrichment of TAG and low abundance of lipid classes Phosphatidylcholines(PC), Phosphatidylethanolamines (PE) and sphingomyelins(SM) was observed.

The TAG and DAG abundance analysis (Fig39) showed TAG subclasses (58:9), (58:10), (56:8) ,(56:9), (56:7), (40:0), (40:1), (40:2), (40:3), (40:5), (42:0), (42:1), (42:2), (42:3), (42:4), (42:5), (44:0)-(44:6), (46:1)-(46:5), (50:6), (52:7), (54:8) were increased and TAG subclasses (60:3), (60:4), (60:5), (60:2), (58:1), (58:2), (58:3), (58:4), (56:1), (54:5) were decreased in maternal obese pups compared to control. There was no change in the DAG profile of the two groups. The obese pups with CD moms showed more abundance in DAG classes compared to others. There was no significant difference found between WT and KO mice within a specific group.

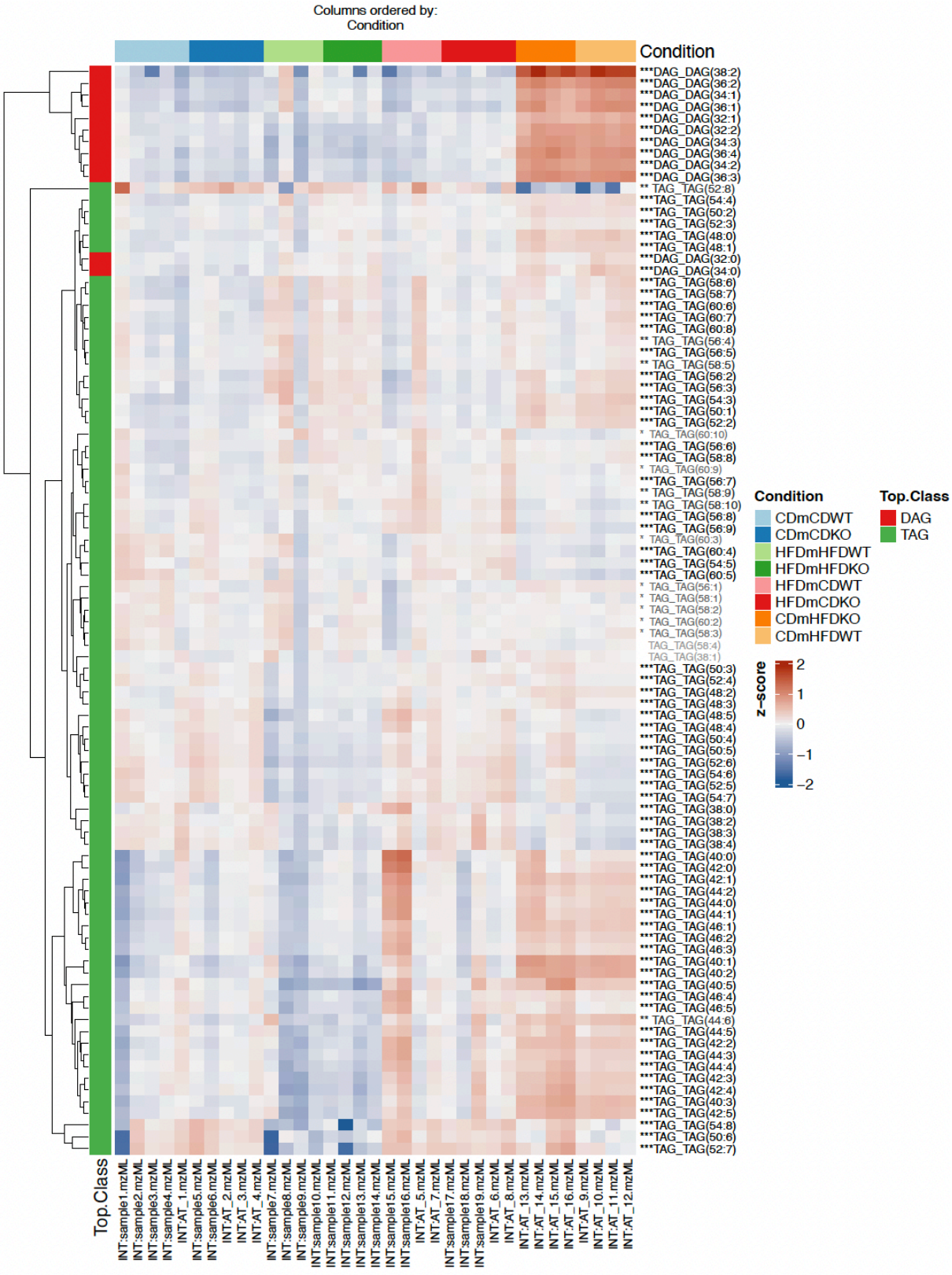

Fig39. Heatmap showing abundance of TAG & DAG identified in gWAT of HIF-1α mice in different dietary conditions, n=4

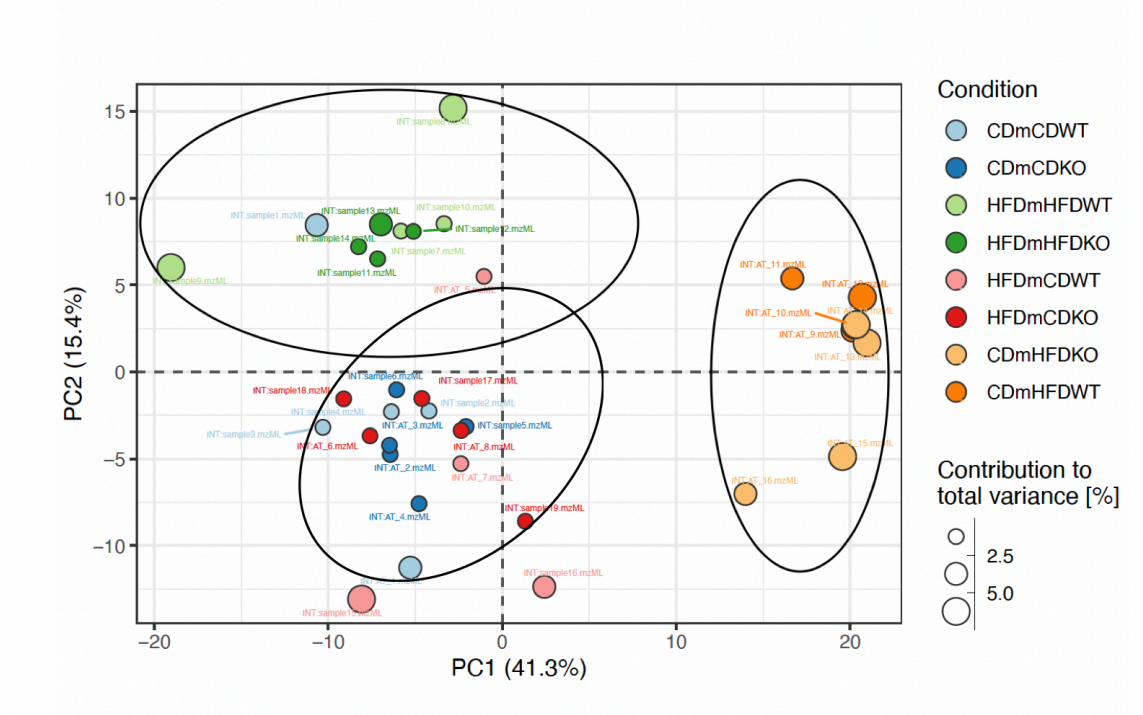

Fig40: PC analysis of the lipidome from gWAT of maternal obese and control groups in HIF-1α mice.

The multivariate (PC) analysis showed 3 main clusters where KO mice from maternal obese group were neighboring with control groups (Fig40). The obese groups formed two other clusters.

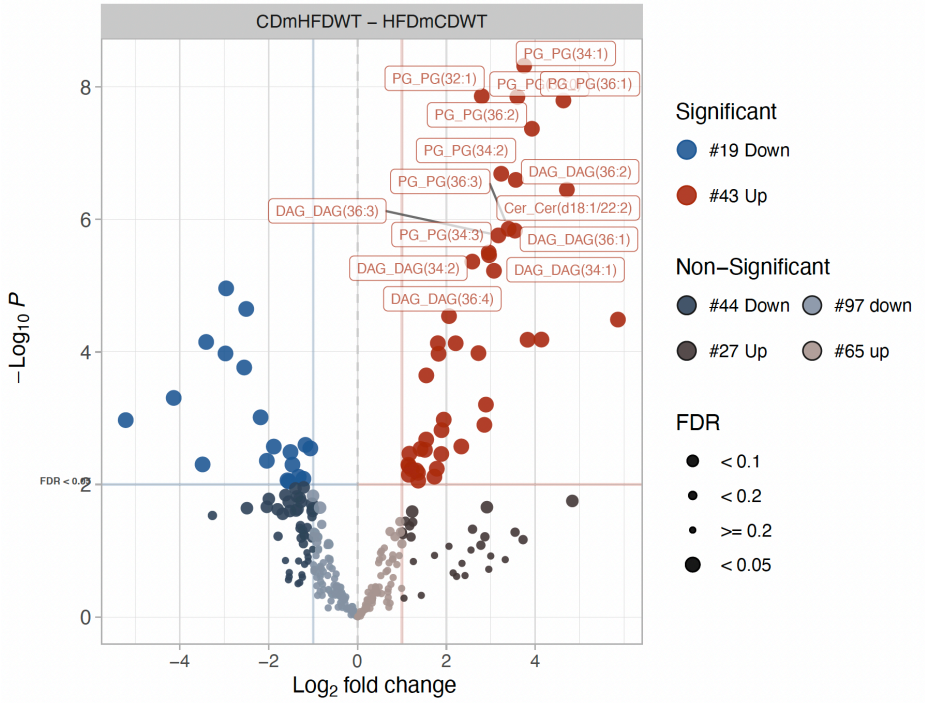

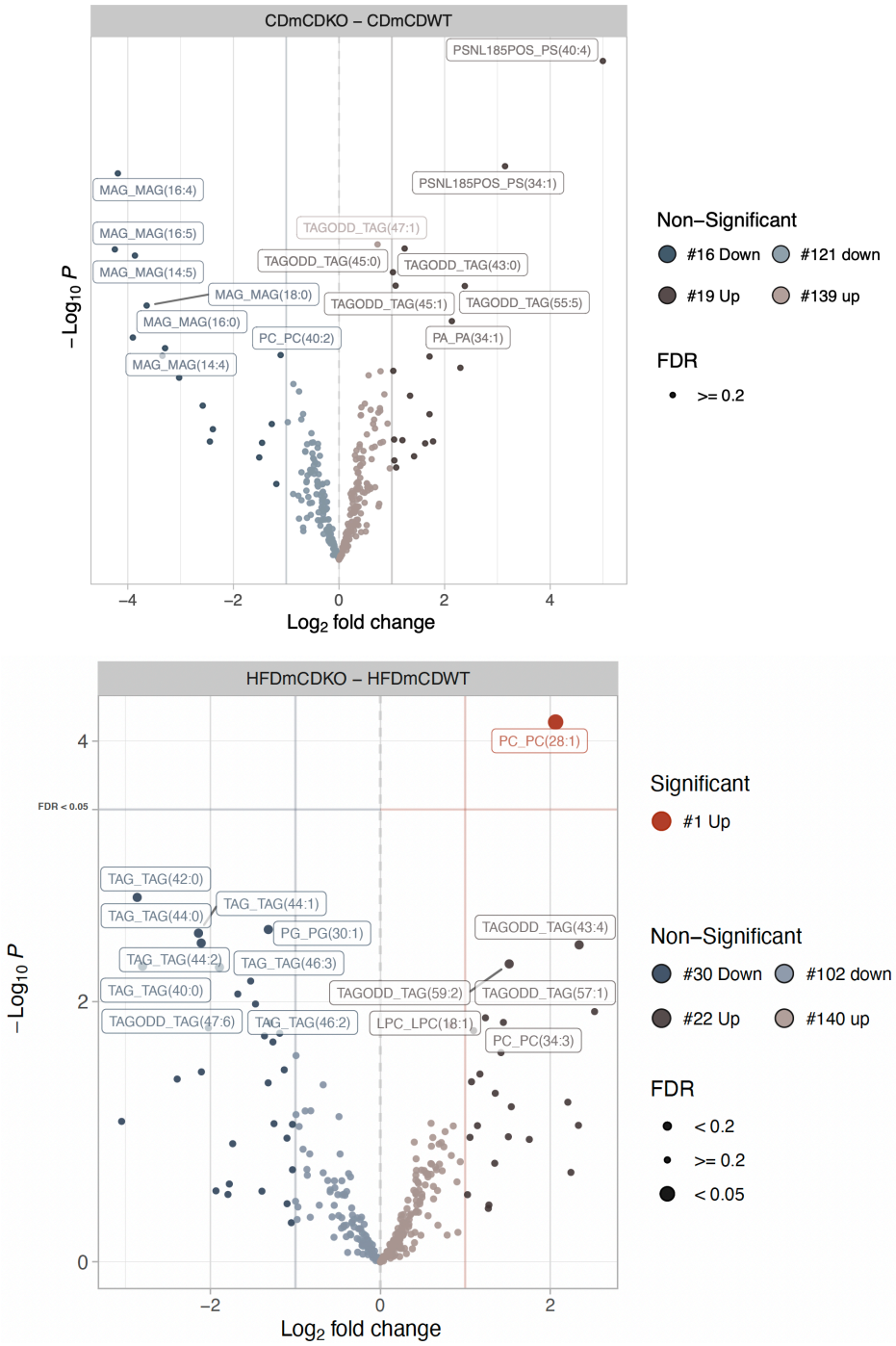

Fig41: Volcano plots displaying differentially expressed lipid species between (a)Control vs maternal Obese group and (b) KO vs WT within control group and (C) KO vs WT within maternal obese group.

The volcano plot displayed significant differential expression of 62 lipid species in between control and maternal obese group, with 43 of them upregulated and 19 of them downregulated. Interestingly, several intermediate and break-down products of TAG were seen to be increase in maternal obese pups compared to control pups. There was no significant change between WT vs KO mice in either control or maternal obese group. Comparison between control and obese groups are shown in the extended data (S4)

4.2.7. APC and macrophage interaction in the gWAT of HIF-1α KO mice

As mentioned earlier, the tissue resident macrophages may start modulating the adipocyte behavior even before their maturity by interacting with adipocyte precursor cells (APCs). Researchers have identified 3 major populations of APCs, P1 or IPCs which are $CD142^-$ $CD55^+$, P2 or committed preadipocytes which are $CD142^-$ $VAP1^+$ and P3 or group3 APCs which are $CD142^+$. The adipogenic potential gradually decreases from P3 to P1. By using flow cytometry panel, it was seen P3 with high adipogenic potential is increased in maternal obese and obese mice in the C57BL/6J mice. In the experiments with HIF-1α mice, this interaction could be identified in obese mice when compared to control(FigS5a,b). Unfortunately, the high cell count required for the analysis could not be achieved in maternal obese mice in repeated experiments.

4.2.8. Pathological HIF-1α signaling results metabolic reprogramming of AT which is rescued by conditional KO of HIF-1α in ATMs

The pathological HIF-1α activation essentially establishes one of the mechanistic pathways which comes into play in the background of maternal obesity. Interestingly, the maternal obese HIF-1α mice were lean, with no significant difference of body or organ weight with the littermate controls. Their abnormal metabolic trait was first noticed subtly in ITT. Though they showed only a slight increase in blood glucose than the controls during GTT, it was quickly reversed by the conditional KO of HIF-1α in macrophages. ITT of the KO maternal obese offspring showed better insulin responsiveness. The remarkable change was seen in the morphology where adipocyte hypertrophy was significant in both gWAT(Visceral) and BAT RIM (subcutaneous) of the maternal obese mice compared to control , which was accompanied by significant crown-like structure formation . This finding was supported by increased influx of the recruited Tim4- macrophages in the tissue microenvironment of the maternal obsess pups. The lipidomics analysis showed lipid class associated with more adipogenic potential in the maternal obese group and the maternal obese KO animals co-localized with control mice in principal component analysis. The rescue of AT hypertrophy and chronic immune activation by conditional KO also strengthen our hypothesis. Altogether these results showed altered HIF-1α signaling is indeed one of the mechanisms behind metabolic reprogramming in the offspring of obese mothers.

4.3. Pathological MYD88 signaling

The recent studies shows the altercation in TLR/IL-1R–MyD88 signaling reprograms cell metabolism in adipocytes, contributing to diet-induced adipose tissue dysfunction and obesity. The current study explores if similar effect is extended in the adipocyte of maternal obese mice .

4.3.1. Body weight and organ weights in MYD88 mice in different dietary groups

The comparison of the body weight and whole organ weight between different dietary groups showed the obese groups had significantly higher body and gWAT weight compared to control, however maternal obese offspring continued to stay phenotypically lean, recapitulating the observation in HIF-1α mice (Fig42a,b). No significant changes in BAT weight could be noted (Fig42c). Comparison of weight gain over time between KO and WT mice within a dietary group showed KO animals gained lower weight compared to WT (Fig42d).

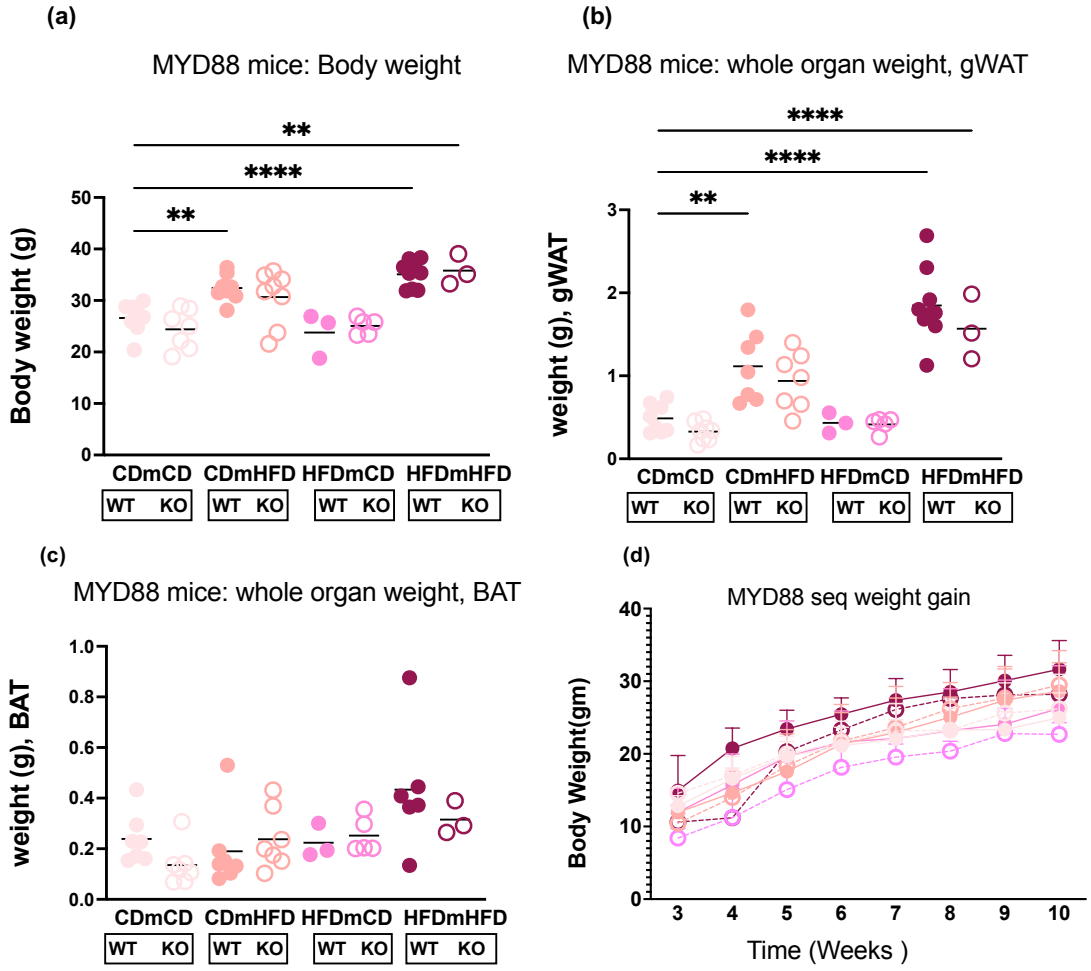

Fig42: **Comparison of body weights and organ weights of MYD88 mice from different dietary groups**

a) Body weight of MYD88 animals from different dietary groups n=3-7 (b) Comparison of whole organ weight of g WAT , n=3-7 & (c) whole organ weight of BAT , n=3-7 (d) weight gain over time in WT mice. P values obtained by one-way ANOVA with Dunnett's multiple comparisons test, *- p<0.05, ** - p < 0.01 , * - p<0.001 , **** - p <0.0001 .**

4.3.2. Quantification of flow cytometry data to assess chronic inflammation in MYD88 mice

Similar to HIF-1α mice, we assessed the chronic inflammatory microenvironment in MYD88 mice. Though not as pronounced as HIF-1α, the results show a mild increase in the recruited macrophages in obese offspring compared to litter-mate controls (Fig44). The macrophage populations in BAT were also explored but no similar influx was detected above the baseline (Fig.S2b).

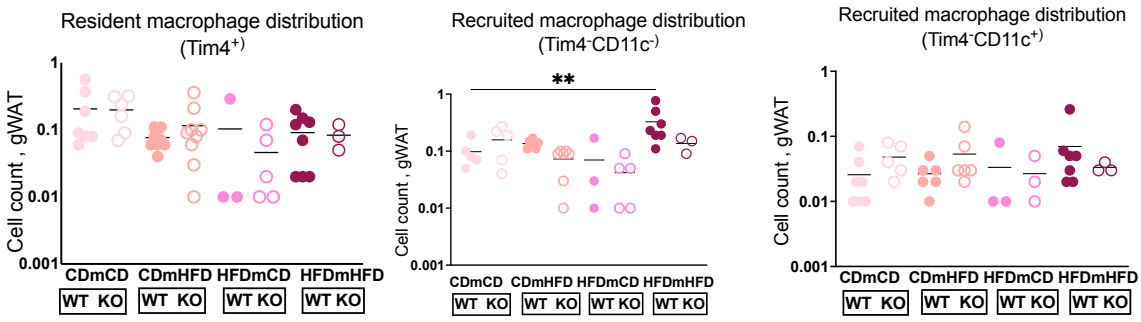

Fig43: Quantification of flow cytometry data of resident vs recruited macrophages in different dietary groups, MYD88 mice n=3-6. p values obtained by one-way ANOVA with Sidak's multiple comparisons test, - p <0.01 .**

4.3.3. UMAP visualization of the flow cytometry data in MYD88 mice

The UMAP clustering of myeloid cells in MYD88 animal in control group recapitulated the observation of HIF-1α mice. In control group the ResMac1 subset was absent in both WT and KO mice, but reappeared in maternal obese group. ResMac 3 subset is a very small group, but persisted across the mouse models including MYD88 mice. In control group, RecMac2 group were depleted with KO while RecMac 1&3 did not show significant changes. In maternal obese group only RecMac 1& monocytes showed minor depletion in KO, while RecMac2&3 showed no visual change. A new $CD9^{+}$ recruited macrophage subset

RecMac4 were noted in both control and maternal obese group which did not significantly change between WT and KO and its significance is not clear.

(a)

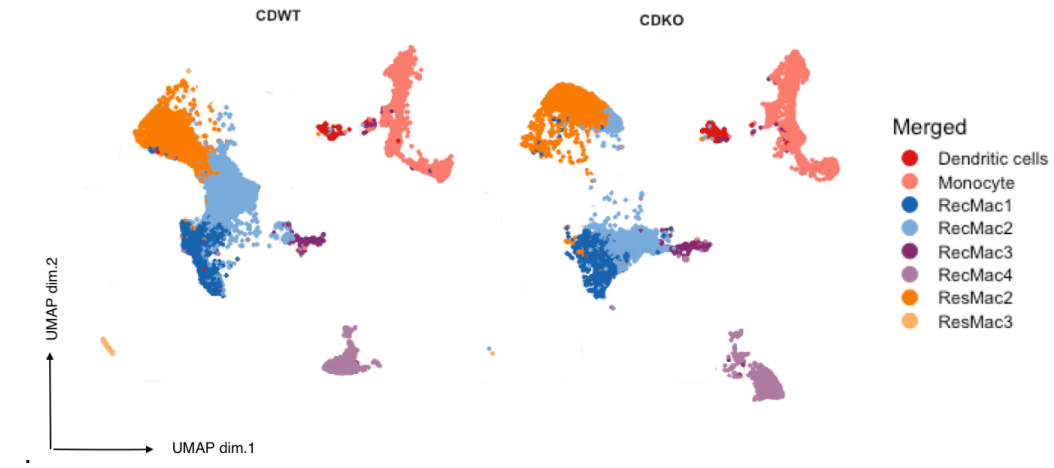

(b)

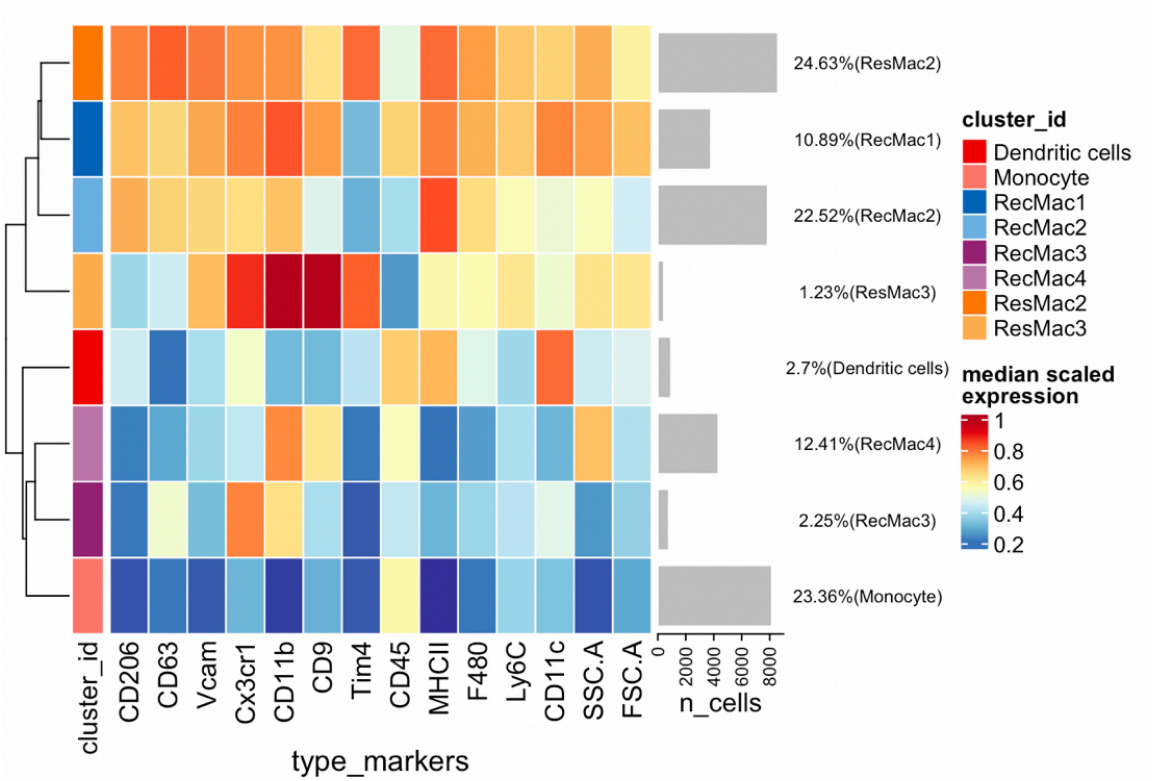

Fig44: UMAP analysis of flow cytometry data showing different macrophage clusters in MYD88 mice, control group WT vs KO

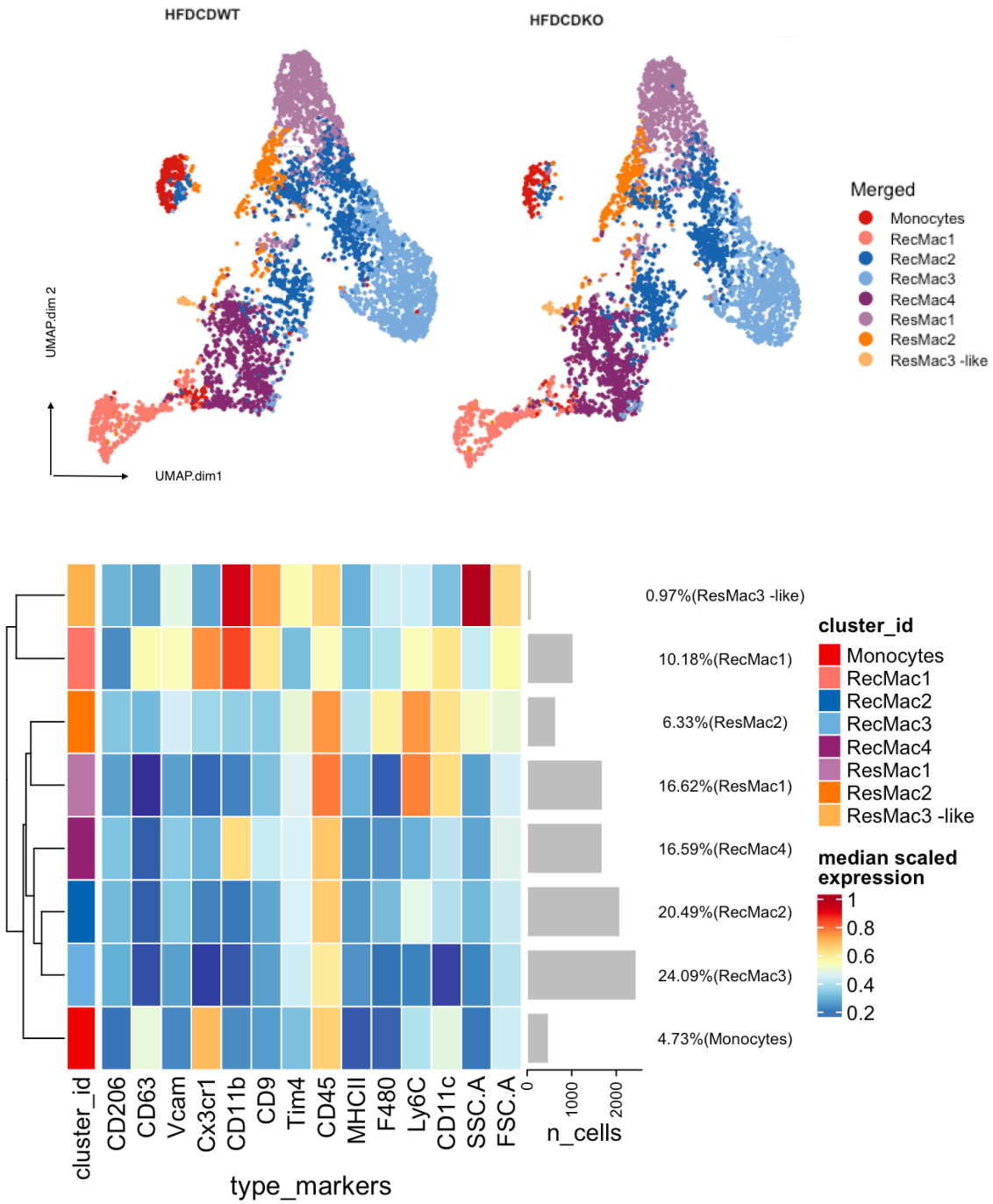

Fig45: UMAP analysis of flow cytometry data showing different macrophage clusters in maternal obese group MYD88 mice, WT vs KO

Overall results of UMAP visualization in MYD88 mice remained inconclusive except minor depletion of monocyte and Tim4$^-$ recruited macrophage in KO mice compared to control. This can be explained by the fact that quantification of macrophages in MYD88 mice showed subtler change than HIF-1α mice in terms of recruited macrophage influx, so the dimension reduction fails to show any visual change (Fig45).

Table 15: Myeloid cell subsets in gWAT in MYD88mice, control group (excluding granulocyte)

Populations	Markers expressed
DC	$CD45^+$ $CD11c^+$ $MHCII^+$
Monocytes	$Ly6c^+$ $CD9^+$
ResMac 2	$Tim4^+$ $CD11c^+$ $MHCII^+$:
ResMac 3	$Tim4^+$ $CD11c^-$ $MHCII^+$
RecMac1	$Tim4^-$ $CD11c^+$ $MHCII^+$
RecMac2	$Tim4^-$ $CD11c^-$ $MHCII^+Ly6c^+$
RecMac3	$Tim4^-$ $CD11c^-$ $MHCII^+$ $Ly6c^-$
RecMac4	$Tim4^-$ $CD11c^-$ $MHCII^-$ $CD9^+$

Table 16: Myeloid subsets in gWAT in MYD88 mice, maternal obese group (excluding granulocytes)

Populations	Markers expressed
DC	$CD45^+$ $CD11c^+$ $MHCII^+$
Monocytes	$F4/80^+$ $Ly6c^+$ $CD9^+$ $MHCII^+$
ResMac 1	$Tim4^+$ $CD11c^+$ $MHCII^-$
ResMac 2	$Tim4^+$ $CD11c^+$ $MHCII^+$
ResMac 3-like	$Tim4^+$ $CD11c^-$ $MHCII^-$
RecMac1	$Tim4^-$ $CD11c^+$ $MHCII^+$
RecMac2	$Tim4^-$ $CD11c^-$ $Ly6c^+$ $CX3CR1^-$
RecMac3	$Tim4^-$ $CD11c^-$ $Ly6c^-$
RecMac4	$Tim4^-$ $CD11c^-$ $MHCII^-$ $CD9^+$

4.3.5. Adipose tissue morphological changes in MYD88 KO mice

Like C57B/L6 mice and HIF-1α mice, the morphology of MYD88 mice was examined. The results looked very similar to the rest and it helped to prove that our hypothesis is consistent across different immune signaling . The morphology is delineated by H&E stain below(Fig46). The control diet mice did not show any difference in size between WT and KO. In all other obese groups, there was an increase in size when compared to control and the hypertrophy was quite nicely rescued by the MYD88 KO. The maternal obese KO offspring showed a distinct phenotype with appearance of lots of small adipocytes which was uniquely observed. We tried to quantify the number of small adipocyte numbers per group, and the results are shown as a discussion point(Fig50). The quantification by (Fiji is just)ImageJ using AdipoQ plugin showed significant increase in size in control vs obese group supporting the morphological observation (Fig 47a).

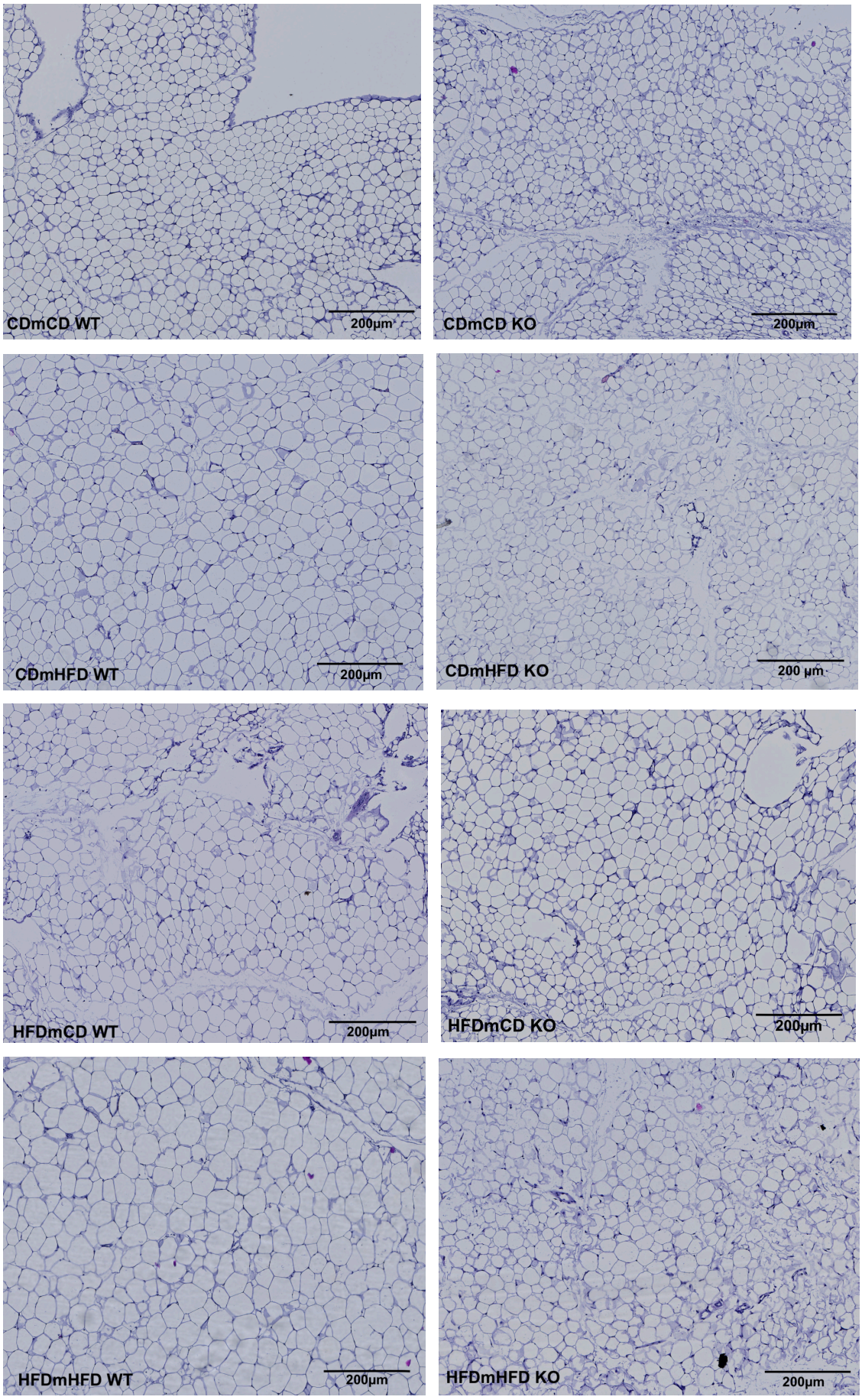
CDmCD WT
200μm
CDmCD KO
200μm
CDmHFD WT
200μm
CDmHFD KO
200 μm
HFDmCD WT
200μm
HFDmCD KO
200μm
HFDmHFD WT
200μm
HFDmHFD KO
200μm

Fig46: Morphological assessment of gWAT on H&E staining of paraffin embedded sections from MYD88 offspring mice, (n=4-6) in different dietary conditions as indicated on the figure.

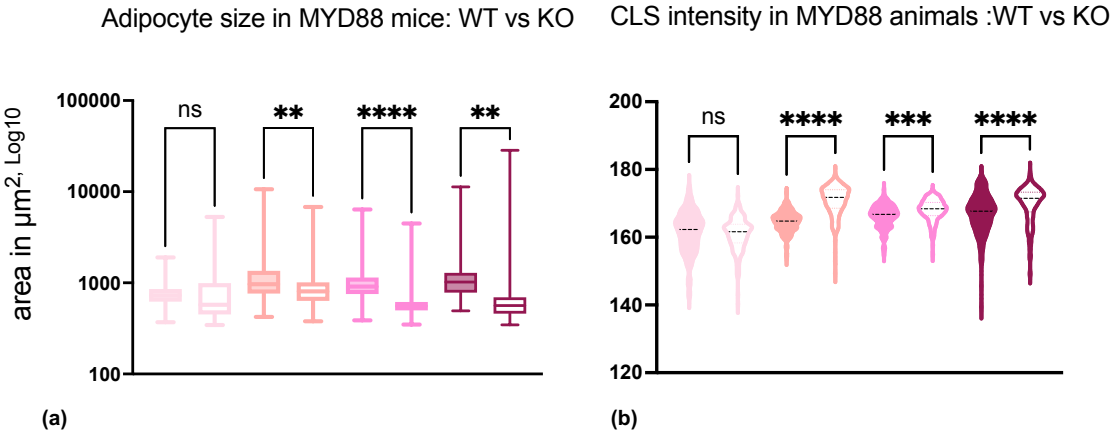

Fig47: Comparative analysis of (a) adipocyte size and (b) Crown like structure intensity in MYD88 mice gWAT among different dietary groups between WT vs KO , p values obtained by one-way ANOVA with Brown-Forsythe test & Bartlett's test, *- p < 0.001, ****- p <0.0001 , ns= nonsignificant , n=4-6.**

4.4 Summary of the results & translational relevance

The overall result over 3 different mouse lines connected through metabolic signaling, consistently shows maternal obesity transmits adverse metabolic effects to the offspring. Activation of certain signaling pathways like HIF-1α or MYD88 signaling are important etiological factors for the same, where even in absence of phenotypical obesity, the underlying microenvironment is insulin resistant and proinflammatory. Macrophage in the adipose tissue and probably in other organs play a central role maintaining the chronic immune activation favorable for metabolic ill-health by infiltrating into the organs or influencing crosstalk locally. Targeting specific macrophage phenotypes or inhibitors of specific immune signaling pathways can provide valuable insight in terms of drug discovery for several immune metabolic diseases like obesity, diabetes mellitus and cancer. To translate the scenario in the clinics, a retrospective study can be designed. A questionnaire on the diet of pregnant mothers having obesity during and before pregnancy or had gestational diabetes in the gynecologist's office can be distributed. Later their children can be monitored for blood glucose, lipid profile and other metabolic tests and compared to the control group from healthy mothers. That can lead to deeper understanding in the clinics without needing significant resources.

5.Discussion

The aim of the thesis was to show the diversity of adipose tissue macrophages brought upon by developmental lineages and if these ATMs reprogram the adipose tissue of the offspring in presence of maternal obesity. Three different mouse models were used to investigate the same: C57BL/6JRccHsd, HIF-1α and MYD88 mouse models. Use of these models explicitly revealed that ontogenic diversity of ATMs exists in the offspring of obese mothers. The presence of such diversity was confirmed by high dimensional flow cytometry. The infiltrating recruited macrophages led to a shift in the metabolic profile of maternal obese offspring towards insulin resistance. Morphological hallmarks of obesity were confirmed by histopathology in those offspring, even when they were phenotypically lean.

Moreover, the next goal was to show if the chronic immune activation has any role in the reprograming of adipose tissue of maternal obese offspring. As macrophage and monocytes are effectors of chronic inflammation, depleting them from targeted tissue would relieve the inflammation, thereby improving the underlying pathology. The offspring of obese mothers had increased macrophage infiltration, adipocyte hypertrophy and formation of crown-like structures. The ATMs in maternal obese pups showed peri-adipocytic inflammatory infiltrates in histology. The morphological changes in the AT were rescued using HIF-1α conditional KO suggesting a mechanism related to immune-metabolic adaptation. Moreover, lipidomic analysis showed co-clustering of lipidome profile of maternal obese HIF-1α KO offspring with that of the control group. This meant the conditional knockout of HIF-1α led back towards lipid homeostasis. These results confirmed that pathologic HIF-1α activation in ATMs is one of the etiological factors for metabolic remodeling of the adipose tissue in offspring of obese mothers. Using a second genetic model targeting MYD88 gene, which is also an activator of HIF-1α, it was possible to recapitulate the morphological changes in AT. Flow cytometry analysis also showed recruited macrophage infiltration to the AT of MYD88 mice, however, in a lesser extent than HIF-1α mice, suggesting it may have an indirect role to the pathogenesis of offspring's metabolic adaptation in the background of maternal obesity. Interestingly, the pathological changes were rescued in Cre positive MYD88 KO mice too, which indicated the role of myeloid cells, specially macrophages (being the predominant myeloid component in AT) in the pathogenesis of maternal obesity induced metabolic syndrome in the offspring .

5.1. Ontogenically different ATMs exist in maternal obese offspring

ATMs are developmentally diverse. Tissue resident macrophages are seen to be already present and maintain themselves within the offspring AT. Line tracing studies in mice showed presence of the tissue resident macrophages'(MΦ) in prenatal stage [138.] On the other hand, the infiltrated short-lived macrophages are recruited from the monocyte derived from bone marrow in metabolically challenged conditions which is also shown by studies on CCR2 [139]. However, none of the earlier studies have addressed the diversity seen in the ATMs of an offspring from an obese mother, especially when it is phenotypically lean or lack any other environmental trigger.

To investigate the macrophage subsets in adipose tissue in the current study, high dimensional flow cytometry was used, which broadly showed two developmentally different macrophage subsets, yolk sac derived resident macrophages which are $Tim4^+$ and monocyte derived recruited macrophages which are $Tim4^-$. Indeed, studies on metabolic reprogramming of skeletal muscle identifies two $Tim4^+$ resident and $Tim4^-$ recruited macrophages in the pathogenesis of muscular dystrophy and parabiosis and line tracing studies confirmed their respective origins[140]. Also, these two subsets have been identified in Kupffer cells which is the tissue specific macrophage for liver in relation to development of non- alcoholic steatohepatitis (NASH)[141]. Similar $Tim4^+$ resident macrophages were also revealed in peritoneal cavity with efficient phagocytic potential[142]. Also the $Tim4^+$ resident macrophages are described in context with cancers with microsatellite instability where they reside in tertiary lymphoid structures facilitating antitumor immunity[143] .

To further deep dive into the ATM subsets from the maternal obese pups, an unbiased clustering was performed on the flow cytometry data for each mouse model with visualization by UMAP. In all 3 mouse models, 3 resident macrophage populations such as $Tim4^+CD11c^+$ $MHCII^-$ (ResMac1), $Tim4^+CD11c^+$ $MHCII^+$ (ResMac2) and $Tim4^+CD11c^-$ $MHCII^+$ ((ResMac3) were found. While ResMac1 was marginally expressed or absent in the control mice, it were observed consistently in the maternal obese pups in all mouse models. It is possible that this particular resident subset proliferated locally in maternal obesity and helped initiate the cascade of events for the pathogenesis of maternal obesity induced metabolic syndrome in offspring. However, this possibility has to be tested further using different methods and ultimately to be confirmed by fate mapping studies. In HIF-1α & MYD88 mice, the resident macrophages additionally showed differential expression of $CD206^+$. It is plausible that a

significant subset of resident macrophages are $CD206^+$ as they are dispersed between blood vessels and adipose epithelial cells in a well vascularized AT in steady state[144]. A study using single cell proteomics reveals eight $CD206^+$ and two $CD206^-$ resident ATM populations defined by Tim4, CD163 & MHCII[145]. In steady state, two different populations of resident macrophages were also described depending on their CD11c positivity in salivary glands, and the $CD11c^+$ resident macrophages were regarded to develop postnatally[146] . In single cell RNA sequencing, resident ATMs can show quite heterogeneous subsets, however, they hold onto their Tim4 positivity [140,143, 145,147,148] .Consistent across all three mouse lines, when compared between control and maternal obese group, the resident macrophages maintained their overall counts though minor shifts within phenotypes could be observed. The significance of specific subset identified in maternal obese group in genetic mouse model and its possible translational importance remains to be confirmed by gene expression profiling.

Among recruited macrophages, 2 recruited macrophage subsets $Tim4^-CD11c^+$ (RecMac1) and $Tim4^-CD11c^-MHCII^+$ (RecMac2) were found in C57BL/6JRccHsd mice which infiltrated the AT of maternal obese pups. When the panel was expanded, there were 3 subsets of recruited macrophages considering Ly6C expression. 2 subsets $Tim4^-CD11c^-MHCII^+Ly6C^+$ (RecMac2) and $Tim4^-CD11c^-MHCII^+Ly6C^-$ (RecMac3) in HIF-1α mice, which was seen to MYD88 mice as well. A fourth population uniquely arose in MYD88 mice which was $Tim4^-CD11c^-MHCII^-CD9^+$ (RecMac4). Among these $Tim4^-$ recruited macrophage phenotypes, differential expression of, CD9, CD63 and Cx3CR1 were noted in different intensities. A recent single cell sequencing of human WAT showed 3 different macrophage population based on CD206 and CD11c positivity : $CD206^+$ $CD11c^+$ $CD9^+$ (LAM), $CD206^+$ $CD11c^-$ perivascular macrophage and $CD206^-$ $CD11c^+$ IM where LAM and IM were particularly associated with obesity[149]. Interestingly, our RecMac1 in HIF-1α mice mimicked LAM and RecMac1 in MYD88 mice resonated IM in maternal obese group. RecMac2 &RecMac3 in both mouse model were similar to the perivascular macrophage profile and unlike the human study, they were also associated with obesity in the current study. This difference can be due to species specific differences in mice model and in human. Moreover, human WAT resident macrophages are still not well defined. A monocyte-independent primitive wave in early yolk sac has been identified from the macrophages sampled from liver, lung, skin and head of aborted human embryos by single cell RNA sequencing (scRNA-seq) on the CD45+ hematopoietic cell population, but in adipose tissue [150]. It clearly point towards for an unmet need for more studies focusing particularly on adipose tissue reprogramming by ATMs. The recruited macrophages showed influx in case of obese and maternal obese group in various extents

but consistently across the mouse models. These observations justifies further studies to be oriented around 3 main ATM phenotypes, such as Tim4^{+} residents and Tim4^{-} CD11c^{-} and Tim4^{-} CD11c^{+} recruited macrophages as their functions are well-defined in the pathogenesis of obesity[53] (Fig48).

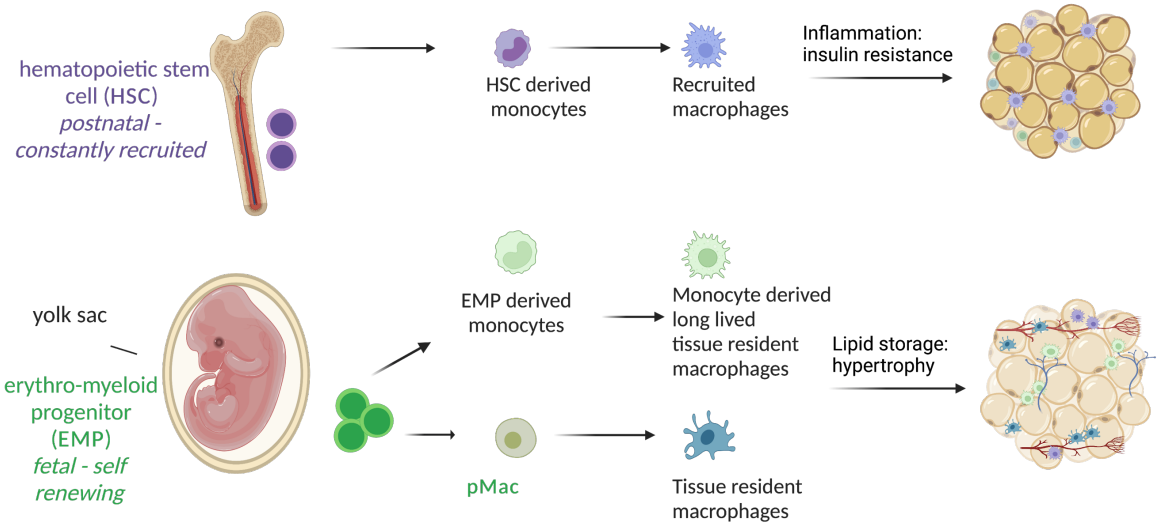

Fig48. Specific functional commitment for ontogenically diverse ATMs.

5.2. ATMs reprogram adipose tissue of offspring with maternal obesity

Obesity is traditionally marked by adipose tissue expansion [151], however, it is not that simple! Development of obesity is orchestrated by much more complex interaction between adipocyte and immune cell in cellular level and adipose tissue remodeling in tissular level. It cannot be explained simply by measurement of BMI or increase of body weight anymore[152]. In fact I observed, while both the obese and maternal obese offspring showed increase in body weight and whole organ weight (gWAT) in C57BL/6JRccHsd mice (Fig18a-c), the HIF1a and MYD88 maternal obsess mice did not show significant change of body weight or the gWAT organ weight when compared to the control pups at P76 time point (Fig 24 a-d, Fig42 a-d). It can be due to the fact '*microscopic obesity'* precedes the phenotypical manifestation in more subtle etiology like transgenerational obesity. It is also possible that using other time-tested and new indicators like Lee index, body water measurement, radiological imaging etc. can give a more correct measurement of adipose content in rodents. rather than only measuring body weight & organ weight, [152,153].

Obesity is primarily characterized by innate immune system induced inflmmation[154]. Obese adipose tissue shows meta-inflammation which is orchestrated by the infiltration of bone marrow derived monocytes and macrophages[26,139,155] . The flow cytometry data showed an increase recruited macrophages influx in obese and maternal obese groups while resident macrophages maintained themselves in the ATME, compared to control. In the C67BL/6J mice, both $Tim4^{-}CD11c^{-}$ & $Tim4^{-}CD11c^{+}$ show an infiltration (Fig19)while in HIF-1α mice, $Tim4^{-}CD11c^{-}$ showed most prominent increase (Fig30). In MYD88 mice the infiltration is much subtle It is worth noting, the number of resident macrophages did not significantly changes in obesity or it may even have increased initially due to local proliferation[156], but due to infiltration by bone marrow derived macrophages in obese mice, percentage of $Tim4^{+}$ macrophages got diluted over time and may seem significantly lower by the time mice reached adulthood. On the other hand the maternal obese pups shows the infiltration of recruited macrophage in a slower rate than an obese offspring. It is not pinpointed what triggers the recruitment of macrophages, but seems to be multifactorial. In ATME, adipose tissue macrophages regulates the lipid uptake[59] and scavenges dead adipocytes to maintain a low annual adipocyte turnover (10%)[57,157]. Due to this low turnover, when there is excess dietary calorie intake, adipocytes undergoes hypertrophy. As the adipocytes starts expanding their size to accommodate more lipid production from excess nutrition, the vasculature can no longer serve increased surface areas, leading to death of some adipocytes, which is a major trigger of adipocyte recruitment[46,72]. It is also proposed that high fat induced EGFR activation leads to proliferation and infiltration of ATMs[156]. Further, diet induced modulation of chromatin remodeling checkpoints can also leads to macrophage recruitment in the obese adipose tissue[158]. These infiltrated macrophages are responsible for inflammation and insulin resistance in the obese adipose tissue [47,139,159-164], as shown by altered GTT and ITT in the obese and maternal obese offspring.

Once it was established by flow cytometry data that specific macrophages are recruited to modulate AT in maternal obese mice, it was necessary to confirm morphological features of metabolic syndrome by histopathology at the tissular level . As mentioned earlier, the hallmark of obese adipose tissue are chronic low-grade inflammation, adipocyte hypertrophy due excessive lipid storage and accumulation of macrophages in the form crown like structures. All these features were noted in obese as well as maternal obese mice in this study. The exact timeline of the events is not so clear, but one may overlap another. Live imaging approaches at single cell resolution showed three events , normal lipid uptake taking average 36 hours,

remnant uptake after death of a storage adipocyte taking few days and no uptake but CLS formation around the whole remnant taking around 48 hours[165]. It is therefore plausible that developmentally reprogrammed resident macrophages induce the adipocyte hypertrophy in maternal obese pups in absence of environmental stimulus such as high fat diet which generally led to excessive fat accumulation in an obese pup. Indeed, maternal obesity programs a heightened capacity of fat storage in adipocytes[166]. Moreover, maternal HFD induced obesity causes insulin resistance before development of obesity by reducing AT insulin signaling protein IRS1[167], which justifies that in our study, microscopic obesity preceded phenotypical weight gain in maternal obese pups. Indeed, maternal obese pups responded to insulin slower than the control group (Fig26). Long term dysregulation of appetite is also observed in the offspring from obese mothers due to reprograming of the hypothalamus-adipose axis caused by hypomethylation of leptin promoter and it causes leptin mediated adipogenesis in them [168-171]. Parabiosis experiments shows adipocyte death leads to metabolic activation of resident ATMs even in lean mice[155]. This activated ATMs promote adipocyte hypertrophy, to accommodate increase amount of fuel leading to an enlarged tissue mass with fewer larger adipocyte, initially as a rescue mechanism. But it leads to capillary rarefication, depletion of multipotent progenitors for angiogenesis leading to pockets of hypoxia[172]. The faulty angiogenesis in obese adipose tissue is one of the keys for AT remodeling. This hypoxic environment leads to adipocyte deaths and resident macrophages again take the wheel by presenting signals through different immune signaling pathways and attracting monocytes and BM derived macrophages into action.

The macrophage has tropism for hypoxic environment[131,132] . Mincle is a type II membrane protein present in macrophages which is a sensor for dead cells in vitro and expressed exclusively in the CLS macrophages under the control of TLR4 signaling[173,174].This is interesting as TLR4 axis directly activates MYD88 signaling. This facilitates the recruited macrophage to get there and attempt to localize the inflammatory process as well as fibrogenesis[175]. Fibrogenesis also trigger more hypertrophy in AT[174,175] contributing to the vicious cycle. The infiltrated macrophages surrounds the debris, released lipid droplets and dead adipocytes to form crown-like structures (CLS). These macrophages express CD64 ,CD11c, CD9 and sometimes TREM2[165] confirming their HSC derived nature. In the current study, the CLS intensity (which is inversely proportional to actual CLS formation) was higher in control and went down in obese and maternal obese offspring, indicating more CLS formation by recruited macrophages in the maternal obese & obese pups. This modulation of CLS was consistently noted in both HIF-1α and MYD88 mice (Fig33 and Fig47b). The quantification was exploratory, but substantiated by morphological demonstration of CLS-

density correlation. CLS density is shown as an important predictive tool for cardiovascular diseases in human epicardial adipose tissue[176]. CLS formation is a vital change in obese environment as it can promote ectopic lipid deposition in liver. Metabolic stress built from lipid accumulation works as part of ' multiple parallel hits' for developing NASH from fatty liver [177]. Finally, the CLS macrophages are HIF-1α activated macrophages. This is proven as ERß agonists helps to reduce CLS formation and inhibits activation of CLS macrophages by inhibiting HIF-1α through PHD2/HIF-1α axis in mice[178]. Thus more CLS formation in maternal obese pups compared to the control ones in the current study, indicated the ATME was hypoxic in maternal obese mice with probable HIF-1α and MYD88 activation in the ATMs.

5.3. Pathological activation of immune-metabolic signaling pathways enables AT reprogramming by ATMs in maternal obese mice

As it was established that ontogenic heterogeneity of the ATMs led to reprogramming of AT, the next focus was to determine the basis of this reprogramming by promoters of chronic immune activation. The ATME is an ideal ground for epithelial-immune interaction and molecular events can precede the phenotypic manifestation of disease. At the onset of obesity, it is rational to think that adipocytes macrophage interaction is limited with resident macrophage as recruitment of macrophages followed several events. On excess calorie intake, first AT response is trying to accommodate by adipocyte hypertrophy leading to insufficient angiogenesis and hypoxia and direct activation of HIF-1α[117,179,180]. Understandably, both HIF-1α & MYD88 signaling pathways are activated in the resident macrophages in early onset of adipocyte hypertrophy, followed by more cytokine release, CLS formation and attraction of recruited macrophages in the ATME. The failed storage system leads adipocytes to release free fatty acids, which interacts with TLR4 signaling and activates nuclear factor kappa-light chain enhancer of activated B cells (NF-κB) in resident macrophages[181] through MYD88 activation. On the other hand, the infiltrated recruited macrophages around CLS express mincle which is also modulated by TLR-4 pathway [173]. At the same time, CLS formation can be directly dependent on the HIF-1α in the later stage of obesity[103]. Resident macrophages release cytokines specially TNF-α, IL-6, IL-4, IL-10 etc. leads to insulin resistance by downregulating glucose transporter 4 (GLUT-4) and Insulin receptor substrate 1 (IRS-1)[182] . These studies point towards the role of HIF-1α and MYD88 activation in obese adipose tissue, but whether these two signaling pathways prime the ATMs for AT remodeling in offspring with obese mothers, that has not been demonstrated directly on mice or human. The current study showed all the morphological features of obesity in mice

gWAT at tissue level and rescue of these morphological features in LysM$^{Cre/+}$ HIF-1$\alpha^{f/f}$ and Rank$^{Cre/+}$ MYD88$^{f/f}$ mice. Further, the knock-out HIF-1α pups with maternal obesity showed comparable glucose tolerance and insulin sensitivity with control pups . The adipocyte size in the knockout mice in maternal obese group was comparable to that of the control (WT) group in both genetic models. In the obese group, the knock-out also showed a reduction in adipocyte size but mixed with bigger adipocytes. Interestingly, many small adipocytes of diameter around 30-80 µm were present in knock-out maternal obese pups and also sometimes in obese pups, whose significance is not yet clear (Fig 49), though study showed that increased number of small sized adipocytes and the decreased number of larger ones in white adipose tissues could be an important mechanism of normalization for increased TNF-alpha and plasma lipids, leading to alleviation of insulin resistance[183]. The adaptation of cellular size modifies metabolic function possibly through beta(1) integrin/ERKs signaling pathway by changing cell and ECM relationships[184]. Lastly, in type-2 diabetes patients, the adipocyte numbers remained low from disease to treatment where no depletion of small adipocytes were noted[185]. Understandably, more research regarding expanding small fat cells, recruitment of new fat will be needed to conclude the significance of this finding[39].

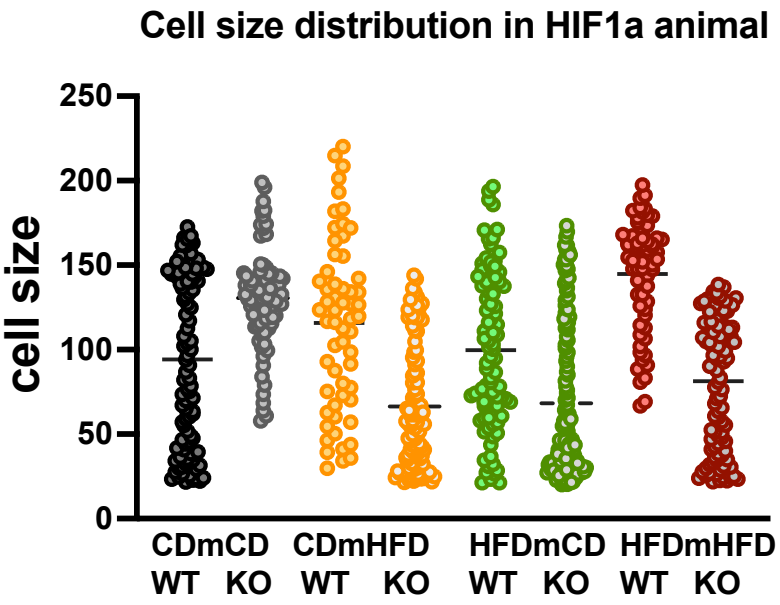

Fig49: Frequency of smaller cells in HIF-1α mice

Taken together, not only I observed the alleviation of adipocyte hypertrophy in knock-out mice compared to control, the CLS formation was also noticeably lower in these knock-out mice compared to the Cre-negative mice in between the same dietary group, as noted by morphology as well as quantification. When adipocyte area, volume and diameter are

quantified, the knock-out pups from maternal obese and obese group showed significant improvement over the WT mice confirming the role of HIF-1α activated ATMs in AT remodeling. Activation of macrophage by HIF-1α has been also noted in dermal adipose tissue [186]. Capability of HIF-1α to induce fibrosis in AT instead of adequate angiogenesis at the onset of obesity [187] or to potentiate FFA induced production of IL-6 and IL-1ß from hypoxic macrophages enriching primary human adipocytes [188] can be different ways of activated macrophages to remodel AT in obesity.

In case of MYD88 mice , the adipocyte size in knock-out mice was relatively comparable to control and much lower to the larger size observed in WT mice of obese and maternal obese group. Thus MYD88 signaling could also be implicated in the activation of ATMs in AT reprogramming. Indeed, similar effects could be observed in other organs. MusMyD88$^{-/-}$ p mice were protected from inactivity induced adiposity while knocking out MYD88 inhibitor miR146a exacerbated weight gain and insulin resistance[189]. Astrocyte-specific Myd88 KO mice improved HFD & saturated free fatty acid induced reactive gliosis and inflammation[122].

Added to this, the increased number of recruited macrophages seen the adipose stroma in obese and maternal obese pups compared to control, was absent in the knock-out mice or only showed minor elevation than steady state. In the UMAP visualization there was no visible difference of the macrophage subsets between the Control group WT and KO, both in HIF-1α and MYD88 mice . However, while comparing the WT and KO pups in maternal obese group, HIF-1α KO mice showed complete depletion of one recruited macrophage subset RecMac3(Tim4^{-} CD11c^{-} MHCII^{+} Ly6c^{-}CX3CR1^{+}), reduction of another recruited subset RecMac2 (Tim4^{-} CD11c^{-} MHCII^{+}Ly6c^{+}CX3CR1^{-}); one last recruited subset RecMac1 (Tim4^{-} CD11c^{+} MHCII^{+}) was unchanged. In MYD88 KO mice, the rescue by KO is more subtle and only mild reduction of RecMac1 (Tim4^{-} CD11c^{+} MHCII^{+}) and RecMac3 (Tim4^{-} CD11c^{-} Ly6c^{-}) were noted compared to WT in maternal obese group while RecMac2&4 subsets remained unaltered. Overall the findings agreed with the fact that, recruited macrophages infiltrate the adipose tissue in obesity[190] similar to monocyte and bone marrow precursor derived macrophages infiltrating hepatic parenchyma during NASH[191]. Indeed, Tim4^{-} macrophages are replenished from blood as seen in smooth muscle in muscular dystrophy[140]. It is noted that small lipid debris after adipocyte death can activate TLR-4-MYD88 pathways, thereby MYD88 can influence the macrophage recruitment in AT[181]. Also saturated FFA mediated activation of TLR4-MYD88-NF-kB activates resident macrophage to release MCP1, and promote monocyte recruitment[164,192,193]. As already discussed in the context of CLS formation, HIF-1α can directly

recruit macrophages in the site of hypoxia. Thus these signaling pathways could influence the recruitment of macrophages in ATME in steady state and obesity.

The resident macrophages maintained their population between WT and KO in both mouse model. As mentioned earlier, one particular resident subset,ResMac1 ($Tim4^+$ $CD11c^+$ $MHCII^-$) was seen to be marginal or absent in control group and consistently came back in maternal obese group in all three mouse models. Whether HIF-1α or MYD88 influences such shift could not be determined, as both WT & KO maternal obese mice displayed this population without much change in between. However, if further studies confirm the consistency of existence of ResMac1, then contribution of either of the signaling pathways in their occurrence or proliferation has to be explored in future.

Maternal HFD modulates the TAG profile in offspring in AT depot and sex dependent manner [95] . As HIF-1α mice showed more recruited macrophage infiltration in flow cytometry and prominent CLS formation in histology, I chose this genetic model to explore the modulation of lipidome by maternal obesity. In the anslysis from 14 major lipid classes which passed the QC check, showed relative abundance of TAG in the maternal obese pups but decrease in sphingolipids(SM) and no change of glycerophospholipids (PC, PE, PS) compared to control, which does not exactly match the selective enrichment of lipid classes such as TAG, glycerophospholipids, and sphingolipids in AT obtained from obese human individuals[194]. Interestingly, TAG, glycerophospholipids (PG, PS) and SM did enrich in obese pups without maternal obesity. It might happen because the human study showed whole spectrum, but no discretion was made between the obese individuals having obese and non-obese mothers. The HIF-1α KO mice resonates the lipidome of control mice in terms of lipid classes.

TAGs is most important lipid species in AT lipidome constituting 99% in healthy individuals[195]. Further analysis on TAG &DAG on gWAT lipidome was performed as TAG was enriched on maternal obese pups and even they are not the signaling molecules, the breakdown or intermediate products of TAG such as FFA, DAG etc. may interfere with insulin signaling pathways to establish insulin resistance in obesity[196]. Among the TAGs found decreased or less abundant in maternal obese pups, TAG(56.1) is negatively correlated with IL-6[197]. TAG association between insulin sensitive, insulin resistance and Type2DM patients showed C40:2, C46:4, C48:5, C48:4, C38:1, C50:3 TAGs were significantly decreased in T2DM compared to other two groups and C56:3, C56:4, C56:7 and C58:7 was increased. No significant difference in TAGs was noted between insulin sensitive and resistant patients[198]. Though I did not observe exactly same lipid species to be changed in the obese groups, that could be due to specific dietary components[199] used among study groups and among species.

The volcano plots did not any significant change between KO and WT mice suggesting that HIF-1α may not be the sole influencer of the lipidome in metabolically challenged conditions like obesity.However, several DAG, PG and CER species were enriched in maternal obese group which has been also seen in HFD induced obese mice[200]. This topic remained less explored and an unmet need for further research on AT lipidome in relation to maternal obesity and insulin resistance exists. While no differences in TAG profile were noted between HIF-1α WT and KO mice within different conditions, maternal obese KO showed proximity with control group in PCA. This may indicate possible role of conditional KO of HIF-1α in ATMs in shifting the lipidome towards steady state, but it is too soon to conclude the same. Enriched ontology analysis of gene screened from LIPID Metabolites And Pathways Strategy (https://www.lipidmaps.org/tools/ms) a multi-institutional database for large number of globally used lipidomics resources) connecting transcriptome with the lipidome [95, 201] of maternal obese mice with deep profiling of adipose tissue-specific lipidomes are needed for understanding of tissue-/organ-specific lipid remodeling mechanisms[202].

Studies in male offspring shows whitening of the BAT and expansion of WAT[95]. While I could not find significant changes in the BAT, the posterior subcutaneous WAT surrounding the BAT showed signs of 'microscopic obesity' i.e. morphological features consistent with obese ATME. The adipocytes in maternal obese and obese group showed hypertrophy which was rescued by KO of HIF-1α. While several studies showed BAT whitening is associated with adverse metabolic effects[203-205], the uniquely observe adipocyte hypertrophy in BAT RIM in this study confirmed the extension of obese micro-environment maternal obesity and could be related to an early onset obesity [206].

Further, I used H&E staining as it has tremendous role in morphological identification and applying machine learning for quantification, but it often falls short to give the context of the spatio-temporal relationship of the cells and matrix in a single tissue. So to dig deeper, I tried multiplex IHC via CODEX (now Phenocyclar) to explore the morphological landscape of adipocyte and macrophages in the same tissue section. The maternal obese gWAT showed an increased influx of F4/80+ Tim4- MHCII+ macrophage infiltration (Fig 50). This concept is completely new in terms of adipose tissue and macrophage microenvironment and not a single study found in PubMed search till May2023 exploring ATME by multiplex IHC. While I did not perform the quantification for multiplexed data, it can be paired with some machine learning techniques to establish plottable quantification from the ATME to give new insight. However, one should keep in mind that AT is a delicate organ in terms of tissue handling and repeated washing used for multiplexing can be damaging to the tissue architecture losing the purpose of spatiotemporal analysis on the process. Additionally, regular IHC can be done in FFPE

tissue as duplex, which is easier, cheaper and can be valuable tool for highlighting interaction between two parties such as adipocytes and macrophages.

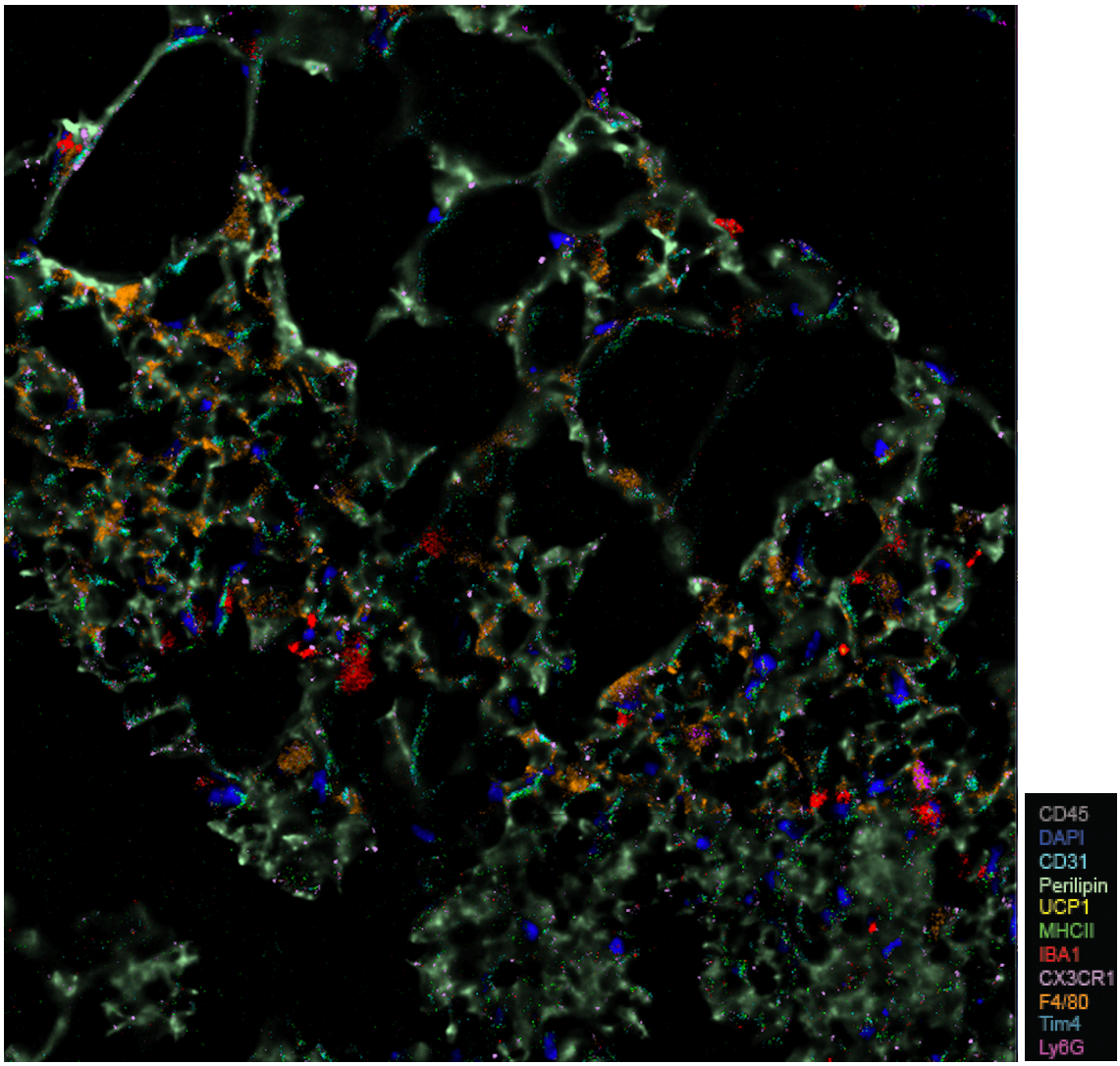

Fig50: Spatiotemporal relation of macrophage with white adipocyte in maternal obese HIF-1a mice, 11 weeks old

Taken together, I could confirm that activation of these two signaling pathways contributes mechanistically in the AT remodeling by ATMs in the pups of obese mothers. Indeed, HIF-1α reprogram myeloid cells in different disease settings such as human monocytes in chronic immune activation in sepsis[207] or mice macrophages in ischemic muscle remodeling[208]. While these studies supported my findings, observation by Lily Boutens and colleagues that HIF-1α does not contribute in the pathogenesis of obesity in early stage[209] was contrary to the current study. Further, Intestinal epithelial cell specific MYD88 KO shown to protect partially against

diet induced obesity and inflmmation[121], but with Rank$^{Cre/+}$ MYD88$^{f/f}$ mice, I could observe an overall improvement on the metabolic profiles of maternal obese and obese pups.

5.4. Maternal Obesity passes on adverse metabolic signature to the offspring

Scientists have recently started exploring the consequences of maternal diet induced obesity on offspring's metabolic life in adulthood. Maternal obesity affects offspring's predisposition to obesity[210-214]. It helps to orchestrate the inflammatory milieu by increased proinflammatory cytokines and gut microbiota dysbiosis[215]. Not only that, two studies showed maternal obesity can contribute to endoplasmic reticulum stress, increase adipocyte size and reprograms adipose tissue transcriptome and lipidome [216,217]. Though several animal models have been studied for mimicking maternal obesity model, mice and rats are most widely used due to their resemblance with human physiology and their short life span to cover transgenerational studies[218]. The current study used all mice with C57BL/6J background, as most appropriate mouse strain for diet induced study are C57BL/6J and its substrains[219] where HFD elicits all metabolic events seen in human such as obesity, hyperinsulinemia , hypertension, diabetes mellitus etc. and CD keeps them lean making them the choice for obesity studies[220-224],
Mice offspring with high-fat high-sucrose maternal and postnatal diet showed obesity and insulin resistance with hypothalamic POMC gene modulation and gut microbiota modulation [225,226]. The effect of maternal obesity is also noted in perivascular adipose tissue by modulating their anticontractile effect[227]. Moreover, maternal HFD has shown to cause adipocyte hypertrophy in offspring without increased adipocyte count[228], thereby driving towards unhealthy obesity without modifying adipogenesis. However, while observational studies started to show these effects, the mechanistic behind transmission of metabolic disease to next generation remains unclear.

Few different hypotheses have been described to address the mechanism of maternal obesity related diseases in offspring with more attention to epigenetic modification and chronic immune activation. Zfp423 promoter methylation in tissue of the offspring of obese dams has been discussed in this context[229]. Alteration of fetal microbiome due to maternal obesity are emerging as one of the mechanisms to long term metabolic and neurologic abnormality in the offspring[230-232]. A recent clinical trial (Clinicaltrials.gov NCT01131117) suggested modulation of fetal gut microbiome by maternal obesity can be one of the predictive indicators for adiposity in later infancy[230]. Though no studies have directly showed HIF-1α activated macrophages to reprogram AT in maternal obese pups, but chronic hypoxic stress has been associated with inflammatory reaction in placenta of gestational diabetic mothers[233]. Male pups from obese dams postnatally treated with HFD had increased CD11c^{-} resident macrophages in

subcutaneous and gWAT [213], mimicked our obese group (HFDmHFD). The current study points towards chronic immune activation as underlying mechanism in maternal obesity related AT pathology in offspring. ATMs drives the central role in AT reprograming in the pups from HFD dams using three different mouse models. I could show that the ATMs remodel the offspring's AT by activation of HIF-1α signaling pathway with contribution from the TLR4-MYD88 signaling in case of maternal obesity. Maternal obesity enhanced cytokine expression in large intestine of offspring, specially TGF-ß and IL-17 which points towards macrophages[234]. Indeed, cytokine profiling by my colleague Iva Spichalova on maternal obese vs control pups showed increased level of several cytokines like IL-1α, CXCL1, IL-7Rα, IL-22, CCL-7 (Tab 17).

Table 17: Cytokine panel for different dietary group in HIF-1α mice

Cytokine Panel for different dietary group, HIF-1α mice														
	CXCL5	CCL11	CSF3	CXCL1	IL-1α	IL-1ß	IL-2R	IL-7Ra	CTLA-8	IL-18	IL-22	IL-23	CCL-2	CCL-7
CDmCD	796	287	4	10	6	6	21	41	3	119	10	48	11	27
CDmHFD	733	227	2	4	9	3	8	50	5	60	4	22	4	29
HFDmCD	626	267	3	14	7	4	17	52	2	107	12	13	10	33
HFDmHFD	365	236	7	18	14	8	13	123	4	151	7	22	9	39

In the fetal monocyte and resident macrophages, translocation of NF-κB and chromatin accessibility at pro-inflammatory gene promoters following TLR stimulation are attenuated by maternal obesity in rhesus macaque pointing towards the MYD88 pathway[235]. Further. Maternal HFD increases noncanonical caspase-11-mediated inflammasome activation and IL-1ß upregulation leading to more CLS formation and insulin resistance[236]. It is quite possible that both epigenetic modification and chronic immune activation act together building the mechanistic or former can influence the latter; ATAC-sequence profiling of hematopoietic stem cells and HSC derived-macrophages in macaques shows inflammatory memory to myeloid cells in utero[237].

Overall results of the current study using 3 different mouse models could establish the influence of maternal obesity in transferring adverse metabolic effects to progeny. Also the study showed ATM ontogenic diversity, remodeling of AT by those ATMs and spot on to HIF-

1α and MYD88 as potential driver of ATM to carry out chronic immune activation. Precisely, this study provides insight to a possible mechanism for developmental reprogramming of AT by maternal obesity.

5.5. Future direction of the current study

As emerging studies started to ask the mechanistic behind maternal transmission of adverse metabolic signature to next generation, the current study will to able answer some questions about how maternal obesity may reprogram offspring's adipose tissue and in turn their metabolic life. However, science never sleeps and every minute, ideas are floating to improve our current understanding of disease processes and supplement our current research with newer innovations.

In future, it will be important to perform transcriptomic analysis of the mice AT to address the heterogeneity of ATM in the background of maternal obesity and to identify the signature genes responsible for the same. Though I have look into it at single cell level through flow cytometry, the data is limited by the panel chosen and more precise clustering is possible only by transcriptomics. Single cell RNA sequencing can identify distinct and unique ATM subsets in the maternal obese pups with insulin resistance or obesity, as was possible for aortic macrophages in atherosclerosis[238]. With the advent of single nuclei RNA sequencing it is also possible to get high through put data on thousands of transcription factors. While we found HIF-1α is one of them enabling macrophage for reprogramming adipocytes, there probably several other genes involved in the full spectrum of pathogenesis which could be identified by single cell approach. Though not many studies have looked particularly into ATM through single cell RNA sequencing, it is an emerging area and so far a study on mice visceral AT (VAT) has demarcated 7 specific macrophage subsets in calorie restricted group compare to obese VAT with better scavenging capacity [239]. In our model it will be possible to identify resident macrophage subsets of AT responsible for AT remodeling in maternal obese pups as well as resident subsets in general associated with obesity.

As discussed earlier, other major hypothesis related to the underpinning mechanism for maternal obesity induced offspring's metabolic ill-health is epigenetic modification. Therefore, it will be important to look into possible DNA methylation or other epigenetic modulation in regard to maternal obesity. The best way to look into it would be through ATAC- seq or CHIP-seq of ATMs related to specific conditions described in the study. So far very few and very recent studies have targeted ATMs for seeing metabolic alteration and identified specific chromatin remodeling complexes and chromatin accessibility status to play a role[240,241]. Only

one study using CHIP-seq showed markedly increased binding HIF-1α sites in visceral WAT in relation to chronic intermittent hypoxia and resulting insulin resistance [242] for sleep apnea disease model. Lastly, only one study published April 2023 used ATAC-seq to show maternal obesity reprogram hematopoietic stem cells and progenitors cells to have a pro-inflammatory phenotype in fetal bone marrow and liver innate immune cells in rhesus macaque[237] but not in AT. Also they did not clarify the role of resident macrophages in this regard. However, these studies show that ATAC or CHIP-seq can add value to current study in future experiments.

Another focused future direction for the current study definitely would be the use of fate mapping model. As macrophage diversity is ontogeny derived, it would be wise to use a fate mapping mouse model to confirm the developmental origins. To depict the macrophage populations, conditional reporter genes and regulated expression of Cre- recombinase are used. Moreover, it can be combined with techniques like single cell RNA-seq and histology to give a complete assessment of the disease process studied[243].

As I have considered chronic immune activation mediated by two important signaling pathways, it would be worth exploring another important signaling pathway: phosphoinositide 3-kinase(PI3K) / Akt pathway for two reasons. First, it is the key pathway in macrophage-adipocyte crosstalk to transduce metabolic information and regulate macrophages' phenotypic switch[244] and secondly, it will directly connect HIF-1α to the pathogenesis of maternal obesity through KEGG pathway easing the understanding on molecular interaction. This can simply be achieved by immunohistochemistry using antiPI3K antibody in the FFPE blocks from gWAT of HIF-1α mice. This is intriguing as most recent preclinical studies show the druggability of PI3K as target for anti-obesity treatment[245].

Other than strengthening our current results by transcriptomics and fate mapping model, few other aspects of adipocyte and ATM crosstalk recently have come into attention which can add value to the study. One interesting recent finding is a transcriptionally defined macrophage subset crosstalk with white adipocyte by mitochondria transfer which is reduced in obesity and altered energy balance[246]. It would be interesting to see how this organelle-bound interaction is affected in the background of maternal obesity.

Another new technical advance called Single Cell omics from Histology Analysis Framework (SCHAF) is recently described to combine histology image with a tissue simple's spatially resolved single cell omics dataset using adversarial machine learning technique[247]. While it has been developed on lung cancer and metastatic breast cancer tissue, certainly this kind of application would bridge the gap between spatial analysis by histology with cellular or deeper molecular understanding by single cell omics[247] for other tissue like AT. Thus it can be

a valuable tool to future studies on our current research. Lastly, in light of recent focus on primary cilia influencing the crosstalk between immune cells and adipose tissue in tissue specific manner[248], their interaction can be explored in terms of maternal obesity reprograming offspring's' white adipose tissue.

5.7 ATMs beyond obesity- Back to the future

While the current study delineates the role of ATMs in an important aspect of obesity pathogenesis, ATMs are not limited to only in the causal role of obesity and metabolic syndrome. Myeloid cells, specially macrophages are emerging as major drivers of tumor immune crosstalk in may solid tumors[249, 250] beyond their role as 'gatekeepers' of homeostasis. Thus the understanding achieved on the obese microenvironment by this study goes past the immediate and direct learning. Hypoxia and HIF-1α plays an important role in engaging macrophages in the tumor microenvironment[251]. Resident macrophage can help recruiting HSC derived macrophages and T-cells in the immune site, modulate immune check points, reprogram tumor cells, deliver drugs as nanoparticles and used for Chimeric Antigen Receptor Macrophages (CAR-M) therapy to exploit patient's immune system to fight tumors [251].

In fact, there are around 184 active and enrolling clinical trials are currently registered in clinicaltrial.gov database for exploiting the unique function of macrophages from bench to bedside[252], but major limiting factor is the lack of understanding about macrophage biology. Also there is a gap in recapitulating disease scenario and therapeutic response in between humans and the transgenic mouse models[253]. Thus, knowledge transfer and translational endeavors centering adipose tissue resident macrophages will guide us to the new direction towards immunotherapy in the future.

6. Supplementary figures

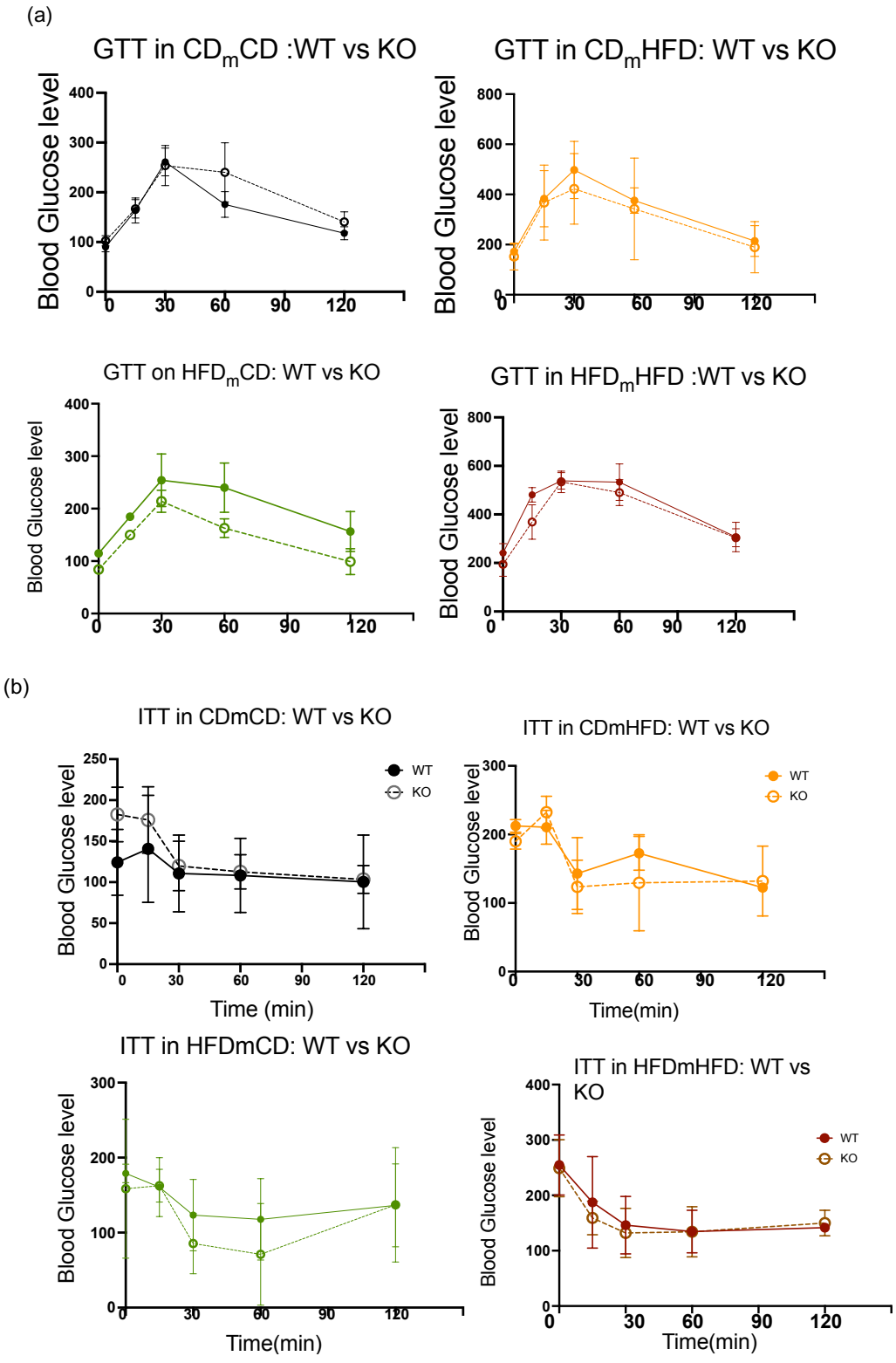

FigS1: (a)Comparison between the blood glucose level after GTT and (b)Comparison between the blood glucose level after ITT, in different obese groups & control in HIF-1α mice, n=3-5

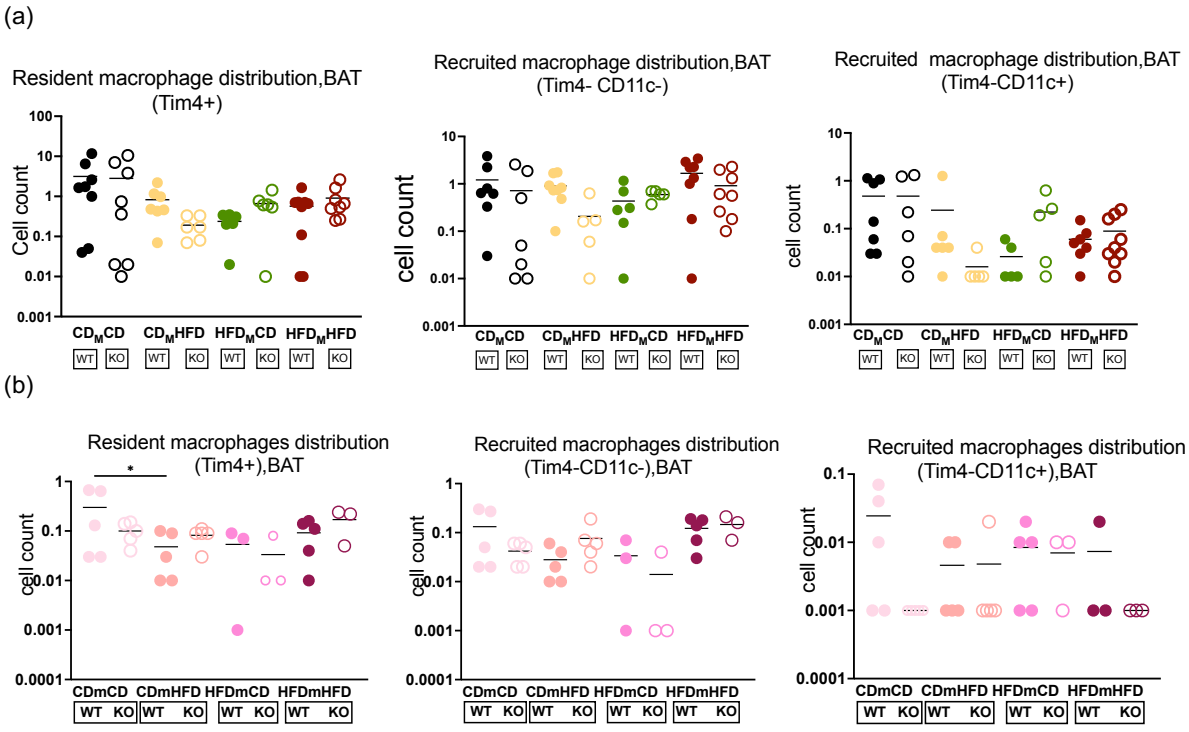

FigS2 : Macrophage landscape in BAT, (a) HIF1α and (b) MYD88 mice

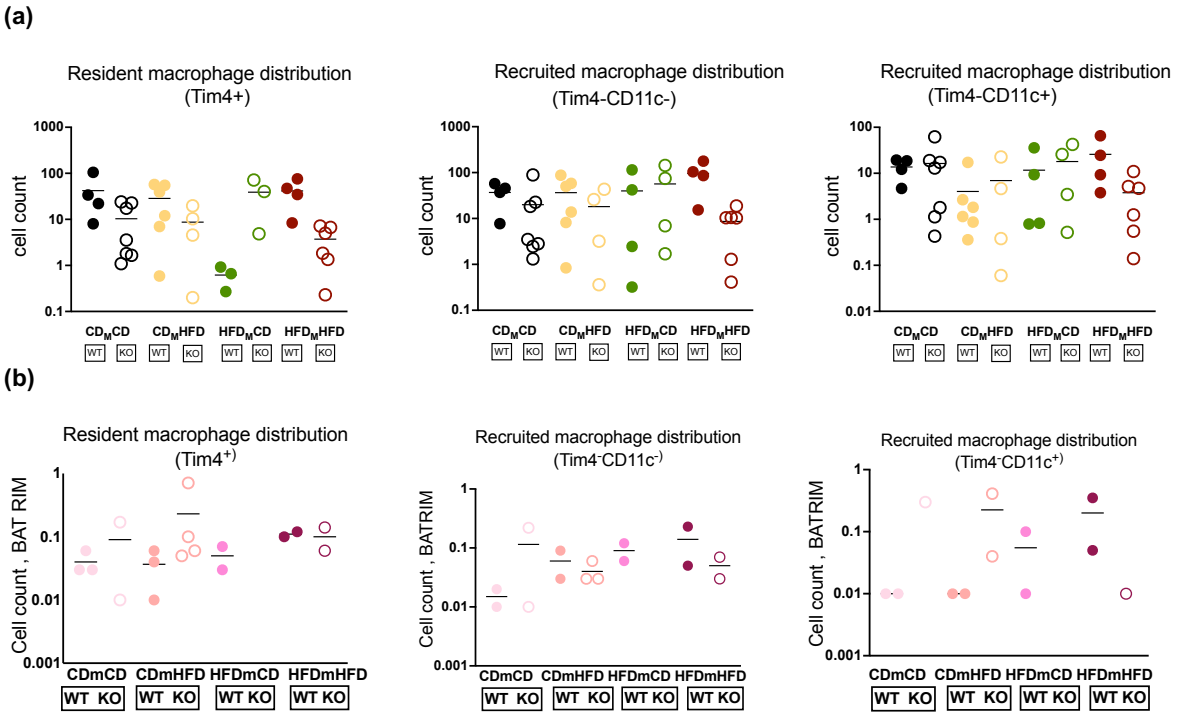

FigS3 : Macrophage landscape in BAT-RIM, (a) HIF1α and (b) MYD88 mice

(a)

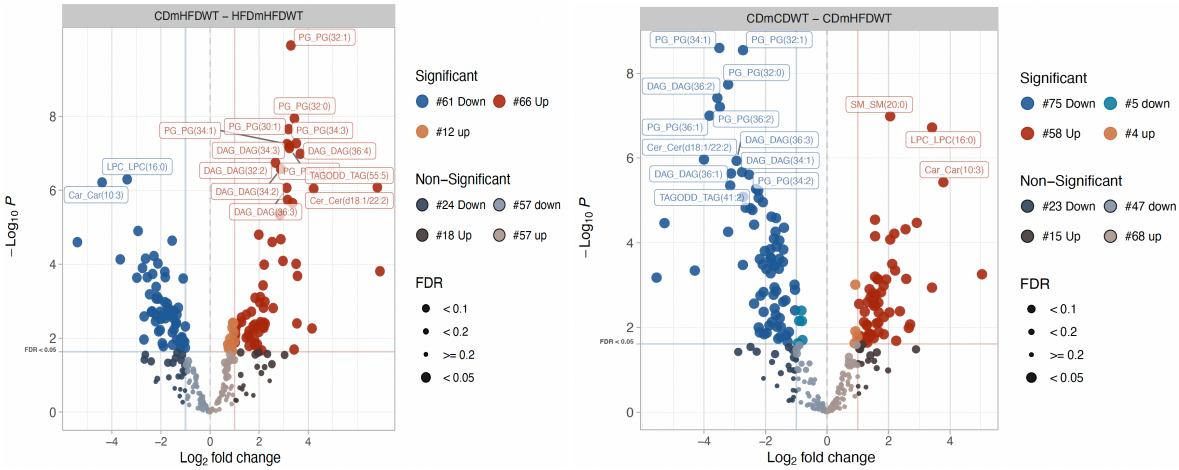

(b)

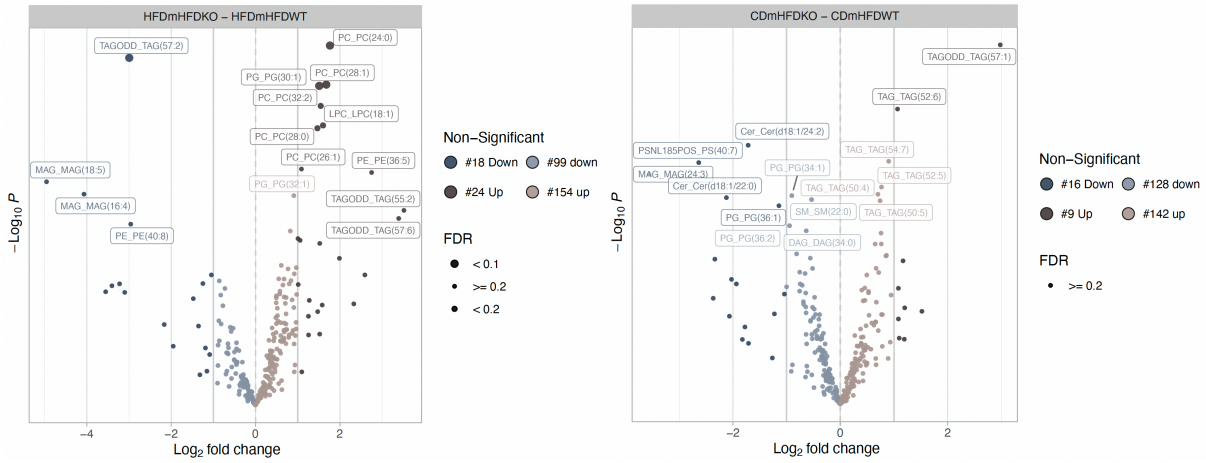

FigS4: Volcano plots displaying differentially expressed lipid species between (a)Control vs Obese groups and (b) KO vs WT within obese groups

(a)

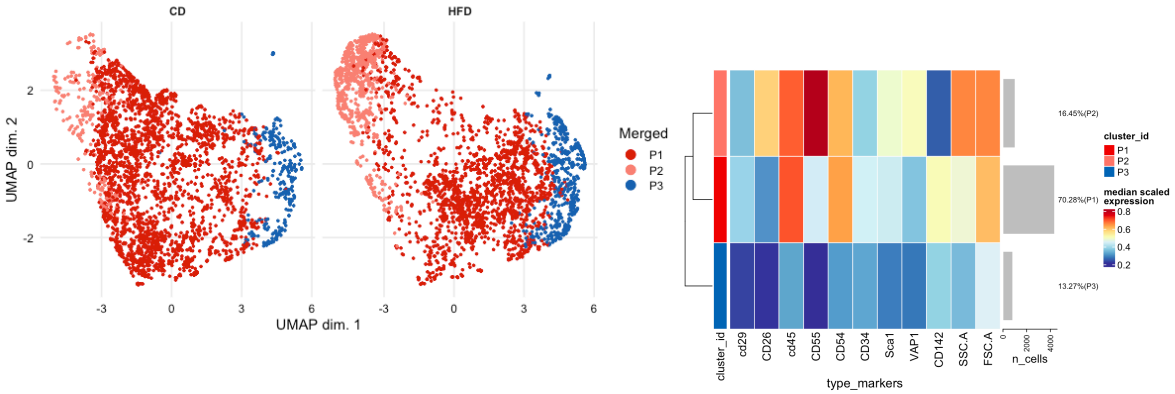

(b)

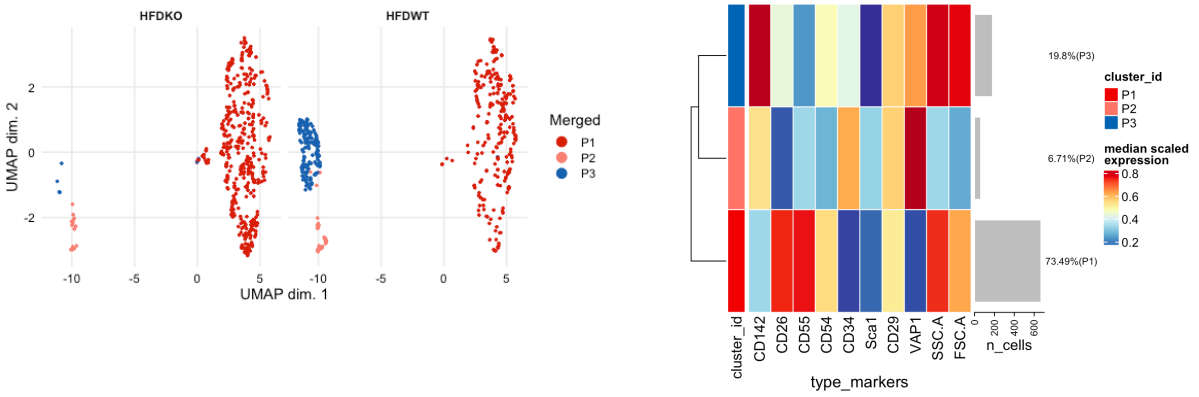

(C)

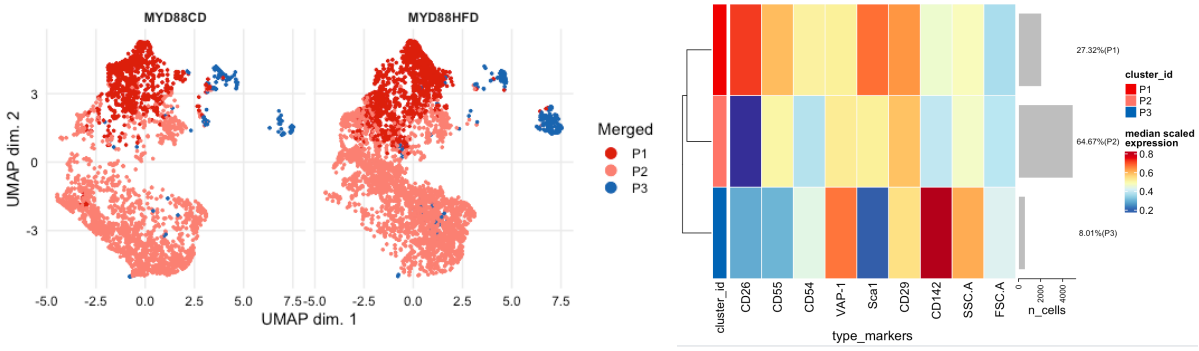

FigS5: APC population comparison in between Control and Obese groups in HIF1-α & MYD88 mice.(a)control vs obese group in HIF1-α mice, (b) WT vs KO within obese group in HIF1-α mice, (c)control vs obese group in MYD88 mice. In both mouse model, the obese group showed an increase in the P2 & P3 APC subset with more adipogenic potential. In HIF1-α KO mice , the P3 subset got depleted.

7.Appendix

7.1.Abbreviations

APC	Adipogenic precursor cells
AT	Adipose tissue
ATM	Adipose tissue macrophage
ATME	Adipose tissue microenvironment
AUC.	Area under the curve
BAT	Brown adipose tissue
BM	Bone marrow
BSA	Bovine Serum Albumin
CD	Control diet
CLS	Crown-like structure
DC	Dendritic cell
DAG	Di-glycerides
EMP	Erythro -myeloid progenitor.
FA	Fatty acid
FFA	Free fatty acid
FFPE.	Formalin fixed -paraffine embedded
gWAT	Gonadal white adipose tissue
GLUT	Glucose transporter
GTT	Glucose tolerance test
HFD	High fat diet
HIF-1α	Hypoxia inducible factor 1 subunit alfa
H&E	Hematoxylin and Eosin
HSC	Hematopoietic stem cell
IHC	Immunohistochemistry
IL	Interleukin
IRS-1	Insulin receptor substrate -1
ITT	Insulin tolerance test
IHC	Immunohistochemistry
KO	Knock-out
MYD88	Myeloid differentiation primary response 88
MPS	Mononuclear phagocyte system
OXPHOS	Oxidative phosphorylation
NFkB	Nuclear factor kappa B
PBS	Phosphate buffered saline
QC	Quality control
RES	Reticuloendothelial system
SVF	Stromal vascular fraction
SPF	Specific pathogen free
scWAT	Subcutaneous white adipose tissue
TAG	Triglyceride
TLR	Toll like receptor
TNF-α	Tumor necrosis factor alfa
TGF-β	Transforming growth factor beta
TVR	Tierversuche Verstehen room
UMAP	Uniform manifold approximation and projection
WT	Wild type
WAT	White adipose tissue
YS	Yolk sac

7.2. List of Figures

7.3. List of Tables

7.4. Contributors

Breeding plan for all mice till March 2021 was carried out by Nora Reka Balzar, including mating and plug check. Carolin Radwaniak performed feeding and scoring of mice. Cornelia Cygon performed majority of the genotyping for transgenic mice. Jelena Zurkovic conducted Mass spectrometry for lipidomics and Farhad Sakeri performed the lipidomics data analysis. David Bejarano performed the multiplex immunohistochemistry by CODEX. Figures were partially created by using online software Biorender.

References

1. Tauber, A. Metchnikoff and the phagocytosis theory. *Nat Rev Mol Cell Biol* **4**, 897–901 (2003). https://doi.org/10.1038/nrm1244

2. Cooper, MD., Alder, MN. The evolution of adaptive immune systems.*Cell* **124**,815-22 (2006). https://doi.org/10.1016/j.cell.2006.02.001

3. Dunnil, M. *The Plato of Praed Street: the Life and Times of Almroth Wright*. RSM Press, London (2000).

4. Gordon, S. The macrophage: past, present and future. *Eur J Immunol* **37 Suppl 1**,S9-17 (2007). https://doi.org/10.1002/eji.200737638

5. Griffin, F. M., Griffin, J. A., Leider, J. E. & Silverstein, S. C. Studies on the mechanism of phagocytosis. I. requirements for circumferential attachment of particle-bound ligands to specific receptors on the macrophage plasma membrane. *Journal of Experimental Medicine* **142,** 1263–1282 (1975). https://doi.org/10.1084/jem.142.5.1263

6. Hume, DA.,Perry, VH. Gordon, S. Mononuclear phagocyte system of the mouse defined by immunohistochemical localization of antigen F4/80: macrophage associated with epithelia. *Anat Rec* **210**,503-512(1984). https://doi.org/10.1002/ar.1092100311

7. Micklem, K. et al. A human macrophage-associated antigen (CD68) detected by six different monoclonal antibodies. *Br J Haematol.* **73**,6-11 (1989). https://doi.org/10.1111/j.1365-2141.1989.tb00210.x

8. Wynn, T., Chawla, A. & Pollard, J. Macrophage biology in development, homeostasis and disease. *Nature* **496**, 445–455 (2013). https://doi.org/10.1038/nature12034

9. Gordon, S., Taylor, P. Monocyte and macrophage heterogeneity. *Nat Rev Immunol* **5**, 953–964 (2005). https://doi.org/10.1038/nri1733

10. Geissmann, F. et al. Development of monocytes, macrophages, and dendritic cells. *Science* **327**,656-661 (2010) https://doi.org/10.1126/science.1178331
    Erratum in: Science**. 330**,1319 (2010).

11. Ginhoux F. et al. Fate mapping analysis reveals that adult microglia derive from primitive macrophages. *Science* **330**,841-5 (2010). https://doi.org/10.1126/science.1194637

12. Sathe, P.et al. Lymphoid tissue and plasmacytoid dendritic cells and macrophages do not share a common macrophage-dendritic cell-restricted progenitor. *Immunity* **41**,104-15 (2014). https://doi.org/10.1016/j.immuni.2014.05.020

13. Yona, S. et al. Fate mapping reveals origins and dynamics of monocytes and tissue macrophages under homeostasis. *Immunity* **38**,79-91 (2013). Erratum in: *Immunity* **38**,1073-9 (2013). https://doi.org/10.1016/j.immuni.2012.12.001

14. Mass E. Delineating the origins, developmental programs and homeostatic functions of tissue-resident macrophages. *Int Immunol.* **30**,493-501(2018). https://doi.org/10.1093/intimm/dxy044

15. Martin, FP., Jacqueline, C., Poschmann, J., Roquilly, A. Alveolar Macrophages: Adaptation to Their Anatomic Niche during and after Inflammation. *Cells* **10**:2720 (2021). https://doi.org/10.3390/cells10102720

16. Chakarov,S.et al. Two distinct interstitial macrophage populations coexist across tissues in specific subtissular niches. *Science* **363**,eaau0964(2019). https://doi.org/10.1126/science.aau0964

17. Martyniak, K., Masternak, MM. Changes in adipose tissue cellular composition during obesity and aging as a cause of metabolic dysregulation. *Exp Gerontol* **94**,59-63 (2017). https://doi.org/10.1016/j.exger.2016.12.007

18. Lee, MJ., Wu, Y., Fried, SK. Adipose tissue heterogeneity: implication of depot differences in adipose tissue for obesity complications. *Mol Aspects Med* **34**,1-11(2013). https://doi.org/10.1016/j.mam.2012.10.001

19. Pfeifer A, Hoffmann LS. Brown, beige, and white: the new color code of fat and its pharmacological implications. *Annu Rev Pharmacol Toxicol* **55**,207-227 (2015). https://doi.org/10.1146/annurev-pharmtox-010814-124346

20. Ergen, AV., Jeong, M., Lin, KK., Challen, GA,. Goodell, MA. Isolation and Characterization of Mouse Side Population cells., *Methods in Molecular Biology* **946**,151-162. (2013). https://doi.org/10.1007/978-1-62703-128-8_10

21. Lumeng, CN. et al. Aging is associated with an increase in T cells and inflammatory macrophages in visceral adipose tissue. *J Immunol* **187**,6208-6216 (2011). https://doi.org/10.4049/jimmunol.1102188

22. Zuk, PA.et al. Human adipose tissue is a source of multipotent stem cells. *Mol Biol Cell* **13,**4279-4295 (2002). https://doi.org/10.1091/mbc.e02-02-0105

23. Cinti S. The adipose organ at a glance. *Dis Model Mech* **5**,588-594(2012). https://doi.org/10.1242/dmm.009662

24. Bjørndal, B., Burri, L., Staalesen, V., Skorve, J., Berge, RK. Different adipose depots: their role in the development of metabolic syndrome and mitochondrial response to hypolipidemic agents. *J Obes* **2011**,490650(2011). https://doi.org/10.1155/2011/490650

25. Kershaw, EE., Flier, JS. Adipose tissue as an endocrine organ. *J Clin Endocrinol Metab* **89**,2548-2556(2004). https://doi.org/10.1210/jc.2004-0395

26. Kawai, T., Autieri, MV., Scalia, R. Adipose tissue inflammation and metabolic dysfunction in obesity. *Am J Physiol Cell Physiol* **320**,C375-C391(2021). https://doi.org/10.1152/ajpcell.00379.2020

27. Zwick RK, Guerrero-Juarez CF, Horsley V, Plikus MV. Anatomical, Physiological, and Functional Diversity of Adipose Tissue. *Cell Metab* **27**,68-83(2018). https://doi.org/10.1016/j.cmet.2017.12.002

28. Sakers, A., De, Siqueira MK., Seale, P., Villanueva, CJ. Adipose-tissue plasticity in health and disease.*Cell* **185**,419-446(2022). https://doi.org/10.1016/j.cell.2021.12.016

29. Kojta, I., Chacińska, M., Błachnio-Zabielska, A. Obesity, Bioactive Lipids, and Adipose Tissue Inflammation in Insulin Resistance. *Nutrients* **12,**1305(2020). https://doi.org/10.3390/nu12051305

30. Coelho, M., Oliveira, T., Fernandes, R. Biochemistry of adipose tissue: an endocrine organ. *Arch Med Sci* **9**,191-200(2013). https://doi.org/10.5114/aoms.2013.33181

31. Scheele, C., Wolfrum, C. Brown Adipose Crosstalk in Tissue Plasticity and Human Metabolism. *Endocr Rev* **41**,53–65 (2020). https://doi.org/10.1210/endrev/bnz007

32. Fitzgibbons, T.P.et al. Similarity of mouse perivascular and brown adipose tissues and their resistance to diet-induced inflammation. *Am. J. Physiol. Heart Circ. Physiol* **301**, H1425–H1437(2011). https://doi.org/10.1152/ajpheart.00376.2011

33. Herrero, L., Shapiro, H., Nayer, A., Lee, J., Shoelson, SE. Inflammation and adipose tissue macrophages in lipodystrophic mice. *Proc Natl Acad Sci U S A* **107**,240-5(2010). https://doi.org/10.1073/pnas.090531010

34. Villarroya, F., Cereijo, R., Villarroya, J. *et al.* Brown adipose tissue as a secretory organ. *Nat Rev Endocrinol* **13**, 26–35 (2017). https://doi.org/10.1038/nrendo.2016.136

35. Lizcano F. The Beige Adipocyte as a Therapy for Metabolic Diseases. *Int J Mol Sci* **20**,5058 (2019). https://doi.org/10.3390/ijms20205058

36. Altshuler-Keylin, S. et al. Beige Adipocyte Maintenance Is Regulated by Autophagy-Induced Mitochondrial Clearance.*Cell Metab* **24**, 402–419 (2016). https://doi.org/10.1016/j.cmet.2016.08.002

37. Roh, HC. et al. Warming Induces Significant Reprogramming of Beige, but Not Brown, Adipocyte Cellular Identity.*Cell Metab* **27**, 1121–1137 (2018). https://doi.org/10.1016/j.cmet.2018.03.005

38. Villarroya, F., Cereijo, R., Villarroya, J., Gavaldà-Navarro, A., Giralt, M. Toward an Understanding of How Immune Cells Control Brown and Beige Adipobiology. Cell Metab **27**,954-961 (2018). https://doi.org/10.1016/j.cmet.2018.04.006

39. Stenkula, KG., Erlanson-Albertsson, C. Adipose cell size: importance in health and disease. *Am J Physiol Regul Integr Comp Physiol* **315**,R284-R295 (2018). https://doi.org/10.1152/ajpregu.00257.2017

40. Klöting, N. et al. Insulin-sensitive obesity. *Am J Physiol Endocrinol Metab* **299**,E506-15(2010). https://doi.org/10.1152/ajpendo.00586.2009

41. Ye, RZ., Richard, G., Gévry, N., Tchernof, A., Carpentier, AC. Fat Cell Size: Measurement Methods, Pathophysiological Origins, and Relationships With Metabolic Dysregulations. *Endocr Rev* **43**,35-60.(2022). https://doi.org/10.1210/endrev/bnab018

42. Honecker, J. *et al.* A distribution-centered approach for analyzing human adipocyte estimates and their association with obesity-related traits and mitochondrial function. *Int J Obes* **45**, 2108–2117 (2021). https://doi.org/10.1038/s41366-021-00883-6

43. Laforest S. et al. Comparative analysis of three human adipocyte size measurement methods and their relevance for cardiometabolic risk. *Obesity (Silver Spring)* **25**,122-131 (2017). https://doi.org/10.1002/oby.21697

44. Fried SK. Adipocyte size redux. *Obesity (Silver Spring)* **25**,15. https://doi.org/10.1002/oby.21717

45. McLaughlin T. et al. Enhanced proportion of small adipose cells in insulin-resistant vs insulin-sensitive obese individuals implicates impaired adipogenesis. *Diabetologia* **50**,1707-1715 (2007). https://doi.org/10.1007/s00125-007-0708-y

46. Yao, J., Wu, D., Qiu, Y. Adipose tissue macrophage in obesity-associated metabolic diseases. *Front Immunol* **13**:977485 (2022). https://doi.org/10.3389/fimmu.2022.977485

47. Weisberg SP. et al. Obesity is associated with macrophage accumulation in adipose tissue. *J Clin Invest* **112**,1796-1808(2003). https://doi.org/10.1172/jci19246

48. Blaszczak, AM., Jalilvand, A., Hsueh, WA. Adipocytes, Innate Immunity and Obesity: A Mini-Review. *Front Immunol* **12**:650768 (2021). https://doi.org/10.3389/fimmu.2021.650768

49. Joffin, N., Gliniak, C.M., Funcke, JB. *et al.* Adipose tissue macrophages exert systemic metabolic control by manipulating local iron concentrations. *Nat Metab* **4**, 1474–1494 (2022). https://doi.org/10.1038/s42255-022-00664-z

50. Sharma, M. et al Netrin-1 Alters Adipose Tissue Macrophage Fate and Function in Obesity. *Immunometabolism* **1**,190010 (2019). https://doi.org/10.20900/immunometab20190010

51. . Cho, CH.et al. Angiogenic role of LYVE-1-positive macrophages in adipose tissue. *Circ Res* **100**,e47-57(2007). https://doi.org/10.1161/01.res.0000259564.92792.93

52. Jaitin DA.et al. Lipid-Associated Macrophages Control Metabolic Homeostasis in a Trem2-Dependent Manner. *Cell* **178**,686-698.e14(2019). https://doi.org/10.1016/j.cell.2019.05.054

53. Cox, N.et al. Diet-regulated production of PDGFcc by macrophages controls energy storage. *Science* **373,**eabe9383(2021). https://doi.org/10.1126/science.abe9383

54. Han, J.et al. The spatiotemporal development of adipose tissue. *Development* **138**,5027-5037(2011). https://doi.org/10.1242/dev.067686

55. Wolf, Y.et al. Brown-adipose-tissue macrophages control tissue innervation and homeostatic energy expenditure. *Nat Immunol* **18**,665-674(2017). https://doi.org/10.1038/ni.3746

56. Boutens, L., Stienstra, R. Adipose tissue macrophages: going off track during obesity. *Diabetologia* **59**,879-94(2016). https://doi.org/10.1007/s00125-016-3904-9

57. Spalding, KL.et al. Dynamics of fat cell turnover in humans. *Nature* **453**,783-787(2008). https://doi.org/10.1038/nature06902

58. Strawford, A., Antelo, F., Christiansen, M., Hellerstein, MK. Adipose tissue triglyceride turnover, de novo lipogenesis, and cell proliferation in humans measured with $2H_2O$. *Am J Physiol Endocrinol Metab* **286**,E577-88(2004). https://doi.org/10.1152/ajpendo.00093.2003

59. Kosteli, A.et al. Weight loss and lipolysis promote a dynamic immune response in murine adipose tissue. *J Clin Invest* **120**,3466-79 (2010). https://doi.org/10.1172/jci42845

60. Yan, C.et al. Macrophage-specific expression of human lysosomal acid lipase corrects inflammation and pathogenic phenotypes in lal-/- mice. *Am J Pathol* **169**,916-926(2006). https://doi.org/10.2353/ajpath.2006.051327

61. . Qu, P., Yan, C., Blum, JS., Kapur, R., Du, H. Myeloid-specific expression of human lysosomal acid lipase corrects malformation and malfunction of myeloid-derived suppressor cells in lal-/- mice. *J Immunol* **187**,3854-3866(2011). https://doi.org/10.4049/jimmunol.1003358

62. Grijalva, A., Xu, X., Ferrante, AW Jr. Autophagy Is Dispensable for Macrophage-Mediated Lipid Homeostasis in Adipose Tissue. *Diabetes* **65**,967-980. https://doi.org/10.2337/db15-1219

63. Nguyen, KD.et al. Alternatively activated macrophages produce catecholamines to sustain adaptive thermogenesis. *Nature* **480**,104-108. https://doi.org/10.1038/nature10653

64. Qiu, Y.et al. Eosinophils and type 2 cytokine signaling in macrophages orchestrate development of functional beige fat. *Cell* **157**,1292-1308 (2014). https://doi.org/10.1016/j.cell.2014.03.066

65. Xu, H.et al. Chronic inflammation in fat plays a crucial role in the development of obesity-related insulin resistance. *J Clin Invest* **112**,1821-1830 (2003). https://doi.org/10.1172/jci19451

66. Osborn, O., Olefsky. JM. The cellular and signaling networks linking the immune system and metabolism in disease. *Nat Med* **18**,363-374 (2012). https://doi.org/10.1038/nm.2627

67. Olefsky, JM., Glass, CK. Macrophages, inflammation, and insulin resistance. *Annu Rev Physiol* **72**,219-246. https://doi.org/10.1146/annurev-physiol-021909-135846

68. . Nagareddy, PR.et al Adipose tissue macrophages promote myelopoiesis and monocytosis in obesity. *Cell Metab* **19**,821-35(). https://doi.org/10.1016/j.cmet.2014.03.029

69. Amano, SU.et al. Local proliferation of macrophages contributes to obesity-associated adipose tissue inflammation. *Cell Metab* **19**,162-171(2014). https://doi.org/10.1016/j.cmet.2013.11.017

70. Nance, SA., Muir, L., Lumeng, C. Adipose tissue macrophages: Regulators of adipose tissue immunometabolism during obesity. *Mol Metab* **66**,101642 (20). https://doi.org/10.1016/j.molmet.2022.101642

71. Weisberg, SP.et al CCR2 modulates inflammatory and metabolic effects of high-fat feeding. *J Clin Invest* **116**,115-124(2006). Erratum in: *J Clin Invest* 116,1457(2006). https://doi.org/10.1172/jci24335

72. Cinti, S.et al. Adipocyte death defines macrophage localization and function in adipose tissue of obese mice and humans. *J Lipid Res* **46**,2347-2355(2005). https://doi.org/10.1194/jlr.m500294-jlr200

73. Sun, K., Kusminski, CM., Scherer PE. Adipose tissue remodeling and obesity. *J Clin Invest* **121**,2094-2101(2011).https://doi.org/10.1172/jci45887

74. Sabaratnam, R., Svenningsen, P. Adipocyte-Endothelium Crosstalk in Obesity. *Front Endocrinol (Lausanne).* **12**:681290(2021). https://doi.org/10.3389/fendo.2021.681290

75. Jin, C., Flavell, RA.Innate sensors of pathogen and stress: linking inflammation to obesity. *J Allergy Clin Immunol* **132**,287-294(2013). https://doi.org/10.1016/j.jaci.2013.06.022

76. Nguyen, MT.et al. A subpopulation of macrophages infiltrates hypertrophic adipose tissue and is activated by free fatty acids via Toll-like receptors 2 and 4 and JNK-dependent pathways. *J Biol Chem* **282**,35279-292(2007). https://doi.org/10.1074/jbc.m706762200

77. Chakarov, S., Blériot, C., Ginhoux, F. Role of adipose tissue macrophages in obesity-related disorders. *J Exp Med* **219**,e20211948(2022). https://doi.org/10.1084/jem.20211948

78. Vishvanath, L., Gupta, RK. Contribution of adipogenesis to healthy adipose tissue expansion in obesity. *J Clin Invest* **129**,4022-4031(2019). https://doi.org/10.1172/jci129191

79. Hepler, C., Vishvanath, L, Gupta RK. Sorting out adipocyte precursors and their role in physiology and disease. *Genes* **31**,127-140(2017). https://doi.org/10.1101/gad.293704.116

80. Chau, YY.et al. Visceral and subcutaneous fat have different origins and evidence supports a mesothelial source. *Nat Cell Biol* **16**,367-75 (2014). https://doi.org/10.1038/ncb2922

81. Sanchez-Gurmaches, J., Guertin, DA. Adipocyte lineages: tracing back the origins of fat. *Biochim Biophys Acta* **1842,**340-351(2014). https://doi.org/10.1016/j.bbadis.2013.05.027

82. Knittle, JL. , Timmers, K. , Ginsberg-Fellner, F., Brown, RE., Katz, DP. The growth of adipose tissue in children and adolescents. Cross-sectional and longitudinal studies of adipose cell number and size. *J Clin Invest* **63**,239-246(1979). https://doi.org/10.1172/jci109295

83. Rodeheffer, MS., Birsoy, K., Friedman, JM. Identification of white adipocyte progenitor cells in vivo. *Cell* **135**,240-249(2008). https://doi.org/10.1016/j.cell.2008.09.036

84. Merrick, D. et al. Identification of a mesenchymal progenitor cell hierarchy in adipose tissue. *Science*. **364**,eaav2501(2019). https://doi.org/10.1126/science.aav2501

85. Rabhi, N. et al. Obesity-induced senescent macrophages activate a fibrotic transcriptional program in adipocyte progenitors. Life Sci Alliance. **5**,e202101286(2022). https://doi.org/10.26508/lsa.202101286

86. Chen, C., Xu, X., Yan Y. Estimated global overweight and obesity burden in pregnant women based on panel data model. PLoS One **13**(8):e0202183. https://doi.org/10.1371/journal.pone.0202183

87. Marchi, J., Berg, M., Dencker, A., Olander, EK., Begley, C. Risks associated with obesity in pregnancy, for the mother and baby: a systematic review of reviews. *Obes Rev*. Aug;16(8):621-638(2015). https://doi.org/10.1111/obr.12288

88. Kereliuk, S. M. & Dolinsky, V. W. Recent Experimental Studies of Maternal Obesity, Diabetes during Pregnancy and the Developmental Origins of Cardiovascular Disease. *International Journal of Molecular Sciences* **23**, 4467 (2022). https://doi.org/10.3390/ijms23084467

89. Gomes, D.et al. Predicting the earliest deviation in weight gain in the course towards manifest overweight in offspring exposed to obesity in pregnancy: a longitudinal cohort study. *BMC Med* **20**,156(2022). https://doi.org/10.1186/s12916-022-02318-z

90. Park, S., Jang, A., Bouret, SG. Maternal obesity-induced endoplasmic reticulum stress causes metabolic alterations and abnormal hypothalamic development in the offspring. *PLoS Biol* **18**,e3000296(2020). https://doi.org/10.1371/journal.pbio.3000296

91. Savva, C., Helguero, L.A., González-Granillo, M. *et al.* Obese mother offspring have hepatic lipidic modulation that contributes to sex-dependent metabolic adaptation later in life. *Commun Biol* **4**, 14 (2021). https://doi.org/10.1038/s42003-020-01513-z

92. Rodgers, A., Sferruzzi-Perri, AN. Developmental programming of offspring adipose tissue biology and obesity risk. *Int J Obes (Lond)* **45**,1170-1192(2021). Erratum in: *Int J Obes (Lond)*. (2021). https://doi.org/10.1038/s41366-021-00790-w

93. Summerfield, M.et al. A long-term maternal diet transition from high-fat diet to normal fat diet during pre-pregnancy avoids adipose tissue inflammation in next generation. *PLoS One* **13**,e0209053(2018). https://doi.org/10.1371/journal.pone.0209053

94. Cirulli, F., De Simone, R., Musillo, C., Ajmone-Cat, M.A., Berry, A. Inflammatory Signatures of Maternal Obesity as Risk Factors for Neurodevelopmental Disorders: Role of Maternal Microbiota and Nutritional Intervention Strategies. *Nutrients* **14**,3150(2022). https://doi.org/10.3390/nu14153150

95. Savva, C.et al. Maternal high-fat diet programs white and brown adipose tissue lipidome and transcriptome in offspring in a sex- and tissue-dependent manner in mice. *Int J Obes (Lond)* **46**,831-842. https://doi.org/10.1038/s41366-021-01060-5

96. Trayhurn, P., Wood, IS. Adipokines: inflammation and the pleiotropic role of white adipose tissue. *Br J Nutr* **92**,347-355(2004). https://doi.org/10.1079/bjn20041213

97. Goossens, GH.et al. Increased adipose tissue oxygen tension in obese compared with lean men is accompanied by insulin resistance, impaired adipose tissue capillarization, and inflammation. *Circulation***124**,67-76(2011). https://doi.org/10.1161/circulationaha.111.027813

98. Gatenby, RA., Gillies, RJ. Why do cancers have high aerobic glycolysis? *Nat Rev Cancer* **4**,891-899(2004). https://doi.org/10.1038/nrc1478

99. . Trayhurn P. Hypoxia and adipose tissue function and dysfunction in obesity. *Physiol Rev* 93,1-21(2013). https://doi.org/10.1152/physrev.00017.2012

100. Huang, S.et al. Saturated fatty acids activate TLR-mediated proinflammatory signaling pathways. *J Lipid Res* **53**,2002-2013(2012). https://doi.org/10.1194/jlr.d029546

101. Snodgrass, RG., Huang, S., Choi, IW., Rutledge, JC., Hwang, DH. Inflammasome-mediated secretion of IL-1β in human monocytes through TLR2 activation; modulation by dietary fatty acids. *J Immunol* **191**,4337-4347(2013). https://doi.org/10.4049/jimmunol.1300298

102. Wen, H.et al. Fatty acid-induced NLRP3-ASC inflammasome activation interferes with insulin signaling. *Nat Immunol* **12**,408-415(2011). https://doi.org/10.1038/ni.2022

103. Fujisaka, S.et al. Adipose tissue hypoxia induces inflammatory M1 polarity of macrophages in an HIF-1α-dependent and HIF-1α-independent manner in obese mice. *Diabetologia* **56**,1403-1412(2013). https://doi.org/10.1007/s00125-013-2885-1

104. Lee, YS.et al. Increased adipocyte O2 consumption triggers HIF-1α, causing inflammation and insulin resistance in obesity. *Cell***157**,1339-1352(2014). https://doi.org/10.1016/j.cell.2014.05.012

105. Keith, B., Johnson, RS., Simon, MC. HIF1α and HIF2α: sibling rivalry in hypoxic tumour growth and progression. *Nat Rev Cancer* **12**,9-22(2011). https://doi.org/10.1038/nrc3183

106. Jiang, C.et al. Disruption of hypoxia-inducible factor 1 in adipocytes improves insulin sensitivity and decreases adiposity in high-fat diet-fed mice. *Diabetes* **60**,2484-2495(2011). https://doi.org/10.2337/db11-0174

107. Takikawa, A.et al. HIF-1α in Myeloid Cells Promotes Adipose Tissue Remodeling Toward Insulin Resistance. *Diabetes* **65**,3649-3659(2016). https://doi.org/10.2337/db16-0012

108. Sharma, M.*et al.* Enhanced glycolysis and HIF-1α activation in adipose tissue macrophages sustains local and systemic interleukin-1β production in obesity. *Sci Rep* **10**,5555 (2020). https://doi.org/10.1038/s41598-020-62272-9

109. Tannahill, G., Curtis, A., Adamik, J. *et al.* Succinate is an inflammatory signal that induces IL-1β through HIF-1α. *Nature* **496**, 238–242 (2013). https://doi.org/10.1038/nature11986

110. McGettrick, AF., O'Neill, LAJ. The Role of HIF in Immunity and Inflammation. *Cell Metab* **32**,524-536(2020). https://doi.org/10.1016/j.cmet.2020.08.002

111. Selak, MA.et al. Succinate links TCA cycle dysfunction to oncogenesis by inhibiting HIF-alpha prolyl hydroxylase. *Cancer Cell* **7**,77-85(2005). https://doi.org/10.1016/j.ccr.2004.11.022

112. Mills, EL.et al. Succinate Dehydrogenase Supports Metabolic Repurposing of Mitochondria to Drive Inflammatory Macrophages. *Cell* **167**,457-470(2016). https://doi.org/10.1016/j.cell.2016.08.064

113. Weidemann, A., Johnson, R. Biology of HIF-1α. *Cell Death Differ* **15**, 621–627 (2008). https://doi.org/10.1038/cdd.2008.12

114. Regazzetti, C.et al. Hypoxia Decreases Insulin Signaling Pathways in Adipocytes. *Diabetes* **58**,95–103(2009). https://doi.org/10.2337/db08-0457

115. Thomas, L.W., Ashcroft, M. Exploring the molecular interface between hypoxia-inducible factor signalling and mitochondria. *Cell. Mol. Life Sci.* **76**, 1759–1777 (2019). https://doi.org/10.1007/s00018-019-03039-y

116.Sun, RC., Denko, NC. Hypoxic regulation of glutamine metabolism through HIF1 and SIAH2 supports lipid synthesis that is necessary for tumor growth. *Cell Metab* **19**,285-292(2014). https://doi.org/10.1016/j.cmet.2013.11.022

117. Poblete, JMS.et al. Macrophage HIF-1α mediates obesity-related adipose tissue dysfunction via interleukin-1 receptor-associated kinase M. *Am J Physiol Endocrinol Metab* **318**,E689-E700(2020). https://doi.org/10.1152/ajpendo.00174.2019

118. Lei ,R.et al. HIF-1α promotes the keloid development through the activation of TGF-β/Smad and TLR4/MyD88/NF-κB pathways. *Cell Cycle* **8**,3239-3250(2019). https://doi.org/10.1080/15384101.2019.1670508

119. Zhou, H., Wang, H., Yu, M. *et al.* IL-1 induces mitochondrial translocation of IRAK2 to suppress oxidative metabolism in adipocytes. *Nat Immunol* **21**, 1219–1231 (2020). https://doi.org/10.1038/s41590-020-0750-1

120. Tran, HQ.et al. "Western Diet"-Induced Adipose Inflammation Requires a Complex Gut Microbiota. *Cell Mol Gastroenterol Hepatol* **9**,313-333(2020). https://doi.org/10.1016/j.jcmgh.2019.09.009

121. Everard, A., Geurts, L., Caesar, R. *et al.* Intestinal epithelial MyD88 is a sensor switching host metabolism towards obesity according to nutritional status. *Nat Commun* **5**, 5648 (2014). https://doi.org/10.1038/ncomms6648

122. Jin, S., Kim, K.K., Park, B.S. *et al.* Function of astrocyte MyD88 in high-fat-diet-induced hypothalamic inflammation. *J Neuroinflammation* **17**, 195 (2020). https://doi.org/10.1186/s12974-020-01846-w

123. Ryan HE.et al. Hypoxia-inducible factor-1alpha is a positive factor in solid tumor growth. *Cancer Res* **60**,4010-4015(2000).

124. Clausen, BE., Burkhardt, C., Reith, W., Renkawitz, R., Förster, I. Conditional gene targeting in macrophages and granulocytes using LysMcre mice. *Transgenic Res* **8**,265-277(1999). https://doi.org/10.1023/a:1008942828960

125. Hou, B., Reizis, B., DeFranco, AL. Toll-like receptors activate innate and adaptive immunity by using dendritic cell-intrinsic and -extrinsic mechanisms. *Immunity* **29,**272-282(2008). https://doi.org/10.1016/j.immuni.2008.05.016

126. Maeda, K. *et al.* Wnt5a-Ror2 signaling between osteoblast-lineage cells and osteoclast precursors enhances osteoclastogenesis. *Nat Med* **18**, 405–412 (2012). https://doi.org/10.1038/nm.2653

127. Crowell, HL. *et al.* An R-based reproducible and user-friendly preprocessing pipeline for CyTOF data. *F1000Research* **9**:1263(2022).[version 2; peer review: 2 approved]. https://doi.org/10.12688/f1000research.26073.2

128. Mclnnes. L. et al. UMAP: Uniform Manifold Approximation and Projection. *Journal of Open Source Sofware* **3,** 861(2018). https://doi.org/10.21105/joss.00861

129. Van Gassen, S.et al. FlowSOM: Using self-organizing maps for visualization and interpretation of cytometry data. *Cytometry A* **87**,636-645(2015). https://doi.org/10.1002/cyto.a.22625

130. Wilkerson, MD., Hayes, DN. ConsensusClusterPlus: a class discovery tool with confidence assessments and item tracking. *Bioinformatics* **26**,1572-1573(2010). https://doi.org/10.1093/bioinformatics/btq170

131. R Core Team. R: A language and environment for statistical computing. R Foundation for Statistical Computing, Vienna, Austria (2018). URL https://www.R-project.org/

132. Lazar, C., Burger, T. (2022). imputeLCMD: A Collection of Methods for Left-Censored Missing Data Imputation. R package version 2.1(2022). https://CRAN.R-project.org/package=imputeLCMD

133. Ritchie, M.E. et al. limma powers differential expression analyses for RNA-sequencing and microarray studies. *Nucleic Acids Research* **43**, e47(2015). https://doi.org/10.1093/nar/gkv007

134. Le,S., Josse, J., Husson, F. FactoMineR: An R Package for Multivariate Analysis. *Journal of Statistical Software* **25**,1-18(2008). https://doi.org/10.18637/jss.v025.i0

135. Gu, Z. Eils R, Schlesner M. Complex heatmaps reveal patterns and correlations in multidimensional genomic data. *Bioinformatics* **32**,2847-2849 (2016). https://doi.org/10.1093/bioinformatics/btw313

136. Jiang, M.et al. Dual Inhibition of Endoplasmic Reticulum Stress and Oxidation Stress Manipulates the Polarization of Macrophages under Hypoxia to Sensitize Immunotherapy. *ACS Nano* **15**,14522-14534 (2021) https://doi.org/10.1021/acsnano.1c04068

137. Leblond, MM.et al. Hypoxia induces macrophage polarization and re-education toward an M2 phenotype in U87 and U251 glioblastoma models. *Oncoimmunology* **5**,e1056442 (2015). https://doi.org/10.1080/2162402x.2015.1056442

138. Hassnain Waqas, SF.et al. Adipose tissue macrophages develop from bone marrow-independent progenitors in *Xenopus laevis* and mouse. *J Leukoc Biol* **102**,845-855(2017). https://doi.org/10.1189/jlb.1a0317-082rr

139. Ito, A.et al. Role of CC chemokine receptor 2 in bone marrow cells in the recruitment of macrophages into obese adipose tissue. *J Biol Chem* **283**,35715-35723(2008). https://doi.org/10.1074/jbc.m804220200

140. Babaeijandaghi, F. Metabolic reprogramming of skeletal muscle by resident macrophages points to CSF1R inhibitors as muscular dystrophy therapeutics. *Sci Transl Med* **14**,eabg7504(2022). https://doi.org/10.1126/scitranslmed.abg7504

141. Daemen, S et al. Dynamic Shifts in the Composition of Resident and Recruited Macrophages Influence Tissue Remodeling in NASH. *Cell Rep* **34**,108626(2021). Erratum in: *Cell Rep* **41**,111660(2022). https://doi.org/10.1016/j.celrep.2020.108626

142. Nishi, C., Toda, S., Segawa, K., Nagata, S. Tim4- and MerTK-mediated engulfment of apoptotic cells by mouse resident peritoneal macrophages. *Mol Cell Biol* **34**,1512-1520(2014). https://doi.org/10.1128/mcb.01394-13

143. Bugatti, M.et al. A Population of TIM4+FOLR2+ Macrophages Localized in Tertiary Lymphoid Structures Correlates to an Active Immune Infiltrate Across Several Cancer Types. *Cancer Immunol Res*. **10**,1340-1353(2022). https://doi.org/10.1158/2326-6066.cir-22-0271

144. Russo, L., Lumeng, CN. Properties and functions of adipose tissue macrophages in obesity. *Immunology* **155,**407-417(2018). https://doi.org/10.1111/imm.13002

145. Félix, I.et al. Single-Cell Proteomics Reveals the Defined Heterogeneity of Resident Macrophages in White Adipose Tissue. *Front Immunol* **12**,719979(2021). https://doi.org/10.3389/fimmu.2021.719979

146. Lu, L.et al. Differential expression of CD11c defines two types of tissue-resident macrophages with different origins in steady-state salivary glands. *Sci Rep* **12**,931(2022). https://doi.org/10.1038/s41598-022-04941-5

147. Huh, J.Y., Kim, J.B. TIM4^{+} adipose tissue-resident macrophages: new modulators of adiposity. *Nat Rev Endocrinol* **17**, 645–646 (2021). https://doi.org/10.1038/s41574-021-00554-6

148. Zhou, TA.et al. Thymic macrophages consist of two populations with distinct localization and origin. *Elife* **11**,e75148(2022). https://doi.org/10.7554/elife.75148

149. Hildreth, AD.et al. Single-cell sequencing of human white adipose tissue identifies new cell states in health and obesity. *Nat Immunol* **22**,639-653(2021). https://doi.org/10.1038/s41590-021-00922-4

150. Bian, Z.et al. Deciphering human macrophage development at single-cell resolution. *Nature* **582**,571-576(2020). https://doi.org/10.1038/s41586-020-2316-7

151. Davidson, S,Passmore, R, Brock, JF and Truswell, *Human Nutrition and Dietetics*, Churchhill Living Stone, Edinburgh (AS 1975).

152. Piché, ME., Tchernof, A., Després, JP. Obesity Phenotypes, Diabetes, and Cardiovascular Diseases. *Circ Res* **126**,1477-1500(2020). https://doi.org/10.1161/circresaha.120.316101

153. Rogers, P., & Webb, G. Estimation of body fat in normal and obese mice. *British Journal of Nutrition* **43**,83-86(1980). https://doi.org/10.1079/bjn19800066

154. Abbas.A, Lichtman,A.,Pillai,S. *Cellular and Molecular Immunology*, 9th ed., Elsevier Health Sciences. Philadelphia, PA.(2017).

155. Parker, R.et al. CC chemokine receptor 2 promotes recruitment of myeloid cells associated with insulin resistance in nonalcoholic fatty liver disease. *Am J Physiol Gastrointest Liver Physiol* **314**,G483-G493(2018). https://doi.org/10.1152/ajpgi.00213.2017

156. Cao, S.et al. EGFR-mediated activation of adipose tissue macrophages promotes obesity and insulin resistance. *Nat Commun* **13**,4684(2022). https://doi.org/10.1038/s41467-022-32348-3

157. Arner, P., Spalding, KL. Fat cell turnover in humans. *Biochem Biophys Res Commun* **396**,101-4(2010). https://doi.org/10.1016/j.bbrc.2010.02.165

158. Dalamaga, M., Liu, J. A chromatin remodeling checkpoint of diet-induced macrophage activation in adipose tissue. *Metabol Open* **15**:100204(2022). https://doi.org/10.1016/j.metop.2022.100204

159. Suganami,T., Ogawa, Y. Adipose tissue macrophages: their role in adipose tissue remodeling. *J Leukoc Biol* **88**,33-39(2010). https://doi.org/10.1189/jlb.0210072

160. Surmi, BK., Hasty, AH. Macrophage infiltration into adipose tissue: initiation, propagation and remodeling. *Future Lipidol* **3**,545-556 (2008). https://doi.org/10.2217/17460875.3.5.545

161. Kim, J.et al. Silencing CCR2 in Macrophages Alleviates Adipose Tissue Inflammation and the Associated Metabolic Syndrome in Dietary Obese Mice. *Mol Ther Nucleic Acids* **5**,e280(2016). https://doi.org/10.1038/mtna.2015.51

162. Sullivan, TJ.et al. Experimental evidence for the use of CCR2 antagonists in the treatment of type 2 diabetes. *Metabolism* **62**,1623-1632(2013). https://doi.org/10.1016/j.metabol.2013.06.008

163. Kanda, H et al. MCP-1 contributes to macrophage infiltration into adipose tissue, insulin resistance, and hepatic steatosis in obesity. *J Clin Invest* **116**,1494-1505(2006). https://doi.org/10.1172/jci26498

164.Kamei, N.et al. Overexpression of monocyte chemoattractant protein-1 in adipose tissues causes macrophage recruitment and insulin resistance. *J Biol Chem* **281**,26602-26614(2006). https://doi.org/10.1074/jbc.m601284200

165. Lindhorst, A., Raulien, N., Wieghofer, P. *et al.* Adipocyte death triggers a pro-inflammatory response and induces metabolic activation of resident macrophages. *Cell Death Dis* **12**, 579 (2021). https://doi.org/10.1038/s41419-021-03872-9

166. Muhlhausler, BS., Vithayathil, MA. Impact of maternal obesity on offspring adipose tissue: lessons for the clinic. *Expert Rev Endocrinol Metab* **9**,615-627(2014). https://doi.org/10.1586/17446651.2014.956088

167. Fernandez-Twinn, DS.et al. Downregulation of IRS-1 in adipose tissue of offspring of obese mice is programmed cell-autonomously through post-transcriptional mechanisms. *Mol Metab* **3**,325-333(2014). https://doi.org/10.1016/j.molmet.2014.01.007

168. Breton, C. The hypothalamus-adipose axis is a key target of developmental programming by maternal nutritional manipulation. *J Endocrinol* **216**,R19-31(2013). https://doi.org/10.1530/joe-12-0157

169: Bol, VV., Delattre, AI., Reusens, B., Raes, M., Remacle, C. Forced catch-up growth after fetal protein restriction alters the adipose tissue gene expression program leading to obesity in adult mice. *Am J Physiol Regul Integr Comp Physiol* **297**,R291-9(2009). https://doi.org/10.1152/ajpregu.90497.2008

170. Bouret, SG., Draper, SJ., Simerly, RB. Trophic action of leptin on hypothalamic neurons that regulate feeding. *Science* **304**,108-110(2004). https://doi.org/10.1126/science.1095004

171. Granado, M., Fuente-Martín, E., García-Cáceres, C., Argente, J., Chowen, JA. Leptin in early life: a key factor for the development of the adult metabolic profile. *Obes Facts* **5**,138-150(2012). https://doi.org/10.1159/000336967

172. Corvera, S., Solivan-Rivera, J., Yang Loureiro, Z. Angiogenesis in adipose tissue and obesity. *Angiogenesis* **25**,439-453(2022). https://doi.org/10.1007/s10456-022-09848-3

173. Ichioka M,et al. Increased expression of macrophage-inducible C-type lectin in adipose tissue of obese mice and humans. *Diabetes* **60**,819-826(2011). https://doi.org/10.2337/db10-0864

174. Hachiya, R., Tanaka, M., Itoh, M., Suganami, T.Molecular mechanism of crosstalk between immune and metabolic systems in metabolic syndrome. *Inflamm Regener* **42**, 13 (2022). https://doi.org/10.1186/s41232-022-00198-7

175. Tanaka, M.et al. Macrophage-inducible C-type lectin underlies obesity-induced adipose tissue fibrosis. *Nat Commun* **5**,4982(2014). https://doi.org/10.1038/ncomms5982

176. Malavazos, AE.et al. The density of crown-like structures in epicardial adipose tissue could play a role in cardiovascular diseases. *Eat Weight Disord* **27**,2905-2910(2022). https://doi.org/10.1007/s40519-022-01420-8

177.Tilg, H., Moschen, AR. Evolution of inflammation in nonalcoholic fatty liver disease: the multiple parallel hits hypothesis. *Hepatology* **52**,1836–1846 (2010). https://doi.org/10.1002/hep.24001

178. Wang, L., Zhao, RP., Song, XY., Wu, WF. Targeting ERβ in Macrophage Reduces Crown-like Structures in Adipose Tissue by Inhibiting Osteopontin and HIF-1α. *Sci Rep* **9**,15762 (2019). https://doi.org/10.1038/s41598-019-52265-8

179. Sun, K., Tordjman, J., Clément, K., Scherer, PE. Fibrosis and adipose tissue dysfunction. *Cell Metab* **18**,470–477, (2013). https://doi.org/10.1016/j.cmet.2013.06.016

180. Goossens, GH., Blaak, EE. Adipose tissue dysfunction and impaired metabolic health in human obesity: a matter of oxygen?*Front Endocrinol* **6,**55(2015). https://doi.org/10.3389%2Ffendo.2015.00055

181. Engin, AB., Engin, A., Gonul, II. The effect of adipocyte-macrophage crosstalk in obesity-related breast cancer. *J Mol Endocrinol* **62**,R201-R222(2019). https://doi.org/10.1530/jme-18-0252

182. Lumeng, CN., Deyoung, SM., Saltiel, AR. Macrophages block insulin action in adipocytes by altering expression of signaling and glucose transport proteins. *Am J Physiol Endocrinol Metab* **292**,E166-74 (2007). https://doi.org/10.1152/ajpendo.00284.2006

183. Okuno A.et al. Troglitazone increases the number of small adipocytes without the change of white adipose tissue mass in obese Zucker rats. *J Clin* **101**,1354-1361(1998). https://doi.org/10.1172/jci1235

184. Farnier, C.et al. Adipocyte functions are modulated by cell size change: potential involvement of an integrin/ERK signalling pathway. *Int J Obes Relat Metab Disord* **27,**1178-1186(2003). https://doi.org/10.1038/sj.ijo.0802399

185. Pasarica, M.et al. Lower total adipocyte number but no evidence for small adipocyte depletion in patients with type 2 diabetes. *Diabetes Care* **32**,900-902(2009). https://doi.org/10.2337/dc08-2240

186. Gawronska-Kozak, B. et al. J. Dermal White Adipose Tissue (dWAT) Is Regulated by Foxn1 and Hif-1α during the Early Phase of Skin Wound. Healing. *Int.J.Mol.Sci* **23**,257(2021). https://doi.org/10.3390/ijms23010257

187.Halberg, N. et al. Hypoxia-inducible factor 1alpha induces fibrosis and insulin resistance in white adipose tissue. *Mol Cell Biol* **29**,4467-4483(2009). https://doi.org/10.1128/mcb.00192-09

188. Snodgrass, RG.et al. Hypoxia Potentiates Palmitate-induced Pro-inflammatory Activation of Primary Human Macrophages. *J Biol Chem* **291**,413-424(2016). https://doi.org/10.1074/jbc.m115.686709

189. Mahmassani, ZS.et al. Absence of MyD88 from Skeletal Muscle Protects Female Mice from Inactivity-Induced Adiposity and Insulin Resistance. *Obesity (Silver Spring* **28**,772-782(2020). https://doi.org/10.1002/oby.22759

190. Bai, Y., Sun, Q. Macrophage recruitment in obese adipose tissue. *Obes Rev* **16**,127-136(2015). https://doi.org/10.1111/obr.12242

191. Fredrickson, G.et al. Exercise of high intensity ameliorates hepatic inflammation and the progression of NASH. *Mol Metab* **53**,101270(2021). https://doi.org/10.1016/j.molmet.2021.101270

192. Suganami, T., Nishida, J., Ogawa, Y. A paracrine loop between adipocytes and macrophages aggravates inflammatory changes: role of free fatty acids and tumor necrosis factor alpha. *Arterioscler Thromb Vasc Biol* **25**,2062-2068(2005). https://doi.org/10.1161/01.atv.0000183883.72263.13

193. Scott, T., Owens, MD. Thrombocytes respond to lipopolysaccharide through Toll-like receptor-4, and MAP kinase and NF-kappaB pathways leading to expression of interleukin-6 and cyclooxygenase-2 with production of prostaglandin E2. *Mol Immunol* **45**,1001-1008(2008). https://doi.org/10.1016/j.molimm.2007.07.035

194. Jové, M. et al. Human omental and subcutaneous adipose tissue exhibit specific lipidomic signatures. *FASEB J* **28**,1071-1081(2014). https://doi.org/10.1096/fj.13-234419

195. Wahle, KW., McIntosh, G., Duncan, WR., James WP. Concentrations of linoleic acid in adipose tissue differ with age in women but not men. *Eur J Clin Nutr* **45**,195–202(1991).

196.Zhang, C., Klett EL., Coleman, RA. Lipid signals and insulin resistance. *Clin Lipidol* **8**:659–667(2013). https://doi.org/10.2217/clp.13.67

197.Huang, WC.et al. Anti-bacterial and anti-inflammatory properties of capric acid against Propionibacterium acnes: a comparative study with lauric acid. *J Dermatol Sci.* **73**:232–240(2014). https://doi.org/10.1016/j.jdermsci.2013.10.010

198. Al-Sulaiti H. et al. Triglyceride profiling in adipose tissues from obese insulin sensitive, insulin resistant and type 2 diabetes mellitus individuals. *J Transl Med* **16**,175(2018). https://doi.org/10.1186/s12967-018-1548-x

199. Perona, JS., Portillo, MP., Teresa Macarulla, M., Tueros, AI., Ruiz-Gutierrez, V. Influence of different dietary fats on triacylglycerol deposition in rat adipose tissue. *Br J Nutr* **84**,765–774(2000).

200. Blandin, A.et al. Lipidomic analysis of adipose-derived extracellular vesicles reveals specific EV lipid sorting informative of the obesity metabolic state. *Cell Rep* **42**,112169(2023). https://doi.org/10.1016/j.celrep.2023.112169

201. Hou, B.et al. Targeted lipidomics and transcriptomics profiling reveal the heterogeneity of visceral and subcutaneous white adipose tissue. *Life Sci* **245**,117352(2020). https://doi.org/10.1016/j.lfs.2020.117352

202. Lange M. et al. AdipoAtlas: A reference lipidome for human white adipose tissue, *Cell Reports Medicine* **2**,100407(2021). https://doi.org/10.1016/j.xcrm.2021.100407.

203. Shimizu, I., Walsh, K. The Whitening of Brown Fat and Its Implications for Weight Management in Obesity. *Curr Obes Rep* **4,**224-229(2015). https://doi.org/10.1007/s13679-015-0157-8

204. Lapa, C. *et al.* Whitening and Impaired Glucose Utilization of Brown Adipose Tissue in a Rat Model of Type 2 Diabetes Mellitus. *Sci Rep* **7**, 16795 (2017). https://doi.org/10.1038/s41598-017-17148-w

205. Kotzbeck, P.et al. Brown adipose tissue whitening leads to brown adipocyte death and adipose tissue inflammation. *J Lipid Res* **59**,784-794(2018). https://doi.org/10.1194/jlr.m079665

206. Arner, P., Andersson, DP., Arner, E., Rydén, M., Kerr, AG. Subcutaneous adipose tissue expansion mechanisms are similar in early and late onset overweight/obesity. *Int J Obes (Lond)* **46**,1196-1203(2022). https://doi.org/10.1038/s41366-022-01102-6

207. Shalova, IN.et al. Human monocytes undergo functional re-programming during sepsis mediated by hypoxia-inducible factor-1.*Immunity* **42**,484–498, (2015). https://doi.org/10.1016/j.immuni.2015.02.001

208. Liu, J.et al. Allogeneic adipose-derived stem cells promote ischemic muscle repair by inducing M2 macrophage polarization via the HIF-1α/IL-10 pathway. *Stem Cells* **38**,1307-1320(2020). https://doi.org/10.1002/stem.3250

209.Boutens, L.et al. Unique metabolic activation of adipose tissue macrophages in obesity promotes inflammatory responses. *Diabetologia* **61**,942-953 (2018). https://doi.org/10.1007/s00125-017-4526-6

210. Larqué, E. *et al.* From conception to infancy — early risk factors for childhood obesity. *Nat Rev Endocrinol* **15**, 456–478 (2019). https://doi.org/10.1038/s41574-019-0219-1

211. Tie, H. T. et al. Risk of childhood overweight or obesity associated with excessive weight gain during pregnancy: a meta-analysis. *Arch. Gynecol. Obstetrics* **289**, 247–257(2014). https://doi.org/10.1007/s00404-013-3053-z

212. Desai, M., Beall, M., Ross, M. G. Developmental origins of obesity: programmed adipogenesis. *Curr. Diabetes Rep* **13**, 27–33 (2013). https://doi.org/10.1007/s11892-012-0344-x

213. Chang, E.et al.Programming effects of maternal and gestational obesity on offspring metabolism and metabolic inflammation. *Sci. Rep* **9**,16027 (2019). https://doi.org/10.1038/s41598-019-52583-x

214. Heerwagen, M. J., Miller, M. R., Barbour, L. A., and Friedman, J. E. Maternal obesity and fetal metabolic programming: a fertile epigenetic soil. *Am. J. Physiol. Regulat. Integrat. Comparat. Physiol* **299**, R711–R722(2010). https://doi.org/10.1152/ajpregu.00310.2010

215. Urbonaite, G., Knyzeliene, A., Bunn, FS., Smalskys, A., Neniskyte, U. The impact of maternal high-fat diet on offspring neurodevelopment. *Front Neurosci* **16**,909762(2022). https://doi.org/10.3389/fnins.2022.909762

216. de Almeida-Faria, J.et al. Maternal obesity during pregnancy leads to adipose tissue ER stress in mice via miR-126-mediated reduction in Lunapark. *Diabetologia* **64**,890-902(2021). https://doi.org/10.1007/s00125-020-05357-4

217. Saullo, C.et al. Effects of a maternal high-fat diet on adipose tissue in murine offspring: A systematic review and meta-analysis. *Biochimie* **201**,18-32(2022). https://doi.org/10.1016/j.biochi.2022.06.009

218. Fusco, S.et al. Maternal insulin resistance multigenerationally impairs synaptic plasticity and memory via gametic mechanisms. *Nat. Commun.* **10,**4799 (2019). https://doi.org/10.1038/s41467-019-12793-3

219. Siersbæk, M. S. et al. C57BL/6J substrain differences in response to high-fat diet intervention. *Sci. Rep* **10**,1–15(2020). https://doi.org/10.1038/s41598-020-70765-w

220. Loria, A., Murphy, M. O., Herald, J., and Cohn, D. High fat diet exacerbates adipose tissue-derived adipokines and hypertension in female C57BL/6 mice exposed to early life stress (ELS).*FASEB J* **31**, 859.3–859.3(2017).

221. Calligaris, S. D. et al. Mice long-term high-fat diet feeding recapitulates human cardiovascular alterations: an animal model to study the early phases of diabetic cardiomyopathy. *PloS One* **8**:e60931(2013). https://doi.org/10.1371/journal.pone.0060931

222. Wang, C.Y., Liao, J. K. A Mouse Model of Diet-Induced Obesity and Insulin Resistance. *Methods Mol Biol* **821**,421-433 (2012). https://doi.org/10.1007/978-1-61779-430-8_27

223. Gregoire, F. M.et al.Diet-induced obesity and hepatic gene expression alterations in C57BL/6J and ICAM-1-deficient mice. *Am. J. Physiol. Endocrinol. Metab* **282**,E703–E713(2002). https://doi.org/10.1152/ajpendo.00072.2001

224. Collins, S., Martin, T. L., Surwit, R. S., and Robidoux, J. Genetic vulnerability to diet-induced obesity in the C57BL/6J mouse: physiological and molecular characteristics. *Physiol Behav* **81**,243–248(2004). https://doi.org/10.1016/j.physbeh.2004.02.006

225.Zheng J. et al. Maternal and post-weaning high-fat, high-sucrose diet modulates glucose homeostasis and hypothalamic POMC promoter methylation in mouse offspring. *Metabolic Brain Disease* **30**,1129-1137(2015). https://doi.org/10.1007/s11011-015-9678-9

226. Zheng J. et al. The effects of maternal and post-weaning diet interaction on glucose metabolism and gut microbiota in male mice offspring. *Bioscience Reports* **36**,1-10 (2016). https://doi.org/10.1042/bsr20160103

227. Corken, A., Thakali, KM. Maternal Obesity Programming of Perivascular Adipose Tissue and Associated Immune Cells: An Understudied Area With Few Answers and Many Questions. *Front Physiol* **12**:798987(2022). https://doi.org/10.3389/fphys.2021.798987

228.Sellayah, D., Thomas, H., Lanham, S. A., and Cagampang, F. R. Maternal obesity during pregnancy and lactation influences offspring obesogenic adipogenesis but not developmental adipogenesis in mice. *Nutrients* **11**,495.(2019). https://doi.org/10.3390/nu11030495

229. Yang, Q. Y. et al. Maternal obesity induces epigenetic modifications to facilitate Zfp423 expression and enhance adipogenic differentiation in fetal mice. *Diabetes* **62**,3727–3735. (2013). https://doi.org/10.2337/db13-0433

230. Gilley SP.et al. Associations between maternal obesity and offspring gut microbiome in the first year of life. *Pediatr Obes* **17**,e12921(2022). https://doi.org/10.1111/ijpo.12921

231. Rubini E.et al. Maternal obesity during pregnancy leads to derangements in one-carbon metabolism and the gut microbiota: implications for fetal development and offspring wellbeing. *Am J Obstet Gynecol* **227**,392-400(2022). https://doi.org/10.1016/j.ajog.2022.04.013

232. Strain, J., Spaans, F., Serhan, M., Davidge, ST., Connor, KL. Programming of weight and obesity across the lifecourse by the maternal metabolic exposome: A systematic review. *Mol Aspects Med* **87,**100986(2022). https://doi.org/10.1016/j.mam.2021.100986

233. Li, HP., Chen, X., Li, MQ. Gestational diabetes induces chronic hypoxia stress and excessive inflammatory response in murine placenta. *Int J Clin Exp Pathol* **6**,650-659(2013).

234. Yan, X.et al. Maternal obesity induces sustained inflammation in both fetal and offspring large intestine of sheep.*Inflamm Bowel Dis* **17**,1513-1522(2011). https://doi.org/10.1002/ibd.21539

235. Sureshchandra, S. et al. Maternal obesity blunts antimicrobial responses in fetal monocytes. *Elife* **12**,e81320(2023). https://doi.org/10.7554/elife.81320

236. Wada, N.et al. Maternal high-fat diet exaggerates diet-induced insulin resistance in adult offspring by enhancing inflammasome activation through noncanonical pathway of caspase-11. *Mol Metab* **37**,100988(2020). https://doi.org/10.1016/j.molmet.2020.100988

237. Nash, MJ.et al. Maternal diet alters long-term innate immune cell memory in fetal and juvenile hematopoietic stem and progenitor cells in nonhuman primate offspring. *Cell Rep* **42**,112393(2023). https://doi.org/10.1016/j.celrep.2023.112393

238. Cochain, C.et al. Single-Cell RNA-Seq Reveals the Transcriptional Landscape and Heterogeneity of Aortic Macrophages in Murine Atherosclerosis. *Circ Res* **122**,1661-1674(2018). https://doi.org/10.1161/circresaha.117.312509

239. Weinstock, A.et al. Single-Cell RNA Sequencing of Visceral Adipose Tissue Leukocytes Reveals that Caloric Restriction Following Obesity Promotes the Accumulation of a Distinct Macrophage Population with Features of Phagocytic Cells. *Immunometabolism* 1,190008(2019). https://doi.org/10.20900/immunometab20190008

240. Kong, Q.et al. BAF60a Deficiency in Macrophage Promotes Diet-Induced Obesity and Metabolic Inflammation. *Diabetes* **71**,2136-2152(2022). https://doi.org/10.2337/db22-0114

241. Hu, RD.et al. Chromatin accessibility analysis identifies the transcription factor ETV5 as a suppressor of adipose tissue macrophage activation in obesity. *Cell Death Dis* **12**,1023(2021). https://doi.org/10.1038/s41419-021-04308-0

242. Gozal, D.et al. Visceral White Adipose Tissue after Chronic Intermittent and Sustained Hypoxia in Mice. *Am J Respir Cell Mol Biol* **56**,477-487(2017). https://doi.org/10.1165/rcmb.2016-0243oc

243. Xu, Y., Schrank, PR., Williams, JW. Macrophage Fate Mapping. *Curr Protoc* **2**,e456(2022). https://doi.org/10.1002/cpz1.456

244. Acosta-Martinez, M., Cabail, MZ. The PI3K/Akt Pathway in Meta-Inflammation. *Int J Mol Sci* **23**,15330(2022). https://doi.org/10.3390/ijms232315330

245. Savova, MS., Mihaylova, LV., Tews, D., Wabitsch, M., Georgiev, MI. Targeting PI3K/AKT signaling pathway in obesity. *Biomed Pharmacother* **159**,114244(2023). https://doi.org/10.1016/j.biopha.2023.114244

246.Brestoff, JR. et al. Intercellular Mitochondria Transfer to Macrophages Regulates White Adipose Tissue Homeostasis and Is Impaired in Obesity. *Cell Metab* **33**,270-282.e8(2021). https://doi.org/10.1016/j.cmet.2020.11.008

247. Charles Comiter. et al. Inference of single cell profiles from histology stains with the Single-Cell omics from Histology Analysis Framework(SCHAF). Preprint at https://www.biorxiv.org/content/10.1101/2023.03.21.533680v1(2023).

248. Picon-Galindo, E., Latz, E., Wachten, D. Primary cilia and their effects on immune cell functions and metabolism: a model. *Trends Immunol* **43**,366-378(2022). https://doi.org/10.1016/j.it.2022.03.001

249. Goswami, S., Anandhan, S., Raychaudhuri, D. *et al.* Myeloid cell-targeted therapies for solid tumours. *Nat Rev Immunol* **23**,106–120 (2023). https://doi.org/10.1038/s41577-022-00737-w

250. Kloosterman, DJ., Akkari, L. Macrophages at the interface of the co-evolving cancer ecosystem. *Cell* **186**,1627-1651(2023). https://doi.org/10.1016/j.cell.2023.02.020

251. Wang, Y. Johnson, KCC., Gatti-Mays, ME., Li, Z.Emerging strategies in targeting tumor-resident myeloid cells for cancer immunotherapy.*J Hematol Oncol* **15**:118(2022). https://doi.org/10.1186/s13045-022-01335-y

252. U.S. National Library of Medicine, National Library of Medicine website, Government of the USA , accessed 23 April, 2023, https://clinicaltrials.gov/ct2/home

253. Mass, E., Nimmerjahn, F., Kierdorf, K. Andreas, Schlitzer. Tissue-specific macrophages: how they develop and choreograph tissue biology. *Nat Rev Immunol* (2023).(ahead of print) https://doi.org/10.1038/s41577-023-00848-y

Figure references

Fig2. Chakarov,S.et al. Two distinct interstitial macrophage populations coexist across tissues in specific subtissular niches. *Science* **363**,eaau0964(2019). https://doi.org/10.1126/science.aau0964

Fig3. Cypess AM. Reassessing Human Adipose Tissue.*N Engl J Med* **386**,768-779(2022). https://doi.org/10.1056/nejmra2032804

Fig5. Vishvanath, L., Gupta, RK. Contribution of adipogenesis to healthy adipose tissue expansion in obesity. *J Clin Invest* **129**,4022-4031(2019). https://doi.org/10.1172/jci129191

Fig6. KEGG Pathway, HIF-1 signaling pathway, map 04066, accessed 5 May2023, https://www.kegg.jp/kegg/pathway.html

Fig7: Szklarczyk D.et al. The STRING database in 2023: protein-protein association networks and functional enrichment analyses for any sequenced genome of interest. *Nucleic Acids Res* **51**,D638-D646(2023). doi: 10.1093/nar/gkac1000. **String database accessed 12 May2023, https://version-11-5.string-db.org**

Mice cohort:

Mouse id	sex	age	genotype	Diet	experiment date	mouse no in the exp	Symphony	Histology :H&E	Lipidomics	APC	Mice generated by	
2787	m	11 weeks	Hif1af/f LysM-+/+	CDCDHFD	191219	Mouse_1	NA	W114			NB	
2788	m	11 weeks	Hif1af/f LysM-Cre/+	CDCDHFD	191219	Mouse_2	NA	W115			NB	
2789	m	11 weeks	Hif1af/f LysM-Cre/+	CDCDHFD	191219	Mouse_3	NA	W116			NB	
2643	m	11 weeks	Hif1af/f LysM-+/+	HFDCDCD	191126	Mouse_1	yes	W112			NB	
2645	m	11 weeks	Hif1af/f LysM-+/+	HFDCDCD	191126	Mouse_2	yes	W113			NB	
2641	m	11 weeks	Hif1af/f LysM-+/+	HFDCDCD	191121	Mouse_1	yes	W117			NB	
2642	m	11 weeks	Hif1af/f LysM-Cre/+	HFDCDCD	191121	Mouse_2	yes	W118			NB	
2644	m	11 weeks	Hif1af/f LysM-+/+	HFDCDCD	191121	Mouse_3	yes	W119			NB	
2517	m	11 weeks	Hif1af/f LysM-Cre/+	CDCDCD	191023	Mouse_1	yes	W120			NB	
2513	m	11 weeks	Hif1af/f LysM-+/+	HFDHFDHFD	191023	Mouse_2	yes	W121			NB	
2514	m	11 weeks	Hif1af/f LysM-Cre/+	HFDHFDHFD	191023	Mouse_3	yes	W122			NB	
2511	m	11 weeks	Hif1af/f LysM-Cre/+	CDCDCD	191016	Mouse_1	yes	W123			NB	
2512	m	11 weeks	Hif1af/f LysM-Cre/+	CDCDHFD	191016	Mouse_2	yes	W124			NB	
2821	m	11 weeks	Hif1af/f LysM-+/+	CDCDCD	200107	Mouse_1	NA	W108			NB	
2953	m	11 weeks	Hif1af/f LysM-+/+	HFDCDCD	200107	Mouse_2	NA	W109			NB	
2954	m	11 weeks	Hif1af/f LysM-+/+	HFDCDCD	200107	Mouse_3	NA	W110			NB	
2862	m	11 weeks	Hif1ap/p LysM-Cre/+	HFDHFDHFD	200107	Mouse_4	NA	W111			NB	
2893	m	11 weeks	Hif1af/f LysM-+/+	CDCDCD	200115	Mouse_1	Yes	W105			NB	
2905	m	11 weeks	Hif1af/f LysM-+/+	CDCDCD	200115	Mouse_2	Yes	W106			NB	
2910	m	11 weeks	Hif1af/f LysM-+/+	CDCDCD	200115	Mouse_3	Yes	W107			NB	
	m	11 weeks	Hif1af/f LysM-+/+	CDCDCD	200123	Mouse_1	NA	W101			not used	
	m	11 weeks	Hif1af/f LysM-+/+	CDCDCD	200123	Mouse_2	NA	W102			not used	
	m	11 weeks	Hif1af/f LysM-Cre/+	CDCDCD	200123	Mouse_3	NA	W103			not used	
	m	11 weeks	Hif1af/f LysM-+/+	CDCDCD	200123	Mouse_4	NA	W104			not used	
2903	m	11 weeks	Hif1af/f LysM-+/+	CDCDCD	200127	Mouse_1	Yes	W98			NB	
2904	m	11 weeks	Hif1af/f LysM-+/+	CDCDCD	200127	Mouse_2	Yes	W99			NB	
2906	m	11 weeks	Hif1ap/p LysM-Cre/+	CDCDCD	200127	Mouse_3	Yes	W100			NB	
3030	m	11 weeks	Hif1ap/pLysM-+/+	CDCDHFD	200218	Mouse_1	Yes	W93			NB	
3028	m	11 weeks	Hif1ap/pLysM-cre/+	HFDCDCD	200218	Mouse_2	Yes	W94			NB	
3063	m	11 weeks	Hif1ap/pLysM-+/+	CDCDCD	200218	Mouse_3	Yes	W95			NB	
3031	m	11 weeks	Hif1ap/p LysM-Cre/+	CDCDHFD	200304	Mouse_1	Yes	W77			NB	
3033	m	11 weeks	Hif1ap/pLysM-+/+	CDCDHFD	200304	Mouse_2	Yes	W78			NB	
3034	m	11 weeks	Hif1ap/pLysM-+/+	HFDHFDHFD	200304	Mouse_3	Yes	W79			NB	
3025	m	11 weeks	Hif1ap/p LysM-Cre/+	HFDCDCD	200304	Mouse_4	Yes	W80			NB	
3128	m	11 weeks	Hif1ap/p LysM-Cre/+	CDCDHFD	200317	Mouse_1	Yes	W81			NB	
3118	m	11 weeks	Hif1ap/p LysM-Cre/+	CDCDHFD	200317	Mouse_2	Yes	W82			NB	
3127	m	11 weeks	Hif1ap/pLysM-+/+	CDCDHFD	200317	Mouse_3	Yes	W83			NB	
3129	m	11 weeks	Hif1ap/pLysM-+/+	CDCDHFD	200317	Mouse_4	Yes	W84			NB	
2307	m	11 weeks	Hif1ap/p LysM-Cre/+	HFDHFDHFD	200414	Mouse_1	Yes	W62			NB	
2304	m	11 weeks	Hif1ap/p LysM-+/+	HFDHFDHFD	200414	Mouse_2	Yes	W63			NB	
3107	m	11 weeks	Hif1af/f LysM-Cre/+	CDCDCD	200312	Mouse_1	Yes	W69			NB	
3119	m	11 weeks	Hif1af/f LysM-+/+	CDCDCD	200312	Mouse_2	Yes	W70			NB	
3120	m	11 weeks	Hif1af/f LysM-Cre/+	CDCDCD	200312	Mouse_3	Yes	W71			NB	
3126	m	11 weeks	Hif1af/f LysM-Cre/+	CDCDCD	200312	Mouse_4	Yes	W72			NB	
3802	m	11 weeks	Hif1af/f LysM-+/+	HFDHFDHFD	200728	Mouse_1	Yes	W46			NB	
3869	m	11 weeks	Hif1af/f LysM-+/+	HFDCDCD	200728	Mouse_2	Yes	W47			NB	
3868	m	11 weeks	Hif1af/f LysM-+/+	HFDCDCD	200728	Mouse_3	Yes	W48			NB	
4653	m	11 weeks	Hif1ap/p LysM-Cre/+	HFDHFDHFD	201104	Mouse_1	Yes	W20			NB	
4654	m	11 weeks	Hif1ap/p LysM-Cre/+	HFDHFDHFD	201104	Mouse_2	Yes	W21			NB	
4655	m	11 weeks	Hif1ap/p LysM-Cre/+	HFDHFDHFD	201104	Mouse_3	Yes	NA			NB	
5463	m	11 weeks	Hif1af/f LysM-+/+	HFDCDCD	210126	Mouse_1	Yes	W227			NB	
5464	m	11 weeks	Hif1ap/p LysM-Cre/+	HFDCDCD	210126	Mouse_2	Yes	W228			NB	
5516	m	11 weeks	Hif1ap/p LysM-Cre/+	HFDHFDHFD	210126	Mouse_3	Yes	W229			NB	
5517	m	11 weeks	Hif1af/f LysM-+/+	HFDHFDHFD	210126	Mouse_4	Yes	W230			NB	
5518	m	11 weeks	Hif1af/f LysM-+/+	HFDHFDHFD	210126	Mouse_5	Yes	W231			NB	
5519	m	11 weeks	Hif1ap/p LysM-Cre/+	HFDHFDHFD	210126	Mouse_6	Yes	W232			NB	
5965	m	11 weeks	Hif1ap/p LysM-Cre/+	HFDHFDHFD	210224	Mouse_3	Yes	W183			NB	
5966	m	11 weeks	Hif1ap/p LysM-Cre/+	HFDHFDHFD	210224	Mouse_4	Yes	W184			NB	
5967	m	11 weeks	Hif1ap/p LysM-Cre/+	HFDHFDHFD	210224	Mouse_5	Yes	W185			NB	
5972	m	11 weeks	Hif1ap/p LysM-Cre/+	HFDHFDHFD	210224	Mouse_6	Yes	W186			NB	

6302	m	11 weeks	Hif1ap/p LysM-Cre/+	HFDCDCD	210310	Mouse_5	Yes	W225			
6303	m	11 weeks	Hif1ap/p LysM-+/+	HFDCDCD	210310	Mouse_6	Yes	W226	Yes		NB/MB
5970	m	11 weeks	Hif1ap/p LysM-Cre/+	CDCDCD	210303	Mouse_1	Yes	W170	Yes		NB/MB
5971	m	11 weeks	Hif1ap/p LysM-+/+	CDCDCD	210303	Mouse_2	Yes	W171	Yes		NB/MB
5974	m	11 weeks	Hif1ap/p LysM-Cre/+	CDCDCD	210303	Mouse_3	Yes	W172	Yes		NB/MB
6086	m	11 weeks	Hif1ap/p LysM-Cre/+	HFDCDCD	210303	Mouse_4	Yes	W173	Yes		NB/MB
6088	m	11 weeks	Hif1ap/p LysM-Cre/+	HFDCDCD	210303	Mouse_5	Yes	W174	Yes		NB/MB
6412	m	11 weeks	Hif1ap/p LysM-Cre/+	HFDHFDHFD	210324	Mouse_5	Yes	W179	Yes		NB/MB
6413	m	11 weeks	Hif1ap/p LysM-+/+	HFDHFDHFD	210324	Mouse_6	Yes	W180	Yes		NB/MB
8909	m	11 weeks	Hif1ap/p LysM-+/+	HFDHFDHFD	211029	Mouse_1	Yes	no	Yes		MB
8910	m	11 weeks	Hif1ap/p LysM-Cre/+	HFDHFDHFD	211029	Mouse_2	Yes	no	Yes		MB
8911	m	11 weeks	Hif1ap/p LysM-+/+	HFDHFDHFD	211029	Mouse_3	Yes	no	Yes		MB
8912	m	11 weeks	Hif1ap/p LysM-Cre/+	HFDHFDHFD	211029	Mouse_4	Yes	no	Yes		MB
8913	m	11 weeks	Hif1ap/p LysM-Cre/+	HFDHFDHFD	211029	Mouse_5	Yes	no	Yes		MB
9077	m	11 weeks	Hif1ap/p LysM-Cre/+	CDCDHFD	211129	Mouse_1	Yes	W233	Yes		MB
9220	m	11 weeks	Hif1ap/p LysM-Cre/+	CDCDHFD	211129	Mouse_2	Yes	W234	Yes		MB
9114	m	11 weeks	Hif1ap/p LysM-+/+	CDCDHFD	211129	Mouse_3	Yes	W235	Yes		MB
9341	m	11 weeks	Hif1ap/p LysM-+/+	CDCDHFD	211129	Mouse_4	Yes	W236	Yes		MB
9790	m	11 weeks	Hif1ap/p LysM-+/+	CDCDCD	220128	Mouse_1	Yes	W237	Yes		MB
9791	m	11 weeks	Hif1ap/p LysM-Cre/+	CDCDCD	220128	Mouse_2	Yes	NA	Yes		MB
9792	m	11 weeks	Hif1ap/p LysM-Cre/+	CDCDCD	220128	Mouse_3	Yes	W238	Yes		MB
9794	m	11 weeks	Hif1ap/p LysM-Cre/+	CDCDCD	220128	Mouse_4	Yes	W239	Yes		MB
9795	m	11 weeks	Hif1ap/p LysM-CRe/+	CDCDCD	220128	Mouse_5	Yes	W240	Yes		MB
11279	m	11 weeks	Hif1ap/p LysM-+/+	CDCDCD	220525	Mouse_1	Yes	no	Yes		MB
11281	m	11 weeks	Hif1ap/p LysM-Cre/+	CDCDHFD	220525	Mouse_2	Yes	W245	Yes	yes	MB
11408	m	11 weeks	Hif1ap/p LysM-+/+	HFDCDCD	220525	Mouse_3	Yes	No	Yes	yes	MB
11410	m	11 weeks	Hif1ap/p LysM-cre/+	HFDCDCD	220525	Mouse_4	Yes	W259	Yes	yes	MB
11411	m	11 weeks	Hif1ap/p LysM-+/+	HFDCDCD	220525	Mouse_5	Yes	W260	Yes	yes	MB
11409	m	11 weeks	Hif1ap/p LysM-+/+	HFDCDCD	220525	Mouse_6	Yes	No	Yes	yes	MB
11622	m	11 weeks	Hif1ap/p LysM-+/+	CDCDCD	220608	Mouse_1	Yes	No	Yes		MB
11620	m	11 weeks	Hif1ap/p LysM-Cre/+	CDCDCD	220608	Mouse_2	Yes	No	Yes		MB
11623	m	11 weeks	Hif1ap/p LysM-Cre/+	CDCDCD	220608	Mouse_3	Yes	No	Yes		MB
11625	m	11 weeks	Hif1ap/p LysM-Cre/+	CDCDCD	220608	Mouse_4	Yes	No	Yes		MB
12099	m	11 weeks	Hif1ap/p LysM-+/+	CDCDHFD	220714	Mouse_1	Yes	W246	Yes		MB
12101	m	11 weeks	Hif1ap/p LysM-+/+	CDCDHFD	220714	Mouse_2	Yes	W247	Yes		MB
12100	m	11 weeks	Hif1ap/p LysM-Cre/+	CDCDHFD	220714	Mouse_3	Yes	W248	Yes		MB
12851	m	11 weeks	Hif1ap/p LysM-+/+	CDCDHFD	220908	Mouse_1	Yes	No	Yes		MB
12852	m	11 weeks	Hif1ap/p LysM-+/+	CDCDHFD	220908	Mouse_2	Yes	No	Yes		MB
12853	m	11 weeks	Hif1ap/p LysM-+/+	CDCDHFD	220908	Mouse_3	Yes	No	Yes		MB
13108	m	11 weeks	Hif1ap/p LysM-+/+	HFDHFDHFD	220926	Mouse_1	Yes	No		yes	MB
13109	m	11 weeks	Hif1ap/p LysM-Cre/+	HFDHFDHFD	220926	Mouse_2	Yes	No		yes	MB
13110	m	11 weeks	Hif1ap/p LysM-Cre/+	HFDHFDHFD	220926	Mouse_3	Yes	No		yes	MB
13111	m	11 weeks	Hif1ap/p LysM-+/+	HFDHFDHFD	220926	Mouse_4	Yes	No		yes	MB
13112	m	11 weeks	Hif1ap/p LysM-Cre/+	HFDHFDHFD	220926	Mouse_5	Yes	No		yes	MB
13548	m	11 weeks	Hif1ap/p LysM Cre/+	CDCDCD	221019	Mouse_1	No	yes		yes	MB
13549	m	11 weeks	Hif1ap/p LysM-+/+	CDCDCD	221019	Mouse_2	No	yes		yes	MB
9464	m	11 weeks	Hif1ap/p LysM-+/+	HFDHFDHFD	211216	Mouse_1	NO	W242	Yes		MB
9465	m	11 weeks	Hif1ap/p LysM Cre/+	HFDHFDHFD	211216	Mouse_2	NO	W241	Yes		MB
9466	m	11 weeks	Hif1ap/p LysM Cre/+	HFDHFDHFD	211216	Mouse_3	NO	W243	Yes		MB
9467	m	11 weeks	Hif1ap/p LysM-+/+	HFDHFDHFD	211216	Mouse_4	NO	W244	Yes		MB
9730	m		Hif1ap/p LysM-+/+	CDCDCD	211207	Mouse_6	Yes	No		Yes	MB
9395	m		Hif1ap/p LysM-+/+	HFDHFDHFD	211207	Mouse_7	Yes	No		Yes	MB
9398	m		Hif1ap/p LysM-+/+	HFDHFDHFD	211207	Mouse_8	Yes	No		Yes	MB
9729	f		Hif1ap/p LysM Cre/+	CDCDCD	220312	Mouse_1				Yes	MB
9738	m		Hif1ap/p LysM-+/+	HFDHFDHFD	220312	Mouse_2				Yes	MB
8480	m		WT		220312	Mouse_3				Yes	MB

Mouse id	sex	age	genotype	Diet	experiment d	mouse no in the exp	Symphony	Histology :H&E	Cryosection	Special stain	Mice generaed by
4710	M	11 weeks	MYD88 f/f Rank +/+	CDCDHFD	201111	WAT animal 002.fcs	NA	W17	No	None	NB
4711	M	11 weeks	MYD88 f/f Rank eGFP-Cre/+	CDCDHFD	201111	WAT animal 003.fcs	NA	W18	No	None	NB
4712	M	11 weeks	MYD88 f/f Rank +/+	CDCDHFD	201111	WAT animal 004.fcs	NA	W19	No	None	NB
4782	M	11 weeks	MYD88 f/+ Rank +/+	CDCDCD	201118	WAT animal 001.fcs	Yes	W10	No	None	NB
4785	M	11 weeks	MYD88 f/+ Rank +/+	CDCDCD	201118	WAT animal 002.fcs	Yes	No	No	None	NB
5063	M	11 weeks	MYD88 f/f Rank Cre/+	CDCDHFD	201202	WAT animal 001.fcs	Yes	W4	No	None	NB
5065	M	11 weeks	MYD88 f/f Rank Cre/+	CDCDHFD	201202	WAT animal 002.fcs	Yes	W5	No	None	NB
5037	M	11 weeks	MYD88 f/f Rank Cre/+	CDCDCD	201209	WAT animal 001.fcs	Yes	W1	No	None	NB
5038	M	11 weeks	MYD88 f/f Rank Cre/+	CDCDCD	201209	WAT animal 002.fcs	Yes	W2	No	None	NB
5039	M	11 weeks	MYD88 f/f Rank Cre/+	CDCDCD	201209	WAT animal 003.fcs	Yes	W3	No	None	NB
5215	M	11 weeks	MYD88 f/f Rank +/+	CDCDCD	210113	WAT animal 001.fcs	Yes	W218	No	None	NB
5220	M	11 weeks	MYD88 f/f Rank +/+	CDCDCD	210113	WAT animal 002.fcs	Yes	W219	No	None	NB
5227	M	11 weeks	MYD88 f/f Rank +/+	HFDHFDHFI	210113	WAT animal 003.fcs	Yes	W220	No	None	NB
5229	M	11 weeks	MYD88 f/f Rank Cre/+	HFDHFDHFI	210113	WAT animal 004.fcs	Yes	W221	No	None	NB
5279	M	11 weeks	MYD88 f/f Rank +/+	HFDHFDHFI	210113	WAT animal 005.fcs	Yes	W222	No	None	NB
5226	M	11 weeks	MYD88 f/f Rank +/+	HFDHFDHFD	210105	WAT animal 001.fcs	Yes	W204	No	None	NB
5281	M	11 weeks	MYD88 f/f Rank +/+	HFDHFDHFD	210105	WAT animal 002.fcs	Yes	W205	No	None	NB
5282	M	11 weeks	MYD88 f/f Rank Cre/+	HFDHFDHFD	210105	WAT animal 003.fcs	Yes	W206	No	None	NB
5228	M	11 weeks	MYD88 f/f Rank +/+	HFDHFDHFD	210105	WAT animal 004.fcs	Yes	W207	No	None	NB
5230	M	11 weeks	MYD88 f/f Rank Cre/+	HFDHFDHFD	210105	WAT animal 005.fcs	Yes	W208	No	None	NB
5815	M	11 weeks	MYD88 f/f Rank +/+	CDCDHFD	210210	WAT animal 001.fcs	Yes	W223	No	None	NB
5816	M	11 weeks	MYD88 f/f Rank Cre/+	CDCDHFD	210210	WAT animal 002.fcs	Yes	W224	No	None	NB
5551	M	11 weeks	MYD88 f/f Rank Cre/+	CDCDHFD	210203	WAT animal 001.fcs	Yes	W198	No	None	NB
5552	M	11 weeks	MYD88 f/+ Rank +/+	CDCDHFD	210203	WAT animal 002.fcs	Yes	W199	No	None	NB
5553	M	11 weeks	MYD88 f/+ Rank +/+	CDCDHFD	210203	WAT animal 003.fcs	Yes	W200	No	None	NB
5535	M	11 weeks	MYD88 f/+ Rank +/+	CDCDHFD	210203	WAT animal 004.fcs	Yes	W201	No	None	NB
5536	M	11 weeks	MYD88 f/f Rank Cre/+	CDCDHFD	210203	WAT animal 005.fcs	Yes	W202	No	None	NB
5537	M	11 weeks	MYD88 f/f Rank +/+	CDCDHFD	210203	WAT animal 006.fcs	Yes	W203	No	None	NB
6295	M	11 weeks	MYD88 f/f Rank Cre/+	CDCDCD	210310	WAT animal 001.fcs	Yes	W214	No	None	NB
6300	M	11 weeks	MYD88 f/f Rank Cre/+	CDCDCD	210310	WAT animal 002.fcs	Yes	W215	No	None	MB
6212	M	11 weeks	MYD88 f/f Rank Cre/+	CDCDHFD	210310	WAT animal 003.fcs	Yes	W216	No	None	MB
6399	M	11 weeks	MYD88 f/f Rank +/+	HFDCDCD	210310	WAT animal 004.fcs	Yes	W217	No	None	MB
6354	M	11 weeks	MYD88 f/f Rank Cre/+	CDCDCD	210324	WAT animal 001.fcs	Yes	W175	No	None	MB
6355	M	11 weeks	MYD88 f/f Rank +/+	CDCDHFD	210324	WAT animal 002.fcs	Yes	W176	No	None	MB
6356	M	11 weeks	MYD88 f/f Rank Cre/+	CDCDHFD	210324	WAT animal 003.fcs	Yes	W177	No	None	MB
6357	M	11 weeks	MYD88 f/+ Rank +/+	CDCDHFD	210324	WAT animal 004.fcs	Yes	W178	No	None	MB
7213	M	11 weeks	MYD88 f/f Rank +/+	HFDHFDHFD	210529	WAT animal 001.fcs	Yes	W190	No	None	MB
7105	M	11 weeks	MYD88 f/f Rank Cre/+	HFDCDCD	210529	WAT animal 002.fcs	Yes	W191	No	None	MB
7108	M	11 weeks	MYD88 f/f Rank +/+	HFDCDCD	210529	WAT animal 003.fcs	Yes	W192	No	None	MB
7109	M	11 weeks	MYD88 f/f Rank Cre/+	HFDCDCD	210529	WAT animal 004.fcs	Yes	W193	No	None	MB
7406	M	11 weeks	MYD88 f/f Rank +/+	CDCDHFD	210618	WAT animal 001.fcs	Yes	W194	No	None	MB
7407	M	11 weeks	MYD88 f/f Rank +/+	CDCDCD	210618	WAT animal 002.fcs	Yes	W195	No	None	MB
7408	M	11 weeks	MYD88 f/f Rank eGFP-Cre/+	CDCDHFD	210618	WAT animal 003.fcs	Yes	W196	No	None	MB
7409	M	11 weeks	MYD88 f/f Rank +/+	CDCDCD	210618	WAT animal 004.fcs	Yes	W197	No	None	MB
7518	M	11 weeks	MYD88 f/f Rank +/+	HFDHFDHFD	210709	WAT animal 001.fcs	Yes	W187	No	None	MB
7519	M	11 weeks	MYD88 f/f Rank +/+	HFDHFDHFD	210709	WAT animal 002.fcs	Yes	W188	No	None	MB
7524	M	11 weeks	MYD88 f/f Rank +/+	HFDHFDHFD	210709	WAT animal 003.fcs	Yes	W189	No	None	MB
8072	M	11 weeks	MYD88 f/f Rank + /+	CDCDCD	210818	WAT animal 001.fcs	Yes	W209	No	None	MB
8143	M	11 weeks	MYD88 f/f Rank +/+	HFDCDCD	210818	WAT animal 002.fcs	Yes	W210	No	None	MB
8144	M	11 weeks	MYD88 f/f Rank eGFP-Cre/+	HFDCDCD	210818	WAT animal 003.fcs	Yes	W211	No	None	MB
8149	M	11 weeks	MYD88 f/f Rank eGFP-Cre/+	HFDCDCD	210818	WAT animal 004.fcs	Yes	W212	No	None	MB
8150	M	11 weeks	MYD88 f/f Rank eGFP-Cre/+	HFDCDCD	210818	WAT animal 005.fcs	Yes	W213	No	None	MB
12730	M	11 weeks	MYD88 f/f Rank + /+	HFDHFDHFD	220824	WAT animal 001.fcs	Yes	W257	No	None	MB
12731	M	11 weeks	MYD88 f/f Rank + /+	HFDHFDHFD	220824	WAT animal 002.fcs	Yes	W258	No	None	MB
13412	M	11 weeks	MYD88 f/f Rank + /+	CDCDHFD	221019	WAT animal 003.fcs	Yes	NA	No	None	MB
13413	M	11 weeks	MYD88 f/f Rank + /+	CDCDHFD	221019	WAT animal 004.fcs	Yes	NA	No	None	MB
13414	M	11 weeks	MYD88 f/f Rank + /+	CDCDHFD	221019	WAT animal 005.fcs	Yes	NA	No	None	MB
13175	M	11 weeks	MYD88 f/f Rank eGFP-Cre/+	CDCDCD	220930	WAT animal 001.fcs	No	W255	No	None	MB
13174	M	11 weeks	MYD88 f/f Rank +/+	CDCDCD	220930	WAT animal 002.fcs	No	W256	No	None	MB
5954	M	11 weeks	MYD88 f/f Rank eGFP-Cre/+	HFDCDCD	210224	WAT animal 001.fcs	Yes	W181	No	None	NB
5955	M	11 weeks	MYD88 f/f Rank +/+	HFDCDCD	210224	WAT animal 002.fcs	Yes	W182	No	None	NB
10046	M	11 weeks	MYD88 f/f Rank +/+	HFDHFDHFD	220422	WAT animal 001.fcs	Yes	No	No	None	MB
10048	M	11 weeks	MYD88 f/f Rank +/+	HFDHFDHFD	220422	WAT animal 002.fcs	Yes	No	No	None	MB
10307	M	11 weeks	MYD88 f/f Rank +/+	CDCDCD	220422	WAT animal 003.fcs	Yes	No	No	None	MB
10308	M	11 weeks	MYD88 f/f Rank +/+	CDCDCD	220422	WAT animal 004.fcs	Yes	No	No	None	MB